Energy, Mines and Resources Canada
Énergie, Mines et Ressources Canada

CANMET
Canada Centre for Mineral and Energy Technology
Centre canadien de la technologie des minéraux et de l'énergie

# PARAMETRIC STUDY OF THE VARIABLES OF SUPPORT DESIGN

M. Gyenge
Rock Mechanics Laboratory

August 1983

This document is the ... interim report ... for discussion ... reporting purposes ... represent ... the opinion of the ... for Mineral and ... (CANMET)

Ce document est un rapport ... préliminaire et rédigé ... pour lui de ... documentation ... nulle- ... on définitive de ... Centre canadien de ... des minéraux et de l'énergie (CANMET)

MAR 14 1984

MICROMEDIA

120 pp

MINERALS RESEARCH PROGRAM
MINING RESEARCH LABORATORIES
DIVISION REPORT MRP/MRL 83-67(TR)

# PARAMETRIC STUDY OF THE VARIABLES OF SUPPORT DESIGN

by

M. Gyenge*

## SUMMARY

The presently available bolting guidelines have been developed in 1970. The needs of the industry require to update them by implementing the present and more advanced state of understanding and the latest technological and analytical developments. The first stage of the updating process, is to establish the significance of the variables of support design through a parametric study and then to correlate and synthesize the obtained data in the form required for implementation.

The results of this study were obtained by using the comprehensive rock bolting design procedure which is based on rock-support interaction analysis. The input data of the analyses were selected by ensuring that they represent the defined ranges of variables.

The procedure of rock-support interaction analysis is discussed by a detailed example. The significance of the variables is evaluated by a series of computations with the selected values of variables in systematic combinations.

The correlation of the computation results yielded the formulation of the concept of critical stress and deformation analysis. This method of analysis could provide an effective and simple procedure for analysing the expected behaviour of an underground opening, and it could be used to estimate the support requirements and to make an initial selection of support types.

Based on the results obtained by this study as well as other available information it is possible to proceed with a draft version of the proposed updated bolting guidelines. Areas of further investigations are identified.

---

*Research Scientist, Rock Mechanics Laboratory, Mining Research Laboratories, Canada Centre for Mineral and Energy Technology (CANMET), Energy, Mines and Resources Canada.

# ETUDE PARAMETRIQUE DES VARIABLES INTERVENANT DANS LE CALCUL DU SOUTENEMENT

par

M. Gyenge*

## RESUME

Les principes directeurs actuels en matière de boulons d'encrage ont été publiés en 1970. Les besoins de l'industrie exigent leur mise à jour pour tenir compte de l'état actuel des connaissances ainsi que les derniers perfectionnements techniques et analytiques. La première étape de la mise à jour consiste d'abord à déterminer par le moyen d'une étude paramétrique l'importance relative des variables intervenant dans le calcul des dispositifs de soutènement, puis à faire la corrélation et la synthèse des données obtenues forme utilie pour mise en oeuvre.

On a obtenu les résultats de cette étude par l'emploi de la méthode globale de calcul du boulonnage de roche, fondée sur une analyse de l'interaction entre la roche et le soutènement. Les données d'entrée des analyses ont été choisies pour représenter des gammes prédéterminées de variables.

La méthode d'analyse de l'interaction roche-soutènement est examinée au moyen d'un exemple précis. On évalue la signification des variables à l'aide d'une série de calculs utilisant des valeurs de variables choisies soumises à des combinaisons systématiques.

La corrélation des résultats de calculs permet de formuler une notion que tient compte à la fois de l'analyse des déformations et des contraintes limites. La méthode d'analyse proposée est susceptible de fournir un moyen efficace et simple pour l'analyse du comportement attendu d'une excavation souterraine et pourrait servir à l'estimation des besoins en matière de soutènement ainsi qu'au choix initial des genres de soutènement.

---

*Chercheur scientifique, Laboratoire de la mécanique des roches, Laboratoires de recherche minière, Centre canadien de la technologie des minéraux et de l'énergie (CANMET), Energie, Mines et Ressources Canada.

Il est possible de procéder à l'elaboration d'un projet de mise à jour des principes directeurs en matière de boulonnage en se fondant sur les résultats de la présente étude et sur d'autres renseignements disponibles. Des domaines d'investigation complémentaires sont signalés.

CONTENTS


| | Page |
|---|---|
| SUMMARY | i |
| RÉSUMÉ | ii |
| INTRODUCTION | 1 |
| INPUT DATA OF THE STUDY | 2 |
| Uniaxial Compressive Strength, $\sigma_c$, and Modulus of Elasticity, E | 3 |
| Poisson's Ratio, $\nu$ | 12 |
| Material Constants, m, s, $m_r$, $s_r$ | 13 |
| Unit Weight of Broken Rock Mass, $\sigma_r$, and In Situ Stress Magnitude, $p_o$ | 15 |
| Radius of Opening, $r_i$ | 16 |
| ROCK-SUPPORT INTERACTION ANALYSIS | 17 |
| Input Data | 17 |
| Rock Mass Strength | 18 |
| Calculation Steps | 20 |
| Support Requirements | 32 |
| RESULT OF PARAMETRIC ANALYSIS | 39 |
| Rock: Type A | 40 |
| Rock: Type B | 58 |
| Rock: Type C | 69 |
| Rock: Type D | 80 |
| Rock: Type E | 91 |
| DISCUSSION OF RESULTS | 102 |
| CONCLUSIONS AND RECOMMENDATIONS | 111 |
| REFERENCES | 112 |


TABLES


| No. | | |
|---|---|---|
| 1. | Lists of paired uniaxial compressive strength and elastic modulus values used in the analyses | 5 |
| 2. | List of material constant values used in the analyses | 15 |
| 3. | List of in situ stress magnitudes used in the analyses | 16 |
| 4. | List of radii considered by the analyses | 17 |
| 5. | Tabulated results, corresponding to the load-deformation curve of the drift at Level 2 in fair quality broken rock mass | 28 |

CONTENTS (cont'd)


| No. | | Page |
|---|---|---|
| 6. | Tabulated results, corresponding to the load-deformation curve of the drift at Level 2 in poor quality broken rock mass ..... | 28 |
| 7. | Tabulated results, corresponding to the load-deformation curve of the drifts at Level 3 ..... | 32 |
| 8. | Summary of calculations for drift at Level 2 in fair quality broken rock mass ..... | 33 |
| 9. | Summary of calculations for drift at Level 2 in poor quality broken rock mass ..... | 33 |
| 10. | Summary of calculations for drift with 3.0 m diameter at Level 3 ..... | 34 |
| 11. | Summary of calculations for drift with 6.0 m diameter at Level 3 ..... | 34 |
| 12. | Listing of selected values of variables for rock Type A ..... | 41 |
| 13. | Calculation and listing of $u_i/r_i$ values for rock Type A ..... | 42 |
| 14. | Calculation and listing of $p_{icr}/p_o$ values for rock Type A ..... | 44 |
| 15. | Calculation and listing of $p_{icr}/p_o$ values for rock Type A ..... | 45 |
| 16. | Listing of selected values of variables for rock Type B ..... | 58 |
| 17. | Calculation and listing of $u_i/r_i$ values for rock Type B ..... | 59 |
| 18. | Calculation and listing of $p_{icr}/p_o$ values for rock Type B ..... | 61 |
| 19. | Calculation and listing of $p_{icr}/p_o$ values for rock Type B ..... | 62 |
| 20. | Listing of selected values of variables for rock Type C ..... | 69 |
| 21. | Calculation and listing of $u_i/r_i$ values for rock Type C ..... | 70 |
| 22. | Calculation and listing of $p_{icr}/p_o$ values for rock Type C ..... | 72 |
| 23. | Calculation and listing of $p_{icr}/p_o$ values for rock Type C ..... | 73 |
| 24. | Listing of selected values of variables for rock Type D ..... | 80 |
| 25. | Calculation and listing of $u_i/r_i$ values for rock Type D ..... | 81 |
| 26. | Calculation and listing of $p_{icr}/p_o$ values for rock Type D ..... | 83 |
| 27. | Calculation and listing of $p_{icr}/p_o$ values for rock Type D ..... | 84 |
| 28. | Listing of selected values of variables for rock Type E ..... | 91 |
| 29. | Calculation and listing of $u_i/r_i$ values for rock Type E ..... | 92 |
| 30. | Calculation and listing of $p_{icr}/p_o$ values for rock Type E ..... | 94 |
| 31. | Calculation and listing of $p_{icr}/p_o$ values for rock Type E ..... | 95 |

CONTENTS (cont'd)

FIGURES


| No. | | Page |
|---|---|---|
| 1. | Uniaxial compressive strength versus modulus of elasticity for rock Type A | 6 |
| 2. | Uniaxial compressive strength versus modulus of elasticity for rock Type B | 7 |
| 3. | Uniaxial compressive strength versus modulus of elasticity for rock Type C | 8 |
| 4. | Uniaxial compressive strength versus modulus of elasticity for rock Type D | 9 |
| 5. | Uniaxial compressive strength versus modulus of elasticity for rock Type E | 10 |
| 6. | Uniaxial compresive strength versus modulus of elasticity for all rock types | 11 |
| 7. | Variation of rock mass strength with material constants | 21 |
| 8. | Load-deformation curves in dimensionless terms | 23 |
| 9. | Load-deformation curves in real terms | 36 |
| 10. | Selection of support system | 38 |
| 11. | Elastic rays of rock Type A | 43 |
| 12. | Load-deformation curves for rock Type A | 46 |
| 13. | Load-deformation curves for rock Type A | 47 |
| 14. | Load-deformation curves for rock Type A | 48 |
| 15. | Load-deformation curves for rock Type A | 49 |
| 16. | Load-deformation curves for rock Type A | 50 |
| 17. | Load-deformation curves for rock Type A | 51 |
| 18. | Load-deformation curves for rock Type A | 52 |
| 19. | Load-deformation curves for rock Type A | 53 |
| 20. | Extent of broken zones for rock Type A | 54 |
| 21. | Extent of broken zones for rock Type A | 55 |
| 22. | Extent of broken zones for rock Type A | 56 |
| 23. | Extent of broken zones for rock Type A | 57 |
| 24. | Elastic rays of rock Type B | 60 |
| 25. | Load-deformation curves for rock Type B | 63 |

CONTENTS (cont'd)


| No. | | Page |
|---|---|---|
| 26. | Load-deformation curves for rock Type B | 64 |
| 27. | Load-deformation curves for rock Type B | 65 |
| 28. | Load-deformation curves for rock Type B | 66 |
| 29. | Extent of broken zones for rock Type B | 67 |
| 30. | Extent of broken zones for rock Type B | 68 |
| 31. | Elastic rays of rock Type C | 71 |
| 32. | Load-deformation curves for rock Type C | 74 |
| 33. | Load-deformation curves for rock Type C | 75 |
| 34. | Load-deformation curves for rock Type C | 76 |
| 35. | Load-deformation curves for rock Type C | 77 |
| 36. | Extent of broken zones for rock Type C | 78 |
| 37. | Extent of broken zones for rock Type C | 79 |
| 38. | Elastic rays of rock Type D | 82 |
| 39. | Load-deformation curves for rock Type D | 85 |
| 40. | Load-deformation curves for rock Type D | 86 |
| 41. | Load-deformation curves for rock Type D | 87 |
| 42. | Load-deformation curves for rock Type D | 88 |
| 43. | Extent of broken zones for rock Type D | 89 |
| 44. | Extent of broken zones for rock Type D | 90 |
| 45. | Elastic rays of rock Type E | 93 |
| 46. | Load-deformation curves for rock Type E | 96 |
| 47. | Load-deformation curves for rock Type E | 97 |
| 48. | Load-deformation curves for rock Type E | 98 |
| 49. | Load-deformation curves for rock Type E | 99 |
| 50. | Extent of broken zones for rock Type E | 100 |
| 51. | Extent of broken zones for rock Type E | 101 |
| 52. | Critical stress and deformation of a rock mass and the expected stability behaviour | 105 |
| 53. | Variation of critical stresses and deformations for rock Type A | 109 |
| 54. | Variation of critical stresses and deformations for rock Types A and E | 110 |

# INTRODUCTION

The objective of the Material Properties and Support Systems Project during the present phase is to evaluate the effectiveness and limitations of the various underground support systems. In a subsequent phase the results of the investigations are to be integrated within ground control guidelines.

A previous study revealed that the existing information and knowledge are sufficient to define those factors which generally have major influence on the stability of underground openings and consequently on the requirements of support [1]. One must, however, be aware that the relationship between the variables probably never could be expressed by exact mathematical equations. Therefore, the design of a support system for an underground opening in rock will remain an art involving the application of practical knowledge and experience. Investigations involving laboratory tests, field measurements and analytical studies are essential. The obtained data, translated into understanding of the interplay between the influencing variables, will then be used for the continuous improvement of the art of support system design.

The result of the survey revealed that rock bolting is the most common artificial support system [1]. It is used to various extents in all of the mining method. For this reason rock bolting is being investigated with first order of priority.

The design of rock bolting requires to specify the system in terms of bolt type, diameter and length, bolt spacing, installation and inspection procedures, monitoring and quality control.

A comprehensive rock bolting design procedure, based on rock-support interaction analysis was developed by Hoek and Brown [2]. The analysis embraces all the essential factors of underground support design, therefore, it is suitable for rock bolting design in mines. However, the procedure is tailored to civil engineering design practice which might represent a drawback in gaining overall acceptance in mining engineering practice.

More familiar to the mining engineering design approach is the code of practice method. One of the codes frequently used by the mining industry has been developed within CANMET [3]. It describes, in the form of formulated rules, the procedures to be followed in selecting rock bolts, bolting patterns, and in monitoring various aspects of ground reactions, that are applicable to the majority of rock bolting cases. The problem is that the recommended procedures are based on the results of studies which were conducted

prior to 1970, as well as, on the understanding of relationships between the influencing variables as it prevailed at that time.

The recent rock-support interaction analysis method, beside including up-to-date measurement data, is based on the present and more advanced state of understanding and on the results of the latest technological and analytical developments.

It is, therefore, desirable to combine the above advantages in one package. The modified rock bolting guidelines will follow the design approach set by the code of practice method, but it will be improved by the latest data base and developments of the rock-support interaction analysis method.

The objective of the present study is to establish a technical data base required for the development of bolting guidelines for hard rocks. Therefore, based on the analytical procedure given by Hoek and Brown [2], the significance of the variables, with respect to the stability of underground openings, is to be determined by parametric analyses.

## INPUT DATA OF THE STUDY

The analysis requires the following input data:

$\sigma_c$ = uniaxial compressive strength of intact rock pieces;
$E$ = modulus of elasticity of original rock mass;
$\nu$ = Poisson's ratio of original rock mass;
$m$ and $s$ = material constants of original rock mass;
$m_r$ and $s_r$ = material constants of broken rock mass;
$\gamma_r$ = unit weigth of broken rock mass;
$p_o$ = in situ hydrostatic stress magnitude;
$r_i$ = radius of opening.

The outcome of the analysis is simultaneously affected by all the above variables. The significance of the variables is to be evaluated by a series of computations, using selected values of variables in systematic combinations.

## UNIAXIAL COMPRESSIVE STRENGTH, $\sigma_c$, AND MODULUS OF ELASTICITY, E

For purposes of this specific study only, it is assumed that for a group of rock types with similar behaviour, the elastic modulus, E, will increase linearly with increase of uniaxial compressive strength, $\sigma_c$.

The rock types are grouped according to the group descriptions of Hoek and Brown [2]. Rock strength and deformation data pairs were collected from various available sources [2,4,5,6].

The analysed data pairs correspond to the following groups of rock types:

Type A - Carbonate rocks with well developed crystal cleavage

CARBONATE
CHALK
DOLOMITE
LIMESTONE
MARBLE

Type B - Lithifield argillaceous rocks

ARGILLITE
CLAYSTONE
MARLSTONE
MUDSTONE
SHALE
SILTSTONE
SLATE
TUFF

Type C - Arenaceous rocks with strong crystals and poorly developed crystal cleavage

CHERT
GRAYWACKE
QUARTZITE
SANDSTONE

Type D - Fine grained polymineralllic igneous crystalline rocks

ACTINOLITE SCHIST
ANDESITE
BASALT
BASIC INTRUSION
CHLORITE SCHIST
DACITE
DIABASE
DOLERITE
GREENSTONE
PERIDOTITE
PHYLLITE
RHYOLITE
SCHIST
SCHISTOSE GNEISS
TREMOLITE SCHIST

Type E - Coarse grained polymineralllic igneous and metamorphic crystalline rocks

AMPHIBOLITE
ANORTHOSITE
DIORITE
ECLOGITE
GABBRO
GNEISS
GRANITE
GRANODIORITE
GRANULITE
MIGMATITE
MONOZONITE
NORITE
PYROXENITE
QUARTZ DIORITE
SYENITE
TONALITE
TOURMALINE GRANITE

A total number of 861 data points were analysed with the following distribution:

Type A: 162 data points
Type B: 162 data points
Type C: 190 data points
Type D: 141 data points
Type E: 206 data points

The assumed linear relationships between uniaxial compressive strength and modulus of elasticity for each rock group were obtained by regression analysis. The results are shown in Figs. 1 to 5, where the confidence bands, as defined by one standard deviation, are also indicated.

The arrived linear relationships for the various rock types, together with the linear relationship of all data points, are plotted in Fig. 6. The analysed data points resulted the lowest and highest elastic modulus values for Type C and Type A, respectively. The elastic modulus for Type C rocks is about 22% lower and for Type A rocks is about 21% higher than the overall modulus of all data points. The range of uniaxial compressive strength and of elastic modulus is the narrowest and widest for Type A and Type E rocks, respectively.

The paired $\sigma_c$ and E values selected for input data of the parametric analyses are indicated by circles in Figs. 1 to 5. These data pairs are also listed in Table 1.

Table 1 - Lists of paired uniaxial compressive strength and elastic modulus values used in the analyses

| Rock Type | | | | | | | | | |
|---|---|---|---|---|---|---|---|---|---|
| A | | B | | C | | D | | E | |
| $\sigma_c$ MPa | E, GPA | $\sigma_c$ MPa | E, GPa | $\sigma_c$ MPa | E, GPa | $\sigma_c$ MPa | E, GPa | $\sigma_c$ MPa | E, GPa |
| 45 | 31 | 50 | 22 | 60 | 18 | 90 | 41 | 100 | 41 |
| 100 | 45 | 130 | 43 | 165 | 40 | 195 | 62 | 200 | 58 |
| 150 | 57 | 210 | 65 | 270 | 63 | 300 | 84 | 300 | 76 |
| 200 | 69 | 300 | 90 | 375 | 86 | 400 | 104 | 375 | 88 |
| | | | | | | | | 450 | 101 |

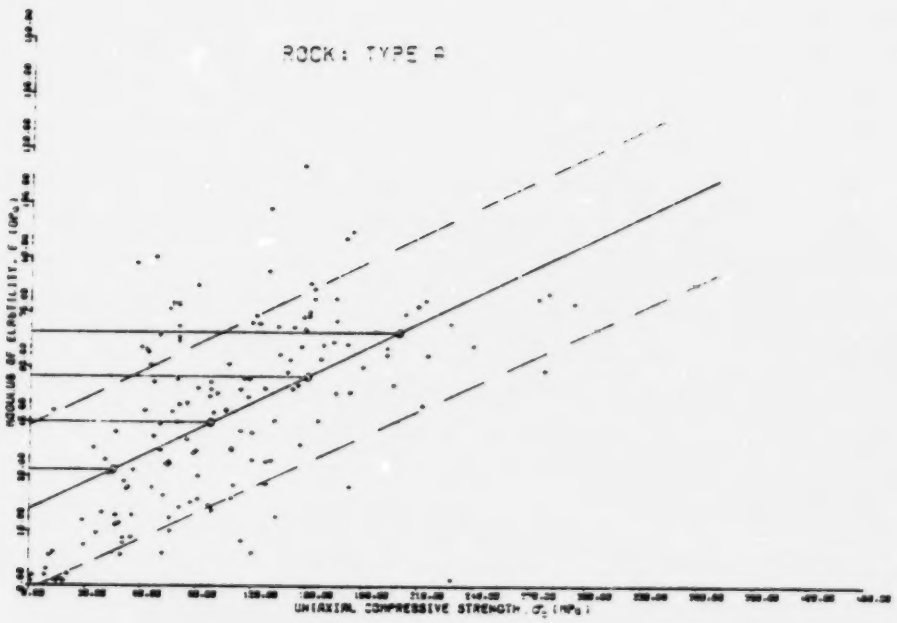


Fig. 1 - Uniaxial compressive strength versus modulus of elasticity for rock Type A

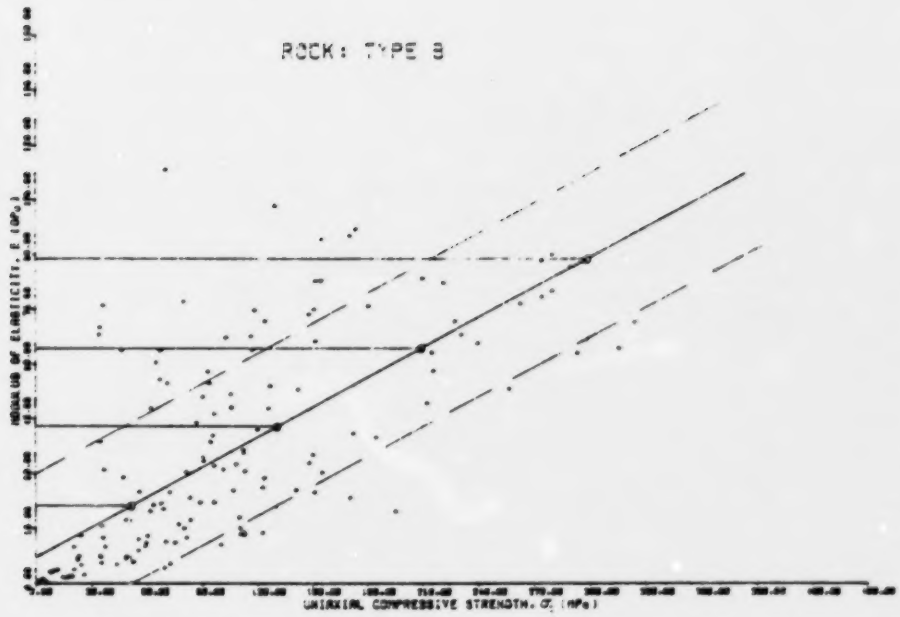


Fig. 2 - Uniaxial compressive strength versus modulus of elasticity for rock Type B

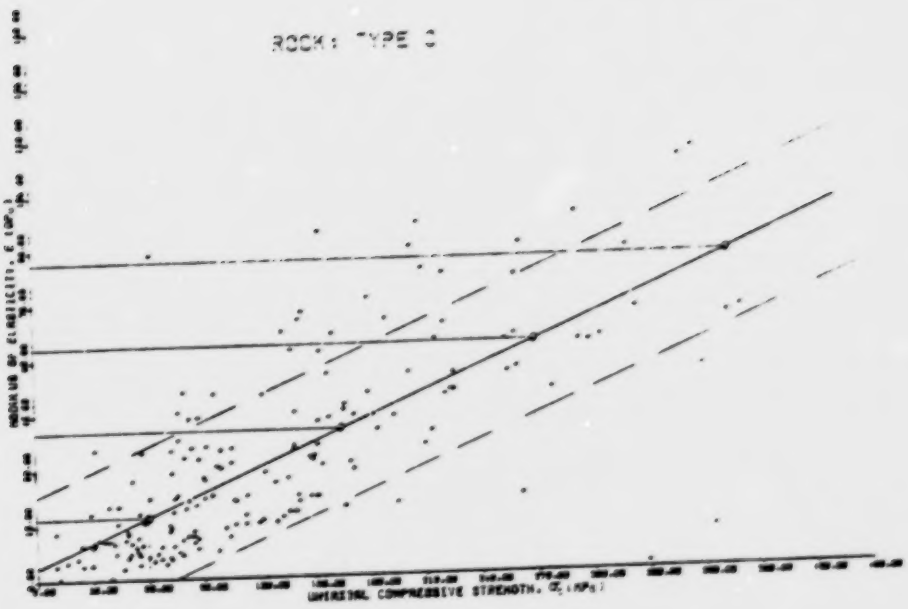


Fig. 3 - Uniaxial compressive strength versus modulus of elasticity for rock Type C

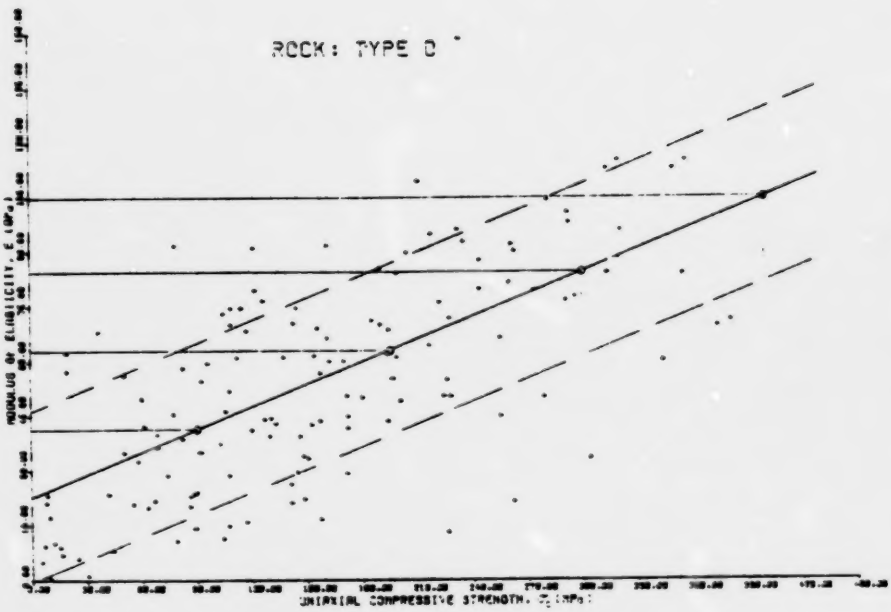


Fig. 4 - Uniaxial compressive strength versus modulus of elasticity for rock Type D

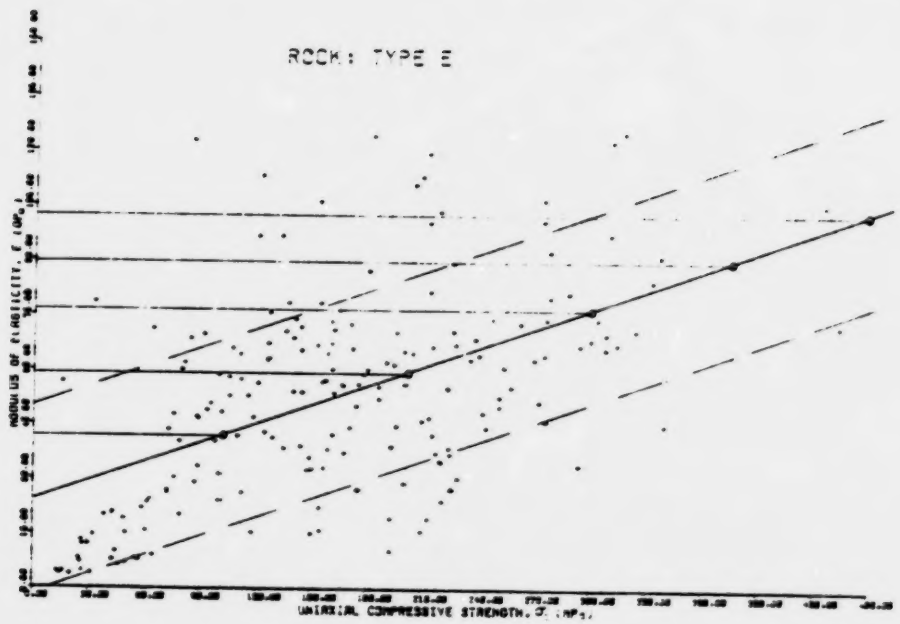


Fig. 5 - Uniaxial compressive strength versus modulus of elasticity for rock Type E

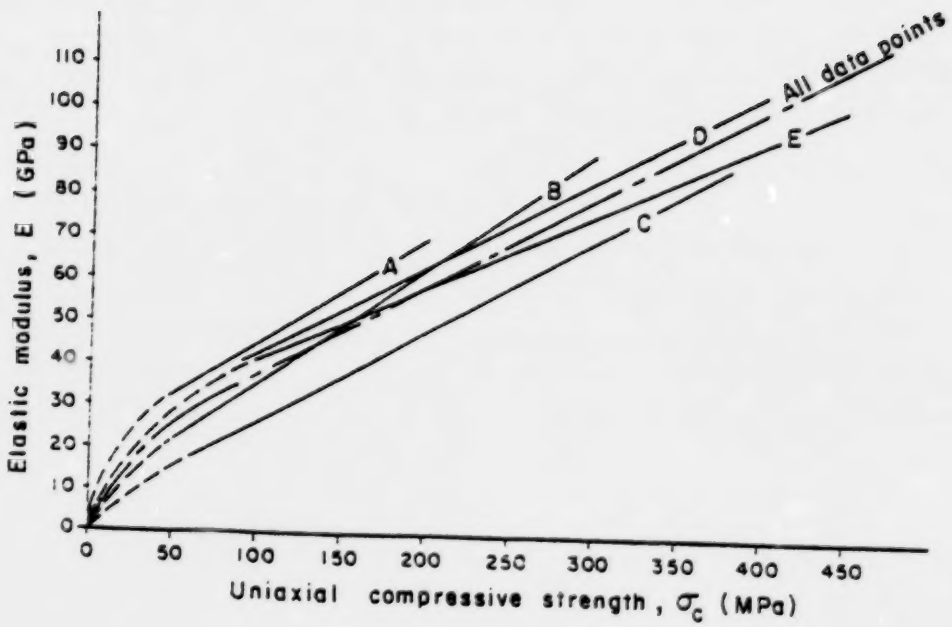


Fig. 6 - Uniaxial compressive strength versus modulus of elasticity for all rock types

POISSON'S RATIO, $\nu$

The rock-support interaction analysis requires the Poisson's ratio of the original rock mass. However, the Poisson's ratio, even in the laboratory, can be determined only for intact rock specimens. Average values for rock mass may be deduced by back-calculations from field deformation measurements.

The range of values recommended by Hoek and Brown is: 0.15 - 0.30. The value of 0.25 is used for the entire study because the Poisson's ratio has only limited effect on the outcome of the analysis.

The Poisson's ratio appears in the following equations of the analysis:

$$\frac{u_i}{r_i} = \frac{(1 + \nu)}{E} (p_o - p_i) \tag{5}$$

and

$$\frac{u_e}{r_e} = \frac{(1 + \nu)}{E} M \sigma_c \tag{6}$$

The rearranged forms of equations (5) and (6) are:

$$\frac{Eu_i}{(p_o - p_i)r_i} - 1 = \nu$$

and

$$\frac{Eu_e}{M \sigma_c r_e} - 1 = \nu$$

The sensitivity of analysis with respect to the Poisson's ratio, $\nu$, can be evaluated by comparing the solution with $\nu = 0.25$ to the solutions corresponding to the lower and the upper limits of the recommended range.

Therefore, if $\nu = 0.25$, it follows that:

$$\frac{Eu_i}{(p_o - p_i)r_i} = \frac{Eu_e}{M \sigma_c r_e} = 1.25$$

if $\nu = 0.15$, it follows that:

$$\frac{Eu_i}{(p_o - p_i)r_i} = \frac{Eu_e}{M\,\sigma_c\,r_e} = 1.15$$

if $\nu = 0.3$, it follows that:

$$\frac{Eu_i}{(p_o - p_i)r_i} = \frac{Eu_e}{M\,\sigma_c\,r_e} = 1.3$$

Consequently, should the actual value of Poisson's ratio be 0.15, then by using the value of $\nu = 0.25$ a possible error of 1.15/1.25 = 0.92, i.e., 8% could occur. The possible error for the upper limit is: 1.3/1.25 = 1.04, i.e., 4%. However, in assigning values to the variables in the expression of $Eu_i/(P_o - p_i)r_i$ or $Eu_e/M\,\sigma_c\,r_e$ a much larger error than 4 or 8 per cent can be made. Therefore, it can be concluded that the Poisson's ratio has only limited effect on the outcome of the analysis.

From equations (5) and (6) it is apparent that the Poisson's ratio has a magnifying effect in calculating the radial deformation, u. To compare the results of the various analysed cases a higher value of $\nu$ offers some advantages. Poisson's ratio of 0.25 is selected with the reasoning that it represents an intermediate value of the upper range.

MATERIAL CONSTANTS, m, s, $m_r$, $s_r$

For each rock type the following rock mass quality designations are considered:

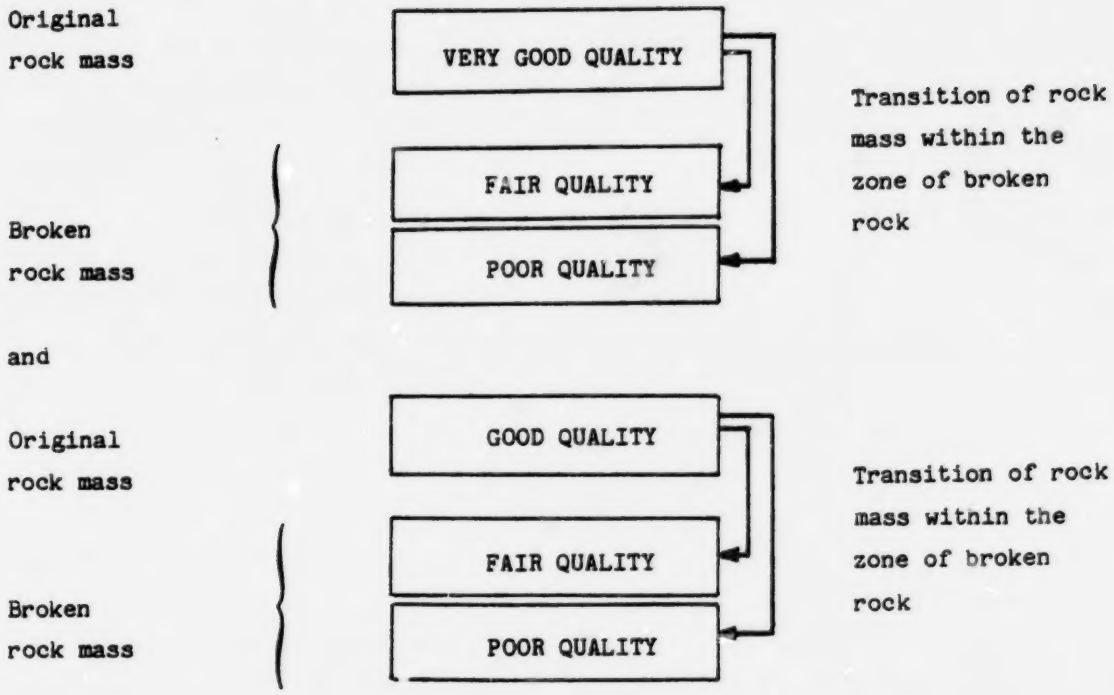


The approximate material constants, as defined by Hoek and Brown [2], of the various rock mass qualities and rock types are listed in Table 2.

Table 2 - List of material constants used in the analyses

| Rock type | Rock mass quality | | | | | | | |
|---|---|---|---|---|---|---|---|---|
| | Very good | | Good | | Fair | | Poor | |
| | m | s | m | s | $m_r$ | $s_r$ | $m_r$ | $s_r$ |
| A | 3.5 | 0.1 | 0.7 | 0.004 | 0.14 | 0.0001 | 0.04 | 0.00001 |
| B | 5.0 | 0.1 | 1.0 | 0.004 | 0.20 | 0.0001 | 0.05 | 0.00001 |
| C | 7.5 | 0.1 | 1.5 | 0.004 | 0.30 | 0.0001 | 0.08 | 0.00001 |
| D | 8.5 | 0.1 | 1.7 | 0.004 | 0.34 | 0.0001 | 0.09 | 0.00001 |
| E | 12.5 | 0.1 | 2.5 | 0.004 | 0.50 | 0.0001 | 0.13 | 0.00001 |

UNIT WEIGHT OF BROKEN ROCK MASS, $\gamma_r$, AND IN SITU STRESS MAGINITUDE, $p_o$

The two terms are interrelated, because of the assumed equal horizontal and vertical in situ stresses. The in situ stress in this case is the product of the vertical depth and the unit weight of broken rock mass.

The unit weight of broken rock mass depends on the rock type and the degree of loosening. For the analyses the following values are used:

Rock type: A and B $\quad \gamma_r = 0.025$ MN/m$^3$

Rock type: C $\quad \gamma_r = 0.0275$ MN/m$^3$

Rock type: D and E $\quad \gamma_r = 0.03$ MN/m$^3$

Because of the wide range of depths being used in the study any possible variations in unit weights became insignificant.

The minimum depth considered by the analyses is 400 m. The maximum depth is 2000 m. In addition, the possibility of highly stressed region is being accounted for by doubling the hydrostatic stress field calculated for the 2000 m depth.

The input data with respect to the in situ stress magnitudes are listed in Table 3.

Table 3 - List of in situ stress magnitudes used in the analyses

| Depth, (m) | In situ stress, po (MPa) | | |
|---|---|---|---|
| | Rock type: A and B | Rock type: C | Rock type: D and E |
| 400 | 10 | 11 | 12 |
| 700 | 17.5 | 19.2 | 21 |
| 1250 | 31.2 | 34.4 | 37.5 |
| 1750 | 43.8 | 48.1 | 52.5 |
| 2000 | 50 | 55 | 60 |
| Highly stressed region | 100 | 110 | 120 |

## RADIUS OF OPENING, $r_i$

The radii of the openings of the study correspond to the commonly used mining drift and stope sizes. The load-deformation curves are calculated in dimensionless terms, therefore, the load-deformation characteristics of a rock mass are independent of the radius. The radius, however, becomes an important variable when the support requirements are being determined.

The radii considered by the study are listed in Table 4.

Table 4 - List of radii considered by the analyses

| Common sizes of mine openings | Metric equivalent |
|---|---|
| 8 ft drift | $r_i$ = 1.5 m |
| 20 ft drift | $r_i$ = 3 m |
| 40 ft stope | $r_i$ = 6 m |
| 60 ft stope | $r_i$ = 9 m |
| 100 ft stope | $r_i$ = 15 m |

## ROCK-SUPPORT INTERACTION ANALYSIS

The procedure of rock-support interaction analysis is to be discussed in connection with a detailed example.

In this example the requirement is to provide a preliminary analysis on the stability and the support requirement of the haulage drifts to be excavated at various depths within the limestone footwall of a lead-zinc orebody.

The haulage drifts to be approximated by circular cross-section and the vertical and horizontal stresses are assumed to be equal.

The drifts to be excavated with 3.0 m diameter at both Level 1 (400 m depth) and Level 2 (700 m depth). For Level 3 (1250 m depth) the mining plan calls for two drifts, one with 3.0 m diameter the other with 6.0 m diameter.

The rock mass can be classified as very good quality. However, the previous mining experienced some supporting difficulties in the vicinity of the orebody at 700 m depth (Level 2). The uniaxial compressive strength of intact rock is 100 ± 12 MPa.

### INPUT DATA

To the described problem the assumed input data of the analysis are as follows:

| | |
|---|---|
| Uniaxial compressive strength of intact rock | $\sigma_c$ = 100 MPa |
| Modulus of elasticity of rock mass | E = 45 GPa |
| Poisson's ratio of rock mass | $\nu$ = 0.25 |
| Material constants for original rock mass | m = 3.5<br>s = 0.1 |
| Material constants for broken rock mass in general | $m_r$ = 0.14<br>$s_r$ = 0.0001 |
| Material constants for broken rock mass at Level 2 near orebody | $m_r$ = 0.04<br>$s_r$ = 0.00001 |
| Unit weight of broken rock | $\gamma_r$ = 0.025 MN/m$^3$ |
| In situ stress magnitudes | |
| at Level 1 (400 m) | $p_o$ = 10 MPa |
| at Level 2 (700 m) | $p_o$ = 17.5 MPa |
| at Level 3 (1250 m) | $p_o$ = 31.2 MPa |
| Drift radius | |
| at Level 1 and Level 2 | $r_i$ = 1.5 m |
| at Level 3 | $r_i$ = 1.5 m and<br>$r_i$ = 3.0 m |

## ROCK MASS STRENGTH

Based on their experience, Hoek and Brown have developed the following empirical relationship between the principal stresses associated with the failure of rock [2]:

$$\sigma_1 = \sigma_3 + \sqrt{m \sigma_c \sigma_3 + s \sigma_c^2} \qquad (1)$$

where $\sigma_1$ = the major principal stress at failure of rock material specimen,

$\sigma_3$ = the minor principal stress applied to the specimen,

$\sigma_c$ = the uniaxial compressive strength of the intact rock material in the specimen,

m,s = material constants, which depend upon the properties of the rock and upon the extent to which it has been broken before being subjected to the stresses $\sigma_1$ and $\sigma_3$

If equation (1) is divided by the uniaxial compressive strength of intact rock, the following dimensionless relationship is obtained:

$$\sigma_{1n} = \sigma_{3n} + \sqrt{m\,\sigma_{3n} + s} \qquad (2)$$

where $\sigma_{1n}$ = the normalized major principal stress at failure, i.e., $\sigma_1/\sigma_c$,

$\sigma_{3n}$ = the normalized minor principal stress, i.e., $\sigma_3/\sigma_c$.

The determination of rock mass constants, m and s, for a specific support design problem should normally be based on the test results of the involved rock. The procedures of testing and data analysis are given by Hoek and Brown [2]. For the purpose of preliminary analyses they recommend to use the rock mass constant values found to be typical for those rock types which belong to the same group (identified in this study by letter from A to E). Within each group the rock mass constants are given for five rock mass qualities, ranging from very good to very poor, in the form of equation (2).

In this example the original rock mass is classified as very good quality. For a limestone very good quality rock mass the approximate equation is:

$$\sigma_{1n} = \sigma_{3n} + \sqrt{3.5\,\sigma_{3n} + 0.1} \qquad (2a)$$

where, 3.5 and 0.1 are the rock mass constants of m and s, respectively.

Within the failure zone the broken rock mass is being classified as fair quality, with material constants of $m_r = 0.14$ and $s_r = 0.0001$.

The approximate equation therefore:

$$\sigma_{1n} = \sigma_{3n} + \sqrt{0.14\,\sigma_{3n} + 0.0001} \qquad (2b)$$

The supporting difficulties in the vicinity of orebody at Level 2, experienced in the past, is being accounted for by assuming a poor quality broken rock mass within the failure zone, with the material constants of $m_r$ = 0.04 and $s_r$ = 0.00001. The approximate equation, defining the principal stress relationship, is:

$$\sigma_{1n} = \sigma_{3n} + \sqrt{0.04\,\sigma_{3n} + 0.00001} \qquad (2c)$$

Solely to demonstrate the effect of material constants on rock mass strength, the relationships expressed by equations (2a), (2b) and (2c) are graphically presented in Fig. 7. The relationships in terms of normalized principal stresses are shown in Fig. 7a. In Fig. 7b the Mohr's strength envelopes are given, which are a more familiar representation of the relationship between failure stresses.

## CALCULATION STEPS

### Level 1 (400 m depth)

The input data are:

$\sigma_c$ = 100 MPa
E = 45 GPa
$\nu$ = 0.25
m = 3.5
s = 0.1
$m_r$ = 0.14
$s_r$ = 0.0001
$p_o$ = 10 MPa
$r_i$ = 1.5 m

The theoretical solution of rock-support interaction analysis, derived by Ladanyi (7), concludes that the zone of broken rock around a circular opening will exist only if the internal support pressure $p_i$ is lower than the critical value given by:

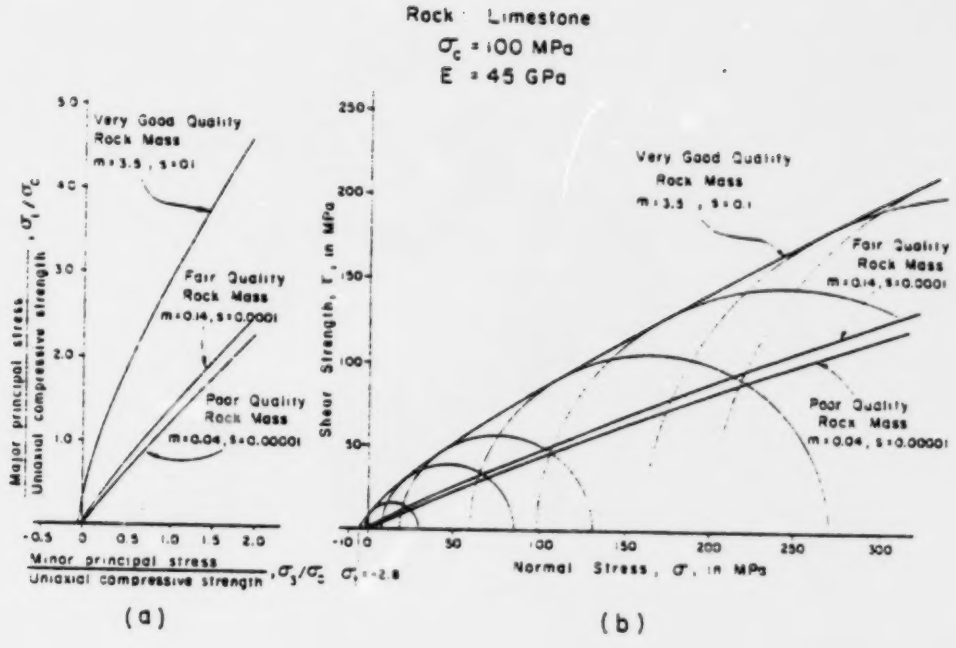


Fig. 7 - Variation of rock mass strength with material constants; (a) normalized principal stresses, (b) Mohr's strength envelopes

$$p_i < p_{icr} \quad p_o - M\sigma_c \tag{3}$$

where,
$$M = \frac{1}{2}\left[\left(\frac{m}{4}\right)^2 + m\, p_o/\sigma_c + s\right]^{1/2} - \frac{m}{8} \tag{4}$$

If $p_{icr} < p_i$, the rock mass surrounding the opening behaves elastically.

For the input data the calculated values are:

$$M = \frac{1}{2}\left[\left(\frac{3.5}{4}\right)^2 + \frac{3.5 \times 10}{100} + 0.1\right]^{1/2} - \frac{3.5}{8} = 0.113$$

$$p_{icr} = 10 - 0.113 \times 100 = -1.13 \text{ MPa}$$

The negative value of $p_{icr}$ indicates that the in situ stress of 10 MPa causes only elastic deformation within the rock mass.

The elastic deformation around the opening is calculated by the following equation:

$$\frac{u_i}{r_i} = \frac{(1 + \nu)}{E}(p_o - p_i) \tag{5}$$

where, $u_i$ is the radial deformation of a circular opening.

The radial deformation, $u_i$, can be calculated by equation (5) for any arbitrary value of $p_i$, within the range of $p_o \geq p_i \geq 0$. However, for both, the calculation and the presentation of calculated results, the load-deformation curve method is used. The load-deformation curves, shown in Fig. 8, are plotted in dimensionless terms, with the abscissa of $u_i/r_i$ and ordinate of $p_i/p_o$.

As shown in Fig. 8 the load-deformation curve of the drift to be excavated at Level 1 is a straight line. This elastic ray begins at $p_i/p_o = 1$ and intersects the abscissa at the point which is obtained by placing $p_i = 0$ value into equation (5).

In the case of our example:

$$\frac{u_i}{r_i} = \frac{1 + 0.25}{45{,}000}(10 - 0) = 2.78 \times 10^{-4}$$

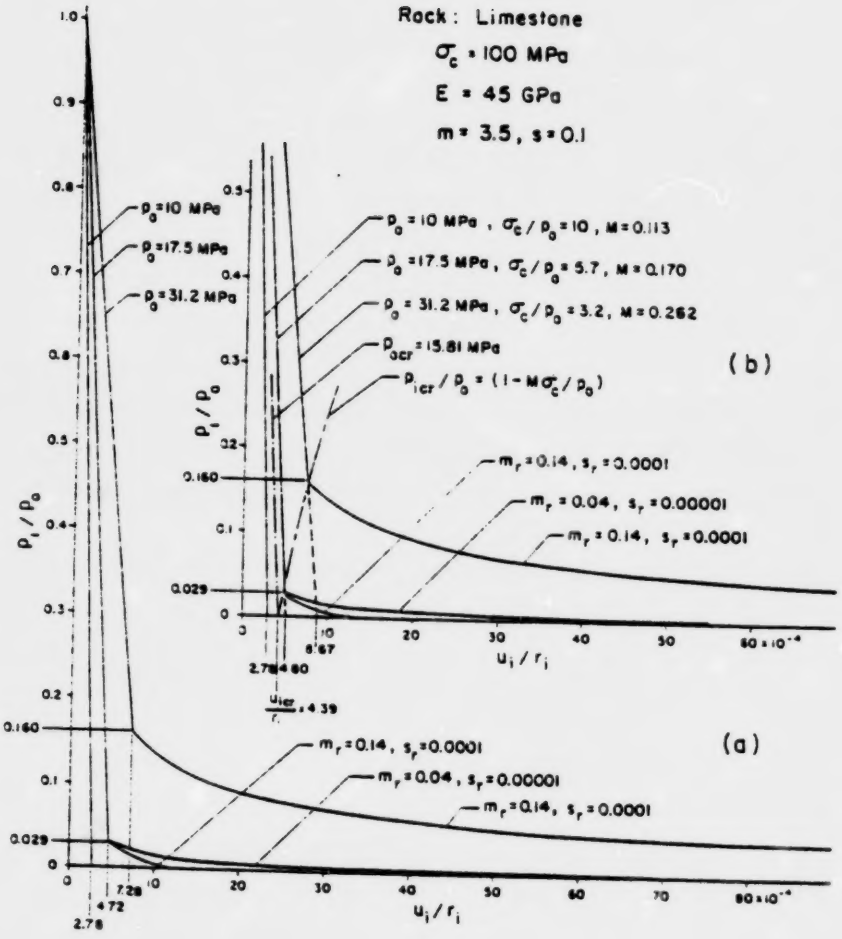
Rock : Limestone
$\sigma_c$ = 100 MPa
E = 45 GPa
m = 3.5, s = 0.1
$p_0$ = 10 MPa
$p_0$ = 17.5 MPa
$p_0$ = 31.2 MPa
$p_0$ = 10 MPa , $\sigma_c / p_0$ = 10 , M = 0.113
$p_0$ = 17.5 MPa , $\sigma_c / p_0$ = 5.7 , M = 0.170
$p_0$ = 31.2 MPa , $\sigma_c / p_0$ = 3.2 , M = 0.262
$p_{0cr}$ = 15.81 MPa
$p_{icr} / p_0 = (1 - M\sigma_c / p_0)$
(b)
(a)
$m_r$ = 0.14 , $s_r$ = 0.0001
$m_r$ = 0.04 , $s_r$ = 0.00001
$m_r$ = 0.14 , $s_r$ = 0.0001
$p_i / p_0$
$u_i / r_i$
$u_{icr} / r_i$ = 4.39
2.78
4.72
7.29
8.67
4.80

Fig. 8 - Load-deformation curves in dimensionless terms

The straight line load-deformation curves means that the entire rock mass, with the strength and deformation properties assigned through the input data and under the assumed in situ stress of $p_o$ = 10 MPa, will behave elastically. Consequently, no zone of broken rock will develop around the drift under these circumstances.

Level 2 (700 m depth)

The input data are:

$\sigma_c$ = 100 MPa
E = 45 GPa
$\nu$ = 0.25
m = 3.5
s = 0.1
$m_r$ = 0.14, $s_r$ = 0.0001 — away from orebody
$m_r$ = 0.04, $s_r$ = 0.00001 — near to orebody
$p_o$ = 17.5 MPa
$r_i$ = 1.5 m

The initial steps are the same as they were for Level 1. Therefore:

$$M = \frac{1}{2}\left[\left(\frac{3.5}{4}\right)^2 + \frac{3.5 \times 17.5}{100} + 0.1\right]^{1/2} - \frac{3.5}{8} = 0.170$$

$$p_{icr} = 17.5 - 0.170 \times 100 = 0.5 \text{ MPa}$$

Now, the positive value of $p_{icr}$ indicates that under the in situ stress of $p_o$ = 17.5 MPa a zone of broken rock will develop around the drift. The transition point, between the elastic and plastic states, on the load-deformation curve can be found by the following modified form of equation (3):

$$p_{icr}/p_o = 1 - M\,\sigma_c/p_o \qquad (3a)$$

The value in our case is:

$$p_{icr}/p_o = 1 - 0.170 \times 100/17.5 = 0.029$$

The $u_i/r_i$ radial deformation ratio, corresponding to this $p_{icr}/p_o$ stress ratio, is calculated by equation (5a):

$$\frac{u_i}{r_i} = \frac{1 + \nu}{E} (p_o - p_{icr}) \qquad (5a)$$

which is:

$$\frac{u_i}{r_i} = \frac{1 + 0.25}{45{,}000} (17.5 - 0.5) = 4.72 \times 10^{-4}$$

The transition point with the coordinates of ($4.72 \times 10^{-4}$, 0.029) is plotted in Fig. 8a. For the pressure ratios of $p_i/p_o > p_{icr}/p_o = 0.029$ the rock mass is in elastic state, therefore, the corresponding load-deformation relationship is linear. The linear portion of the load-deformation curve is drawn by connecting the points of $p_{icr}/p_o = 0.029$ and $p_i/p_o = 1.0$. For the pressure ratios of $p_i/p_o < p_{icr}/p_o = 0.029$ the behaviour of rock mass is plastic, represented by the curved-line portion of the load-deformation curves.

A somewhat different method of plotting is shown in Fig. 8b. The elastic ray, corresponding to 17.5 MPa in situ stress, intersects the horizontal axis at:

$$\frac{u_i}{r_i} = \frac{1 + 0.25}{45{,}000} (17.5 - 0) = 4.86 \times 10^{-4}$$

Then, the transition point is located on this elastic ray at $p_i/p_o = 0.029$.

The transition point signifies the boundary between the elastic and plastic (i.e., zone of broken rock) rock mass. Consequently, the $u_i/r_i = 4.72 \times 10^{-4}$ value, corresponding to the critical internal pressure of $p_{icr} = 0.5$ MPa, should be identical with the value calculated by the following equation:

$$\frac{u_e}{r_e} = \frac{(1 + \nu)}{E} M \sigma_c \qquad (6)$$

where, $u_e$ = radial displacement of the elastic boundary,

$r_e$ = radius of the broken zone

The substitution into equation (6) will indeed yield the same result, that is:

$$\frac{u_e}{r_e} = \frac{1 + 0.25}{45{,}000}\, 0.170 \times 100 = 4.72 \times 10^{-4}$$

The points of the curved-line portion of load-deformation curves, for any desired $p_i/p_o < 0.029$ values, are calculated by the steps of calculation sequence as had been defined by Hoek and Brown [2].

In our example the analysis for Level 2 (700 m depth) must consider two different broken rock mass qualities. Away from the orebody the broken rock mass is assumed to be fair quality with the rock mass constants of $m_r$ = 0.14 and $s_r$ = 0.0001. While, the broken rock mass near to the orebody is designated as poor quality rock mass, with $m_r$ = 0.04 and $s_r$ = 0.00001 rock mass constants values.

These two rock mass quality designations will result in two load-deformation curves, both originate from the common transition point. The following detailed calculation corresponds to the load-deformation curve which defines the rock-support interaction for the fair quality broken rock mass.

$$D = \frac{-m}{m + 4\left[m/\sigma_c(p_o - M\,\sigma_c) + s\right]^{1/2}} \tag{7}$$

$$D = \frac{-3.5}{3.5 + 4\left[3.5/100(17.5 - 0.17 \times 100) + 0.1\right]^{1/2}} = -0.719$$

$$N = 2\left[\frac{p_o - M\,\sigma_c}{m_r\,\sigma_c} + \frac{s_r}{m_r^2}\right]^{1/2} \tag{8}$$

$$N = 2\left[\frac{17.5 - 0.170 \times 100}{0.14 \times 100} + \frac{0.0001}{0.14^2}\right]^{1/2} = 0.404$$

Let the first point of calculation be $p_i/p_o = 0.025$, therefore:

$$p_i = 0.025 \times p_o = 0.025 \times 17.5 = 0.438 \text{ MPa}$$

$$\frac{r_e}{r_i} = e^{N - 2\left(\frac{p_i}{m_r \sigma_c} + \frac{s_r}{m_r^2}\right)^{1/2}} \tag{9}$$

$$\frac{r_e}{r_i} = e^{0.404 - 2\left(\frac{0.438}{0.14 \times 100} + \frac{0.0001}{0.14^2}\right)^{1/2}} = 1.022$$

since,

$$\frac{r_e}{r_i} = 1.022 < \sqrt{3}$$

then

$$R = 2D \ln r_e/r_i \tag{10a}$$

$$R = 2(-0.719) \ln 1.022 = -0.031$$

The required two intermediate values are calculated by:

$$e_{av} = \frac{2\left(u_{e/r_e}\right)\left(r_{e/r_i}\right)^2}{\left[\left(r_e/r_i\right)^2 - 1\right](1 + 1/R)} \tag{11}$$

$$e_{av} = \frac{2(4.72 \times 10^{-4})\ (1.022)^2}{\left[(1.022)^2 - 1\right]\ (1 - 1/0.031)} = -7.09 \times 10^{-4}$$

and

$$A = (2\ u_e/r_e - e_{av})\ (r_e/r_i)^2 \tag{12}$$

$$A = (2 \times 4.72 \times 10^{-4} + 7.09 \times 10^{-4})\ (1.022)^2 = 17.27 \times 10^{-4}$$

Finally,

$$\frac{u_i}{r_i} = 1 - \left[\frac{1 - e_{av}}{1 + A}\right]^{1/2} \tag{13}$$

$$\frac{u_i}{r_i} = 1 - \left[\frac{1 + 7.09 \times 10^{-4}}{1 + 17.27 \times 10^{-4}}\right]^{1/2} = 5.08 \times 10^{-4}$$

The similar calculation procedure has been followed for the other selected $p_i/p_o$ values. The calculation results are tabulated in Table 5.

Table 5 - Tabulated results, corresponding to the load-deformation curve of the drift at Level 2 in fair quality broken rock mass

| $p_i/p_o$ | $p_i$ | $r_e/r_i$ | R | $e_{av} \times 10^{-4}$ | $A \times 10^{-4}$ | $u_i/r_i \times 10^{-4}$ |
|---|---|---|---|---|---|---|
| 0.029 | 0.500 | 1.000 | | | | 4.72 |
| 0.025 | 0.438 | 1.022 | -0.031 | -7.09 | 17.27 | 5.08 |
| 0.020 | 0.350 | 1.059 | -0.082 | -7.79 | 19.32 | 5.76 |
| 0.015 | 0.263 | 1.100 | -0.137 | -8.63 | 21.87 | 6.61 |
| 0.010 | 0.175 | 1.149 | -0.200 | -9.73 | 25.31 | 7.77 |
| 0.005 | 0.088 | 1.210 | -0.274 | -11.24 | 30.28 | 9.49 |
| 0 | 0 | 1.298 | -0.375 | -13.93 | 39.68 | 12.68 |

The $u_i/r_i$ and $p_i/p_o$ coordinates define the load-deformation curve shown in Figs. 8a and 8b by the lower curve, originating from the common transition point of $p_i/P_o = 0.029$.

The coordinates of the points of the curved-line portion for the drift in poor quality broken rock mass, were calculated by the previously described procedure. Without giving the details, the results of these calculations are summarized in Table 6.

Table 6 - Tabulated results, corresponding to the load-deformation curve of the drift at Level 2 in poor quality broken rock mass

| $p_i/p_o$ | $p_i$ | $r_e/r_i$ | R | $e_{av} \times 10^{-4}$ | $A \times 10^{-4}$ | $u_i/r_i \times 10^{-4}$ |
|---|---|---|---|---|---|---|
| 0.029 | 0.500 | 1.000 | | | | |
| 0.025 | 0.438 | 1.046 | -0.065 | -7.64 | 18.69 | 5.52 |
| 0.020 | 0.350 | 1.119 | -0.162 | -9.07 | 23.18 | 7.04 |
| 0.015 | 0.263 | 1.207 | -0.271 | -11.19 | 30.05 | 9.41 |
| 0.010 | 0.175 | 1.320 | -0.399 | -14.72 | 42.10 | 13.64 |
| 0.005 | 0.088 | 1.475 | -0.559 | -22.13 | 68.68 | 23.14 |
| 0 | 0 | 1.763 | -0.791 | -52.72 | 193.20 | 69.15 |

Note that for the ratio of $p_i/p_o = 0$ the value of $r_e/r_i > \sqrt{3}$, therefore, to calculate R the following equation is used:

$$R = 1.1\ D \tag{10b}$$

which is in our case:

$$R = -1.1 \times 0.719 = -0.791$$

The upper curve, in Figs. 8a and 8b, originating from the common transition point, represents the load-deformation relationship of the drift to be excavated at Level 2 within the poor quality broken rock mass.

Level 3 (1250 m depth)

The input data are:

$\sigma_c$ = 100 MPa
E = 45 GPa
$\nu$ = 0.25
m = 3.5
s = 0.1
$m_r$ = 0.14
$s_r$ = 0.0001
$p_o$ = 31.2 MPa
$r_i$ = 1.5 m and 3.0 m

The calculation steps are as follows:

$$M = \frac{1}{2}\left[\left(\frac{3.5}{4}\right)^2 + \frac{3.5 \times 31.2}{100} + 0.1\right]^{1/2} - \frac{3.5}{8} = 0.262$$

$$p_{icr} = 31.2 - 0.262 \times 100 = 5.0 \text{ MPa}$$

Due to the larger in situ stress, the critical pressure, $p_{icr}$, is much larger than at Level 2. The larger critical internal pressure signifies a thicker zone of broken rock around the drift.

The ordinate of the transition point is:

$$p_{icr}/p_o = 1 - 0.262 \times 100/31.2 = 0.160$$

and its abscissa is:

$$\frac{u_i}{r_i} = \frac{1 + 0.25}{45,000} (31.2 - 5.0) = 7.28 \times 10^{-4}$$

With these coordinates the transition point is plotted in Fig. 8a. It defines the end point of the elastic range of load-deformation curve.

The second method to locate the transition point is shown in Fig. 8b. Although it has already been described, some of the details will be repeated because of the important role of transition points within the overall analysis.

The ray of linear elastic deformation originates from the point with (0,1.0) coordinates. It intersects the horizontal axis, i.e., $p_i/p_o = 0$, at:

$$\frac{u_i}{r_i} = \frac{1 + 0.25}{45,000} (31.2 - 0) = 8.67 \times 10^{-4}$$

Then, the transition point is located on this elastic ray with the ordinate of $p_{icr}/p_o = 0.160$.

The transition points are, as shown in Fig. 8b, on a curved line which is being called as transition curve. The transition curve is defined by equation (3a).

The origin of the transition curve is defined by the following equations:

$$p_{ocr} = \left(\frac{s\ \sigma_c^2}{4}\right)^{1/2} \tag{14}$$

and then

$$\frac{u_{icr}}{r_i} = \frac{1 + \nu}{E} p_{ocr} \tag{15}$$

where, $p_{ocr}$ = the critical in situ stress,

$u_{icr}$ = the critical radial deformation.

In the case of our example the values are:

$$p_{ocr} = \left(\frac{0.1 \times 100^2}{4}\right)^{1/2} = 15.81 \text{ MPa}$$

and

$$\frac{u_{icr}}{r_i} = \frac{1 + 0.25}{45{,}000}\, 15.81 = 4.39 \times 10^{-4}$$

From Fig. 8b the importance of the critical in situ stress, the critical radial deformation and the transition curve in stability analysis is quite evident. For the rock mass, with the strength and deformation properties as defined by the input data ($\sigma_c$, m, s, E, $\nu$), they indicate the expected stability behaviour of a circular opening, in function of prevailing in situ stresses.

The rock mass around the drift will behave elastically if the in situ stress $p_o < 15.81$ MPa. The radial deformation of the rock mass for this in situ stress region is elastic. The limit of elastic deformation is defined by the value of $u_{icr}/r_i = 4.39 \times 10^{-4}$. Broken rock zone will develop if the in situ stress $p_o > 15.81$ MPa. At the stress ratios of $p_{icr}/p_o$, as defined by the transition curve, the elastic behaviour of the rock mass change to plastic.

The results of calculations, with respect to the plastic portion of the load-deformation curve of the drifts at Level 3, are summarized below:

$$D = \frac{-3.5}{3.5 + 4\,[3.5/100\,(31.2 - 0.262 \times 100) + 0.1]^{1/2}} = -0.625$$

$$N = 2\left[\frac{31.2 - 0.262 \times 100}{0.14 \times 100} + \frac{0.0001}{0.14^2}\right]^{1/2} = 1.204$$

The uppermost curve in Figs. 8a and 8b represents the load-deformation curve for both the 3.0 m and 6.0 m diameter drifts, to be excavated at Level 3 (1250 m depth).

Table 7 - Tabulated results, corresponding to the load-deformation curve of the drifts at Level 3

| $p_i/p_o$ | $p_i$ | $r_e/r_i$ | R | $e_{av} \times 10^{-4}$ | $A \times 10^{-4}$ | $u_i/r_i \times 10^{-4}$ |
|---|---|---|---|---|---|---|
| | | | | | | 8.67 |
| 0.16 | 5.000 | 1.000 | | | | |
| 0.14 | 4.368 | 1.081 | -0.097 | -10.84 | 29.68 | 9.40 |
| 0.12 | 3.744 | 1.174 | -0.201 | -13.35 | 38.46 | 12.52 |
| 0.10 | 3.120 | 1.283 | -0.312 | -16.83 | 51.67 | 17.35 |
| 0.08 | 2.496 | 1.416 | -0.435 | -22.36 | 74.03 | 25.68 |
| 0.06 | 1.872 | 1.582 | -0.573 | -32.54 | 117.89 | 42.26 |
| 0.04 | 1.248 | 1.804 | -0.688 | -46.41 | 198.41 | 74.80 |
| 0.02 | 0.624 | 2.134 | -0.688 | -41.18 | 253.86 | 104.25 |
| 0 | 0 | 2.889 | -0.688 | -36.52 | 426.31 | 188.71 |

SUPPORT REQUIREMENTS

The load-deformation curves of Fig. 8 actually represent the behaviour of the sidewalls of the drifts. Due to the dead weight of the broken rock the support pressure, $p_i$, obtained by the above analysis, can be increased and decreased for the roof and floor, respectively, by the amount of $\delta_p = \gamma_r (r_e - r_i)$.

The load-deformation curves presented in Fig. 8 are in dimensionless terms. To analyse the rock mass behaviour for various conditions the dimensionless expression is very useful and convenient. However, to determine the support requirements and support methods it is necessary to convert the dimensionless data of Fig. 8 into real terms data. The relevant calculations are summarized in Tables 8 to 11.

The results of these calculations are presented in Fig. 9. Note that in case of our example the dead weight of broken rock is negligable. The differences between the load-deformation cuves of the roof, sidewalls and floor are very small.

The support design, based on the concept of rock-support interaction, is demonstrated in Fig. 9. Let us assume, for example, a steel set support system for the 6 m diameter drift at Level 3. According to Hoek and Brown [2], the support capacity of the well blocked steel sets system, with 12 W 65 members spaced at 1 m intervals, in case of 6 m diameter opening is 2.05 MPa.

Table 8 - Summary of calculations for drift at Level 2 in fair quality broken rock mass

| $p_i/p_o$ | $r_e/r_i$ | $r_e$, m | $r_e-r_i$, m | $\delta_p$, MPa | $p_i$, MPa | $p_i+\delta_p$, MPa | $p_i-\delta_p$, MPa | $u_i/r_i$ x $10^{-4}$ | $u_i$, mm |
|---|---|---|---|---|---|---|---|---|---|
| 0.029 | 1.000 | 1.500 | 0 | 0 | 0.500 | 0.500 | 0.500 | 4.72 | 0.71 |
| 0.025 | 1.022 | 1.533 | 0.033 | 0.001 | 0.438 | 0.439 | 0.437 | 5.08 | 0.76 |
| 0.020 | 1.059 | 1.589 | 0.089 | 0.002 | 0.350 | 0.352 | 0.348 | 5.76 | 0.86 |
| 0.015 | 1.100 | 1.650 | 0.150 | 0.004 | 0.263 | 0.267 | 0.259 | 6.61 | 0.99 |
| 0.010 | 1.149 | 1.724 | 0.224 | 0.006 | 0.175 | 0.181 | 0.169 | 7.77 | 1.17 |
| 0.005 | 1.210 | 1.815 | 0.315 | 0.008 | 0.088 | 0.096 | 0.080 | 9.49 | 1.42 |
| 0 | 1.298 | 1.947 | 0.447 | 0.011 | 0 | 0.011 | -0.011 | 12.68 | 1.90 |

Table 9 - Summary of calculations for drift at Level 2 in poor quality broken rock mass

| $p_i/p_o$ | $r_e/r_i$ | $r_e$, m | $r_e-r_i$, m | $\delta_p$, MPa | $p_i$, MPa | $p_i+\delta_p$, MPa | $p_i-\delta_p$, MPa | $u_i/r_i$ x $10^{-4}$ | $u_i$, mm |
|---|---|---|---|---|---|---|---|---|---|
| 0.029 | 1.000 | 1.500 | 0 | 0 | 0.500 | 0.500 | 0.500 | 4.72 | 0.71 |
| 0.025 | 1.046 | 1.569 | 0.069 | 0.002 | 0.438 | 0.440 | 0.436 | 5.52 | 0.83 |
| 0.020 | 1.119 | 1.679 | 0.179 | 0.004 | 0.350 | 0.354 | 0.344 | 7.04 | 1.06 |
| 0.015 | 1.207 | 1.811 | 0.311 | 0.008 | 0.263 | 0.271 | 0.255 | 9.41 | 1.41 |
| 0.010 | 1.320 | 1.980 | 0.480 | 0.012 | 0.175 | 0.187 | 0.163 | 13.64 | 2.05 |
| 0.005 | 1.475 | 2.176 | 0.676 | 0.017 | 0.088 | 0.105 | 0.071 | 23.14 | 3.47 |
| 0 | 1.763 | 2.645 | 1.145 | 0.029 | 0 | 0.029 | -0.029 | 69.15 | 10.37 |

Table 10 - Summary of calculations for drift with 3.0 m diameter at Level 3

| $p_i/p_o$ | $r_e/r_i$ | $r_e$, m | $r_e-r_i$, m | $\delta_p$, MPa | $p_i$, MPa | $p_i+\delta_p$, MPa | $p_i-\delta_p$, MPa | $u_i/r_i$ x $10^{-4}$ | $u_i$, mm |
|---|---|---|---|---|---|---|---|---|---|
| 0.16 | 1.000 | 1.500 | 0 | 0 | 5.000 | 5.000 | 5.000 | 7.28 | 1.09 |
| 0.14 | 1.081 | 1.622 | 0.122 | 0.003 | 4.368 | 4.371 | 4.365 | 9.40 | 1.41 |
| 0.12 | 1.174 | 1.761 | 0.261 | 0.007 | 3.744 | 3.751 | 3.737 | 12.52 | 1.88 |
| 0.10 | 1.283 | 1.925 | 0.425 | 0.011 | 3.120 | 3.131 | 3.109 | 17.35 | 2.60 |
| 0.08 | 1.416 | 2.124 | 0.624 | 0.016 | 2.496 | 2.512 | 2.480 | 25.68 | 3.85 |
| 0.06 | 1.582 | 2.373 | 0.873 | 0.022 | 1.872 | 1.894 | 1.850 | 42.26 | 6.34 |
| 0.04 | 1.804 | 2.706 | 1.206 | 0.030 | 1.248 | 1.278 | 1.218 | 74.80 | 11.22 |
| 0.02 | 2.134 | 3.201 | 1.701 | 0.043 | 0.624 | 0.667 | 0.581 | 104.25 | 15.64 |
| 0 | 2.889 | 4.334 | 2.834 | 0.071 | 0 | 0.071 | -0.071 | 188.71 | 28.31 |

Table 11 - Summary of calculations for drift with 6.0 m diameter at Level 3

| $p_i/p_o$ | $r_e/r_i$ | $r_e$, m | $r_e-r_i$, m | $\delta_p$, MPa | $p_i$, MPa | $p_i+\delta_p$, MPa | $p_i-\delta_p$, MPa | $u_i/r_i$ x $10^{-4}$ | $u_i$, mm |
|---|---|---|---|---|---|---|---|---|---|
| 0.16 | 1.000 | 3.000 | 0 | 0 | 5.000 | 5.000 | 5.000 | 7.28 | 2.18 |
| 0.14 | 1.081 | 3.243 | 0.243 | 0.006 | 4.368 | 4.374 | 4.362 | 9.40 | 2.82 |
| 0.12 | 1.174 | 3.522 | 0.522 | 0.013 | 3.744 | 3.757 | 3.731 | 12.52 | 3.76 |
| 0.10 | 1.283 | 3.849 | 0.849 | 0.021 | 3.120 | 3.141 | 3.099 | 17.35 | 5.21 |
| 0.08 | 1.416 | 4.248 | 1.248 | 0.031 | 2.496 | 2.572 | 2.465 | 25.68 | 7.70 |
| 0.06 | 1.582 | 4.764 | 1.746 | 0.044 | 1.872 | 1.916 | 1.828 | 42.26 | 12.63 |
| 0.04 | 1.804 | 5.412 | 2.412 | 0.060 | 1.248 | 1.308 | 1.188 | 74.80 | 21.84 |
| 0.02 | 2.134 | 6.402 | 3.402 | 0.085 | 0.624 | 0.709 | 0.539 | 104.25 | 31.23 |
| 0 | 2.889 | 8.667 | 5.667 | 0.142 | 0 | 0.142 | -0.142 | 188.71 | 56.61 |

In Fig. 9 on the load-deformation curve of the 6 m diameter drift the value of $p_i$ = 2.05 MPa is reached at point A, with a radial deformation of $u_i$ = 10.4 mm.

The properly installed support system while it takes the load, equal to its support capacity, will itself undergo an allowable deformation. The allowable deformation of a well blocked steel sets system is about 5 mm.

In order to utilize the safe and full capcity of the steel sets system and also to restrain the rock mass from further deformation, the steel sets are to be installed when the radial deformation of the drift reached about 6 mm.

The proper and timely installation of the steel sets system would ensure that at point A a stable condition could be reached through the rock-support interaction. The load equivalent to $p_i$ = 2.05 MPa would be carried by the support. The much larger portion of the acting load would be borne by the broken but stabilized rock around the drift.

The selection of support system must simultaneously consider the radial deformation and the stress level, i.e., support capacity. This is evident from Fig. 10 where beside the load-deformation curves the capacities of various support systems are also given. The support capacities applicable for circular openings with diameters of 6 m and 3 m are shown by the scales on the right hand side.

The steel sets support with 12 W 65 members (G), as shown in Fig. 10 (and also in Fig. 9), will stabilize the 6 m diameter drift at the radial deformation of 10.4 mm. However, the deterioration of wall rocks is the function of the radial deformation. It is possible that the 10.4 mm deformation causes unacceptable loosening of roof rocks. In this case a concrete lining of 30 cm thickness (C) must be used which will stabilize the rock at a radial deformation of 5.4 mm. It is certain that neither the 5 cm shotcrete lining (B) nor the heaviest rock bolt system (K) can be considered as viable support system for the 6 m diameter drift at 1250 m depth (Level 3). The related radial deformations of 39.5 mm and 51 mm, respectively, will cause unacceptably extensive deterioration of roof rocks.

The procedure and considerations of support selection are the same for the other cases. To avoid overcrowding, however, the support possibilities of the following discussions are not marked in Fig. 10. Since the drift radius is 1.5 m for all the remaining cases the support capacity is to be read from the second (1.5 m) scale.

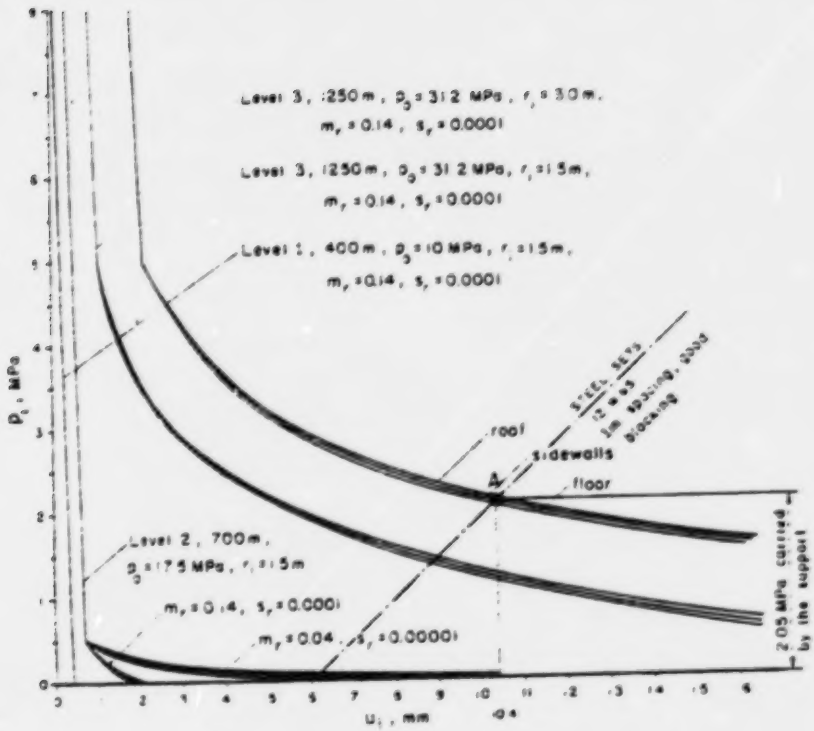
Level 3, 1250 m, $p_3$ = 31.2 MPa, $r_i$ = 3.0 m,
$m_r$ = 0.14, $s_r$ = 0.0001
Level 3, 1250 m, $p_3$ = 31.2 MPa, $r_i$ = 1.5 m,
$m_r$ = 0.14, $s_r$ = 0.0001
Level 1, 400 m, $p_3$ = 10 MPa, $r_i$ = 1.5 m,
$m_r$ = 0.14, $s_r$ = 0.0001
roof
sidewalls
floor
A
Level 2, 700 m,
$p_3$ = 17.5 MPa, $r_i$ = 1.5 m
$m_r$ = 0.14, $s_r$ = 0.0001
$m_r$ = 0.04, $s_r$ = 0.00001
$p_i$, MPa
$u_i$, mm

Fig. 9 - Load-deformation curves in real terms

To support the 3 m diameter drift at 1250 m depth either the 5 cm shotcrete lining (B) or steel sets with 8I23 members at 1.5 m spacing (F) can be considered. The radial deformation of effective support capacity is about 9 mm for both systems.

The use of steel sets with 12 W 65 members at 1 m spacing (G) would result in this case in an overconservative and uneconomic support. It would virtually eliminate any broken rock zone development. This would be contrary to the basic principle of support design. The role of the rock support is to help the rock in supporting itself. The proper support design must, therefore, utilize the self-supporting capability of the broken rock zone.

A not yet mentioned aspect of support selection is the cast factor. The lighter systems, in general, are less expensive. The lower the value of unbalanced pressure along the load-deformation curve, the lighter the required support system. However, the decrease of unbalanced pressure is coupled with the increase in radial deformation, consequently, with the increase of roof rock deterioration. This takes back the problem of support selection to the allowable radial deformation of the drift.

A further aspect of support selection is related to the installation technique. Some of the support type can be installed right at the face while the others can only be installed at several meters behind the face. For example, for the drift at Level 2 located in poor quality broken rock mass ($m_r$ = 0.04, $s_r$ = 0.00001), the 5 cm shotcrete lining (A) would probably be an ideal support type, because of the full surface coverage of the shotcrete. In the case of poor quality rock mass the expected time of response is short. To retain the broken rock the support should be installed immediately at the face. This is not possible with shotcrete lining. To avoid interference with the other activities, shotcreting can only be performed at several meters behind the face. Furthermore, the full strength of shotcrete lining is reached only after 28 days.

To support the 3 m diameter drift in poor quality broken rock mass at Level 2, either the heavy rockbolts (K) or the steel sets with 6I12 members at 2 m spacing (E) can be considered. Both systems can be installed near to the face. The adequate capacities of the two systems are almost equal. The selection can be based on cost factors.

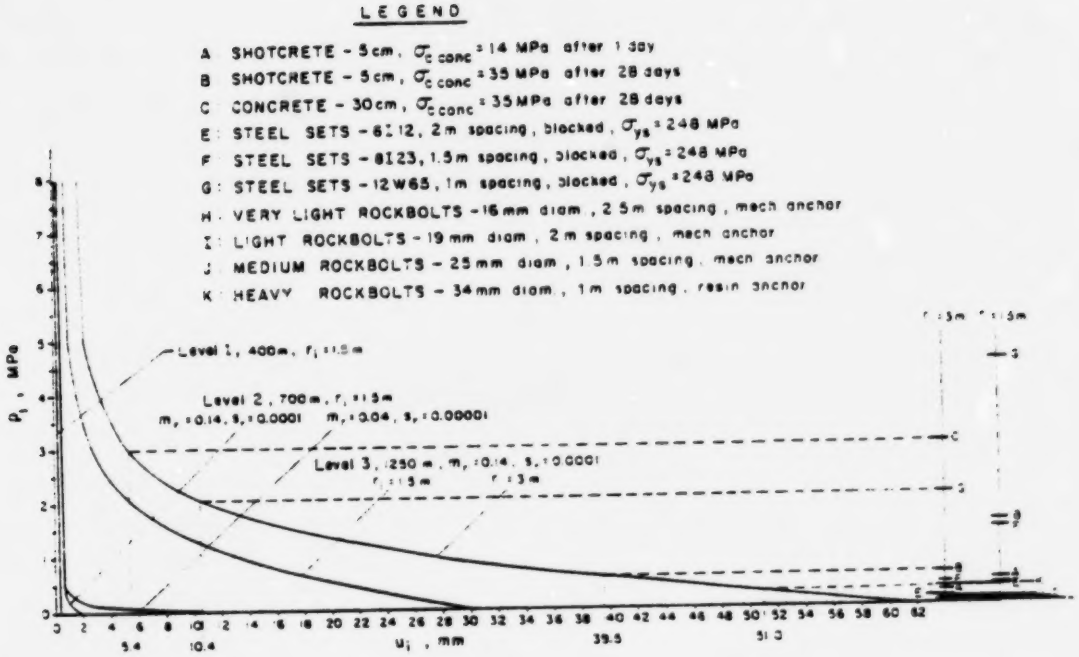
LEGEND
A SHOTCRETE - 5 cm, $\sigma_{c\,conc}$ = 14 MPa after 1 day
B SHOTCRETE - 5 cm, $\sigma_{c\,conc}$ = 35 MPa after 28 days
C CONCRETE - 30 cm, $\sigma_{c\,conc}$ = 35 MPa after 28 days
E STEEL SETS - 8I 12, 2 m spacing, blocked, $\sigma_{ys}$ = 248 MPa
F STEEL SETS - 8I 23, 1.5 m spacing, blocked, $\sigma_{ys}$ = 248 MPa
G STEEL SETS - 12W65, 1 m spacing, blocked, $\sigma_{ys}$ = 248 MPa
H VERY LIGHT ROCKBOLTS - 16 mm diam, 2.5 m spacing, mech anchor
I LIGHT ROCKBOLTS - 19 mm diam, 2 m spacing, mech anchor
J MEDIUM ROCKBOLTS - 25 mm diam, 1.5 m spacing, mech anchor
K HEAVY ROCKBOLTS - 34 mm diam, 1 m spacing, resin anchor
Level 1, 400 m, $r_i$ = 1.5 m
Level 2, 700 m, $r_i$ = 1.5 m
$m_r$ = 0.14, $s_r$ = 0.0001 $m_r$ = 0.04, $s_r$ = 0.00001
Level 3, 1250 m, $m_r$ = 0.14, $s_r$ = 0.0001
$r_i$ = 1.5 m $r_i$ = 3 m
$p_i$, MPa
$u_i$, mm
5.4
10.4
39.5
51.0

Fig. 10 - Selection of support system

To support the drift at Level 2 in fair quality broken rock mass, the medium rockbolts (J) system would be the first choice. However, it is possible that the light bolts (I) system could provide an adequate support. The decision can be made after underground bolting trial and performance evaluation.

The behaviour of the rock mass around the drift excavated at 400 m depth (Level 1) will be entirely elastic. The rock mass is self-supporting. No additional support is required.

## RESULTS OF PARAMETRIC ANALYSES

The detailed example of the previous section demonstrates the effectiveness of the load-deformation curve in analysing the stability behaviour of a rock mass around a circular underground opening. The strength and deformation properties of the rock mass is charaterized by the input data of $\sigma_c$, E, $\nu$, m, s, $m_r$, $s_r$. The load condition and the dimension of the opening is given by the input data of $p_o$ and $r_i$, respectively.

In this section the significance of the above variables is being evaluated by a series of computations. These computations are performed for the systematic combinations of selected values of variables of each rock type.

The steps of calculations are explained in the example of the previous section. The equations used for the calculations are summarized below:

$$p_i < p_{icr} = p_o - M\,\sigma_c \tag{3}$$

$$p_{icr}/p_o = 1 - M\,\sigma_c/p_o \tag{3a}$$

$$M = \frac{1}{2}\left[\left(\frac{m}{4}\right)^2 + m\,p_o/\sigma_c + s\right]^{1/2} - \frac{m}{8} \tag{4}$$

$$\frac{u_i}{r_i} = \frac{(1+\nu)}{E}(p_o - p_i) \tag{5}$$

$$\frac{u_i}{r_i} = \frac{(1+\nu)}{E}(p_o - p_{icr}) \tag{5a}$$

$$\frac{u_e}{r_e} = \frac{(1+\nu)}{E} M\,\sigma_c \tag{6}$$

$$D = \frac{-m}{m + 4\left[m/\sigma_c\,(p_o - M\,\sigma_c) + s\right]^{1/2}} \tag{7}$$

$$N = 2\left[\frac{p_o - M\,\sigma_c}{m_r\,\sigma_c} + \frac{s_r}{m_r^2}\right]^{1/2} \tag{8}$$

$$\frac{r_e}{r_i} = e^{N - 2\left[\frac{p_i}{m_r\,\sigma_c} + \frac{s_r}{m_r^2}\right]^{1/2}} \tag{9}$$

$$R = 2\,D \ln r_e/r_i \tag{10a}$$

$$R = 1.1\,D \tag{10b}$$

$$e_{av} = \frac{2(u_e/r_i)\,(r_e/r_i)^2}{\left[(r_e/r_i)^2 - 1\right](1 + 1/R)} \tag{11}$$

$$A = (2\,u_e/r_e - e_{av})\,(r_e/r_i)^2 \tag{12}$$

$$\frac{u_i}{r_i} = 1 - \left[\frac{1 - e_{av}}{1 + A}\right]^{1/2} \tag{13}$$

$$p_{ocr} = \left(\frac{s\,\sigma_c^2}{4}\right)^{1/2} \tag{14}$$

$$\frac{u_{icr}}{r_i} = \frac{(1 + \nu)}{E}\,p_{ocr} \tag{15}$$

ROCK: TYPE A

The computations were made for the systematic combinations of the selected values of variables listed in Table 12.

The values of $u_i/r_i$, corresponding to the various in situ stress magnitudes, $p_o$, calculated by equation (5), are listed in Table 13. The elastic rays, representing a linear load-deformation relationship for each in situ stress level, are drawn in Fig. 11.

Table 12 - Listing of selected values of variables for rock Type A

| Variables | Selected values | |
|---|---|---|
| Material constants | Original rock mass quality | Very good m = 3.5, s = 0.1 |
| | | Good m = 0.7, s = 0.004 |
| | Broken rock mass quality | Fair $m_r$ = 0.14, $s_r$ = 0.0001 |
| | | Poor $m_r$ = 0.04, $s_r$ = 0.00001 |
| Paired uniaxial compressive strength and modulus of elasticity | $\sigma_c$ = 45 MPa, E = 31 GPa<br>$\sigma_c$ = 100 MPa, E = 45 GPa<br>$\sigma_c$ = 150 MPa, E = 57 GPa<br>$\sigma_c$ = 200 MPa, E = 69 GPa | |
| In situ stress, $p_o$ (MPa) | 10, 17.5, 31.2, 43.8, 50, 100 | |
| Poisson's ratio, $\nu$ | 0.25 | |
| Unit weight, $\gamma_r$, ($MN/m^3$) | 0.025 | |
| Radius of opening, $r_i$ (m) | 1.5, 3, 6, 9, 15 | |

The transition points on the elastic rays are calculated by using equations (3a) and (4). The calculations were made in tabulated forms. Tables 14 and 15 correspond to very good and good quality original rock mass, respectively. The calculated points of $p_{icr}/p_o$ define the transition curves. The transition curves for each analysed data pair of E and $\sigma_c$ are shown in Fig. 11 by separate graphs. The transition curves indicated by m = 3.5, s = 0.1 and m = 0.7, s = 0.004 material constant values correspond to very good and good original rock mass qualities, respectively.

The origin of the transition curves, i.e., the critical radial deformation ratio, $u_{icr}/r_i$, and the critical in situ stresses, $p_{ocr}$, are calculated by equations (14) and (15).

The points of the load-deformation curves, for each combination of the variables listed in Table 12, were calculated and then plotted by computer. Figures numbered from 12 to 19 show the load-deformation curves, drawn from the computer plots. In each of these figures two computer plots are combined. The common variables in each combined plot are: the quality of the original rock mass (i.e., m and s values), the strength and deformation properties (i.e., $\sigma_c$, E and $\nu$) and the in situ stress magnitudes, $p_o$. Consequently, Figs. 12 to 19 indicate the effect of the quality designation of the broken rock mass, expressed by the material constant values of $m_r$ and $s_r$.

Figures numbered by 20 to 23 were plotted, from the computer output, to illustrate the extent of broken zones. For the conditions indicated by the marked variables, the extent of broken zone are given in $r_e/r_i$ terms. The graphs at left hand and right hand sides show the relationships between $r_e/r_i$ and $p_i/p_o$ and between $u_i/r_i$ and $r_e/r_i$, respectively. These plots correspond to the curved line portion of the load-deformation curves, therefore, for the transition points the ratio of $r_e/r_i$ = 1.

Table 13- Calculation and listing of $u_i/r_i$ values for rock Type A

| E | $\frac{1+\nu}{E}$ | $u_i/r_i$ for $p_o$ of | | | | | |
|---|---|---|---|---|---|---|---|
| | | 10 | 17.5 | 31.2 | 43.8 | 80 | 100 |
| 31.000 | $4.03\times10^{-5}$ | $4.03\times10^{-4}$ | $7.05\times10^{-4}$ | $1.26\times10^{-3}$ | $1.77\times10^{-3}$ | $2.02\times10^{-3}$ | $4.03\times10^{-3}$ |
| 45.000 | $2.78\times10^{-5}$ | $2.78\times10^{-4}$ | $4.86\times10^{-4}$ | $8.67\times10^{-4}$ | $1.22\times10^{-3}$ | $1.39\times10^{-3}$ | $2.78\times10^{-3}$ |
| 57.000 | $2.19\times10^{-5}$ | $2.19\times10^{-4}$ | $3.84\times10^{-4}$ | $6.84\times10^{-4}$ | $9.61\times10^{-4}$ | $1.10\times10^{-3}$ | $2.19\times10^{-3}$ |
| 69.000 | $1.81\times10^{-5}$ | $1.81\times10^{-4}$ | $3.17\times10^{-4}$ | $5.65\times10^{-4}$ | $7.93\times10^{-4}$ | $9.05\times10^{-4}$ | $1.81\times10^{-3}$ |

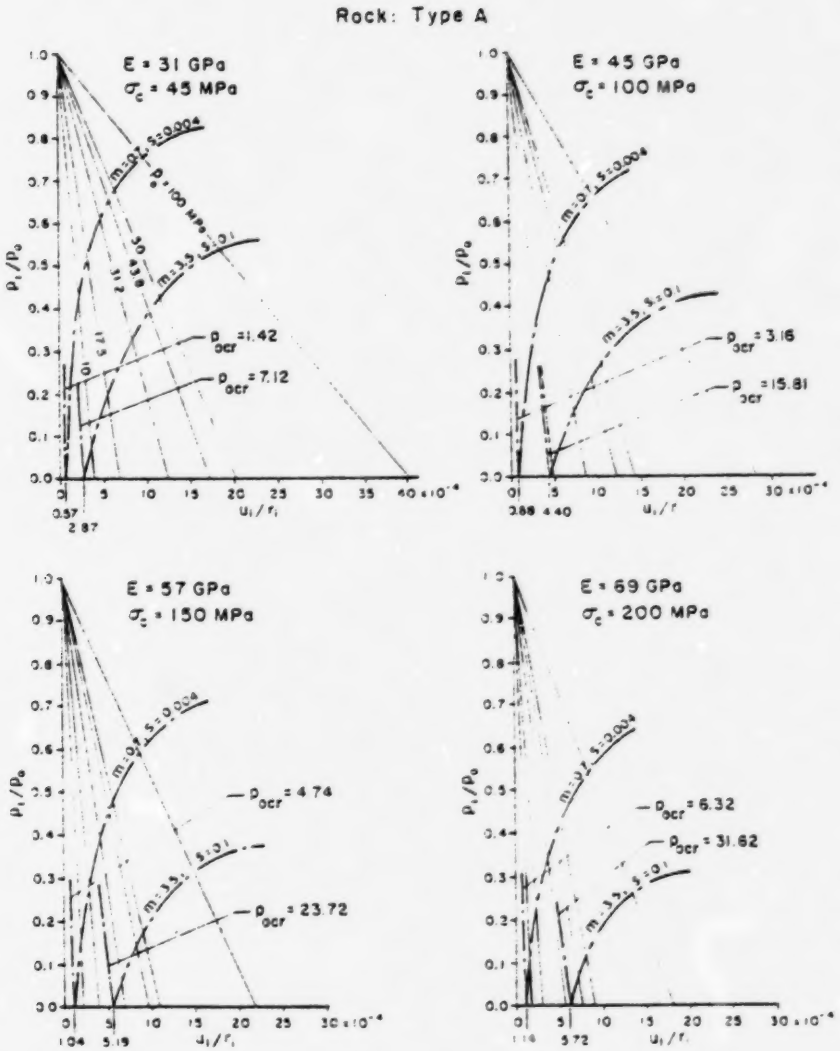


Fig. 11 - Elastic rays of rock Type A

Table 14- Calculation and listing of $p_{icr}/p_o$ values for rock Type A

| $p_o$ | | $\sigma_c$ | | | |
|---|---|---|---|---|---|
| | | 45 | 100 | 150 | 200 |
| 10 | $p_o/\sigma_c$ | 0.222 | 0.100 | 0.067 | 0.050 |
| | 3.5 $p_o/\sigma_c$ | 0.778 | 0.350 | 0.233 | 0.175 |
| | M | 0.203 | 0.113 | 0.086 | 0.072 |
| | M $\sigma_c/p_o$ | 0.914 | 1.130 | 1.290 | 1.440 |
| | $p_{icr}/p_o$ | 0.086 | -0.130 | -0.290 | -0.440 |
| 17.5 | $p_o/\sigma_c$ | 0.389 | 0.175 | 0.117 | 0.088 |
| | 3.5 $p_o/\sigma_c$ | 1.361 | 0.613 | 0.408 | 0.306 |
| | M | 0.308 | 0.170 | 0.125 | 0.102 |
| | M $\sigma_c/p_o$ | 0.792 | 0.971 | 1.080 | 1.177 |
| | $p_{icr}/p_o$ | 0.208 | 0.029 | -0.080 | -0.177 |
| 31.2 | $p_o/\sigma_c$ | 0.693 | 0.312 | 0.208 | 0.156 |
| | 3.5 $p_o/\sigma_c$ | 2.427 | 1.092 | 0.728 | 0.546 |
| | M | 0.469 | 0.262 | 0.193 | 0.150 |
| | M $\sigma_c/p_o$ | 0.675 | 0.841 | 0.925 | 1.000 |
| | $p_{icr}/p_o$ | 0.325 | 0.159 | 0.072 | 0 |
| 43.8 | $p_o/\sigma_c$ | 0.973 | 0.438 | 0.292 | 0.219 |
| | 3.5 $p_o/\sigma_c$ | 3.407 | 1.533 | 1.022 | 0.767 |
| | M | 0.596 | 0.336 | 0.249 | 0.201 |
| | M $\sigma_c/p_o$ | 0.614 | 0.766 | 0.852 | 0.919 |
| | $p_{icr}/p_o$ | 0.386 | 0.234 | 0.148 | 0.081 |
| 50 | $p_o/\sigma_c$ | 1.111 | 0.500 | 0.333 | 0.250 |
| | 3.5 $p_o/\sigma_c$ | 3.889 | 1.750 | 1.167 | 0.875 |
| | M | 0.652 | 0.371 | 0.275 | 0.222 |
| | M $\sigma_c/p_o$ | 0.587 | 0.742 | 0.825 | 0.888 |
| | $p_{icr}/p_o$ | 0.413 | 0.258 | 0.175 | 0.112 |
| 100 | $p_o/\sigma_c$ | 2.222 | 1.000 | 0.667 | 0.500 |
| | 3.5 $p_o/\sigma_c$ | 7.778 | 3.500 | 2.333 | 1.750 |
| | M | 1.032 | 0.607 | 0.456 | 0.371 |
| | M $\sigma_c/p_o$ | 0.464 | 0.607 | 0.684 | 0.742 |
| | $p_{icr}/p_o$ | 0.536 | 0.393 | 0.316 | 0.258 |

$m = 3.5, \quad s = 0.1$

$$M = \frac{1}{2}\left(\left(\frac{3.5}{4}\right)^2 - 3.5\ p_o/\sigma_c + 0.1\right)^{1/2} - 3.5/8$$

$$M = \frac{1}{2}\left(0.866 - 3.5\ p_o/\sigma_c\right)^{1/2} - 0.438$$

Table 15 - Calculation and listing of $p_{ier}/p_o$ values for rock Type A

| $p_o$ | | $\sigma_c$ | | | |
|---|---|---|---|---|---|
| | | 45 | 100 | 150 | 200 |
| 10 | $p_o/\sigma_c$ | 0.222 | 0.100 | 0.067 | 0.050 |
| | $0.7\ p_o/\sigma_c$ | 0.156 | 0.070 | 0.047 | 0.035 |
| | M | 0.131 | 0.074 | 0.055 | 0.044 |
| | $M\ \sigma_c/p_o$ | 0.590 | 0.740 | 0.825 | 0.880 |
| | $p_{ier}/p_o$ | 0.410 | 0.260 | 0.175 | 0.120 |
| 17.5 | $p_o/\sigma_c$ | 0.389 | 0.175 | 0.117 | 0.088 |
| | $0.7\ p_o/\sigma_c$ | 0.272 | 0.123 | 0.082 | 0.061 |
| | M | 0.189 | 0.111 | 0.083 | 0.067 |
| | $M\ \sigma_c/p_o$ | 0.486 | 0.634 | 0.711 | 0.769 |
| | $p_{ier}/p_o$ | 0.514 | 0.366 | 0.289 | 0.234 |
| 31.2 | $p_o/\sigma_c$ | 0.693 | 0.312 | 0.208 | 0.156 |
| | $0.7\ p_o/\sigma_c$ | 0.485 | 0.218 | 0.146 | 0.109 |
| | M | 0.273 | 0.163 | 0.125 | 0.102 |
| | $M\ \sigma_c/p_o$ | 0.393 | 0.523 | 0.601 | 0.654 |
| | $p_{ier}/p_o$ | 0.607 | 0.477 | 0.399 | 0.346 |
| 43.8 | $p_o/\sigma_c$ | 0.973 | 0.438 | 0.292 | 0.219 |
| | $0.7\ p_o/\sigma_c$ | 0.681 | 0.307 | 0.204 | 0.153 |
| | M | 0.335 | 0.204 | 0.156 | 0.129 |
| | $M\ \sigma_c/p_o$ | 0.345 | 0.465 | 0.534 | 0.590 |
| | $p_{ier}/p_o$ | 0.655 | 0.535 | 0.466 | 0.410 |
| 50 | $p_o/\sigma_c$ | 1.111 | 0.500 | 0.333 | 0.250 |
| | $0.7\ p_o/\sigma_c$ | 0.778 | 0.350 | 0.233 | 0.175 |
| | M | 0.363 | 0.222 | 0.171 | 0.141 |
| | $M\ \sigma_c/p_o$ | 0.327 | 0.444 | 0.513 | 0.564 |
| | $p_{ier}/p_o$ | 0.673 | 0.556 | 0.487 | 0.436 |
| 100 | $p_o/\sigma_c$ | 2.222 | 1.000 | 0.667 | 0.500 |
| | $0.7\ p_o/\sigma_c$ | 1.556 | 0.700 | 0.467 | 0.350 |
| | M | 0.543 | 0.341 | 0.256 | 0.222 |
| | $M\ \sigma_c/p_o$ | 0.244 | 0.341 | 0.399 | 0.444 |
| | $p_{ier}/p_o$ | 0.756 | 0.659 | 0.601 | 0.556 |

$a = 0.7, \quad s = 0.004$

$$M = \frac{1}{2}\left(\left(\frac{0.7}{4}\right)^2 + 0.7\ p_o/\sigma_c + 0.004\right)^{1/2} - 0.7/8$$

$$M = \frac{1}{2}\left(0.035 + 0.7\ p_o/\sigma_c\right)^{1/2} - 0.088$$

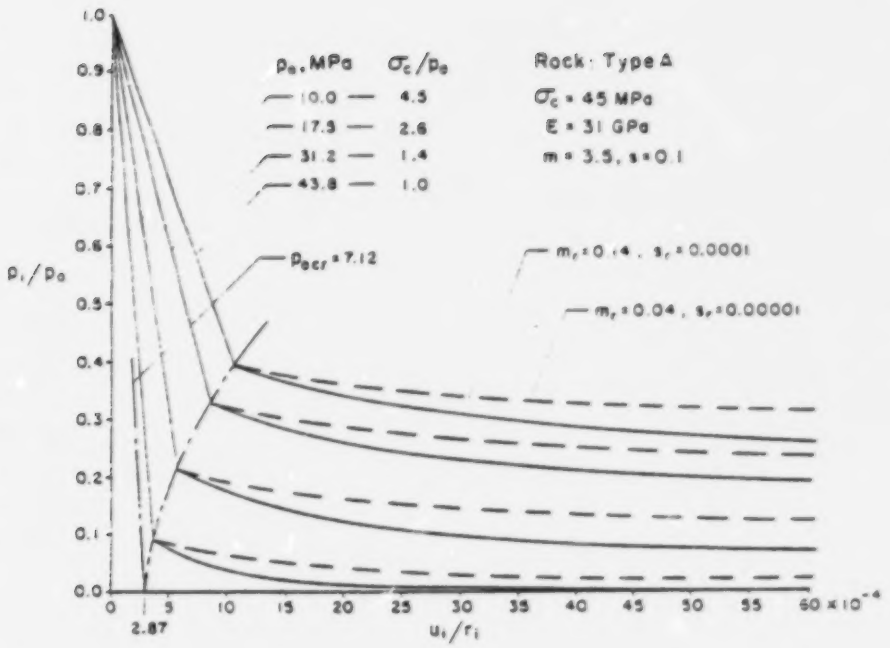


Fig. 12 - Load-deformation curves for rock Type A

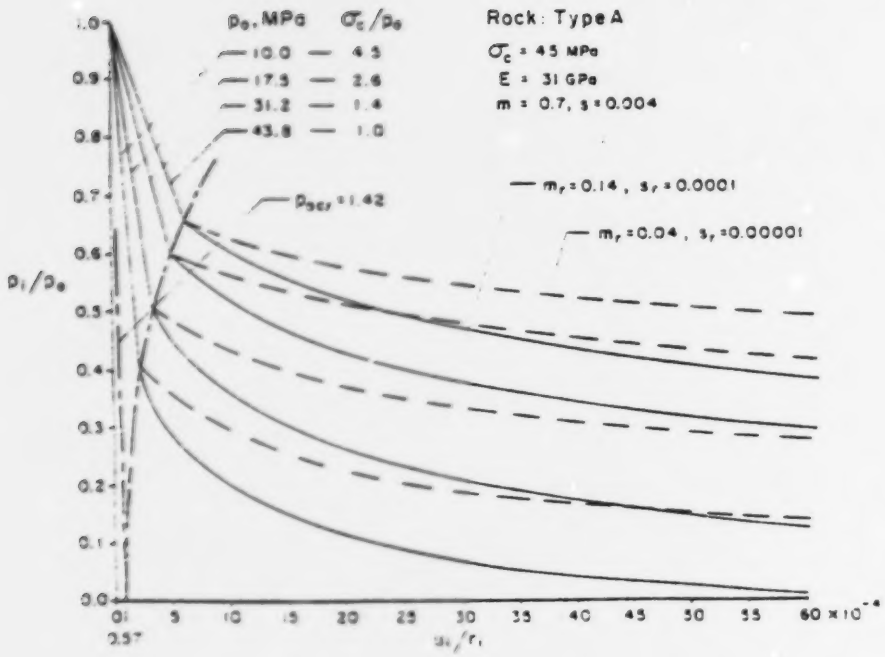


Fig. 13 - Load-deformation curves for rock Type A

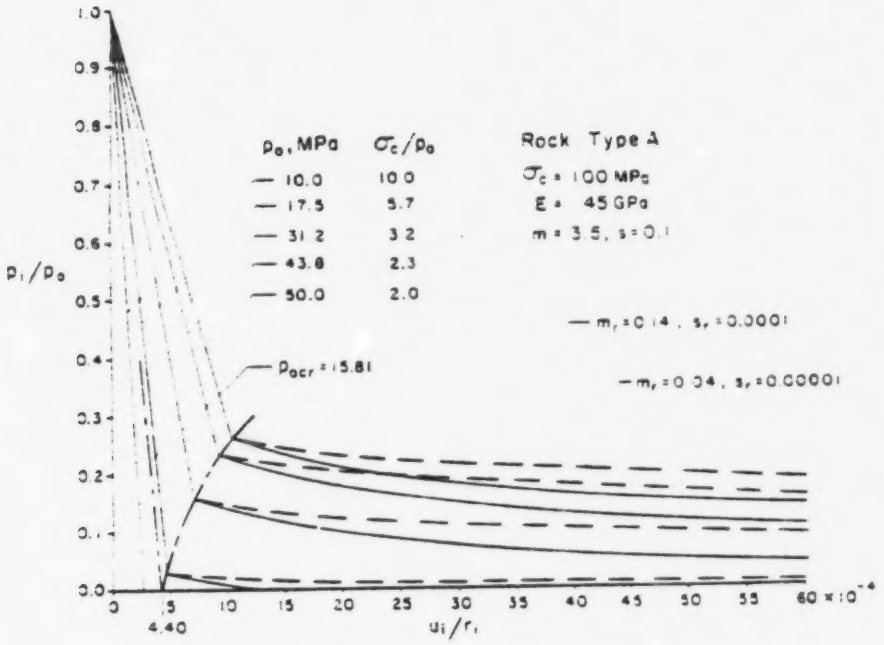


Fig. 14 - Load-deformation curves for rock Type A

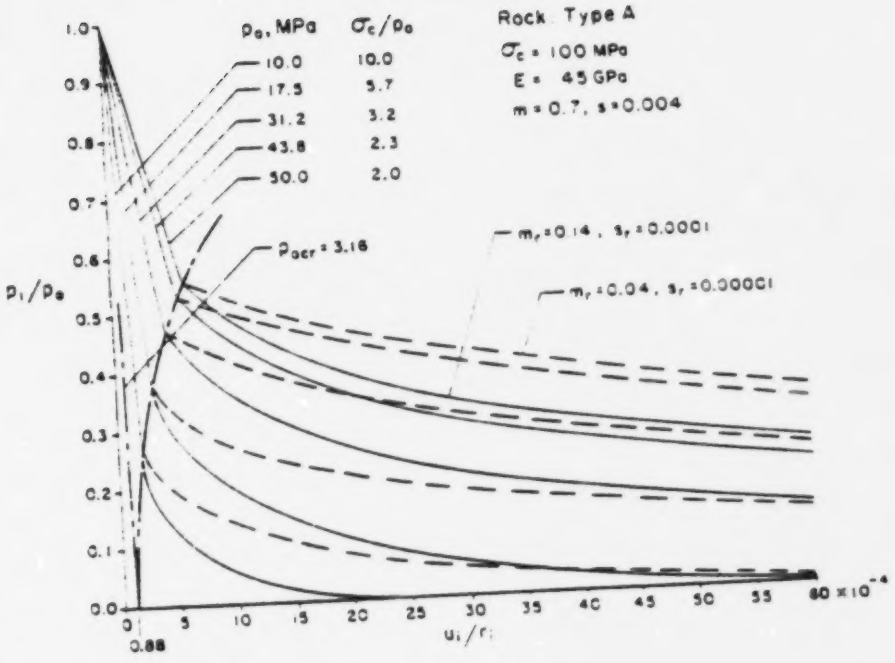


Fig. 15 - Load-deformation curves for rock Type A

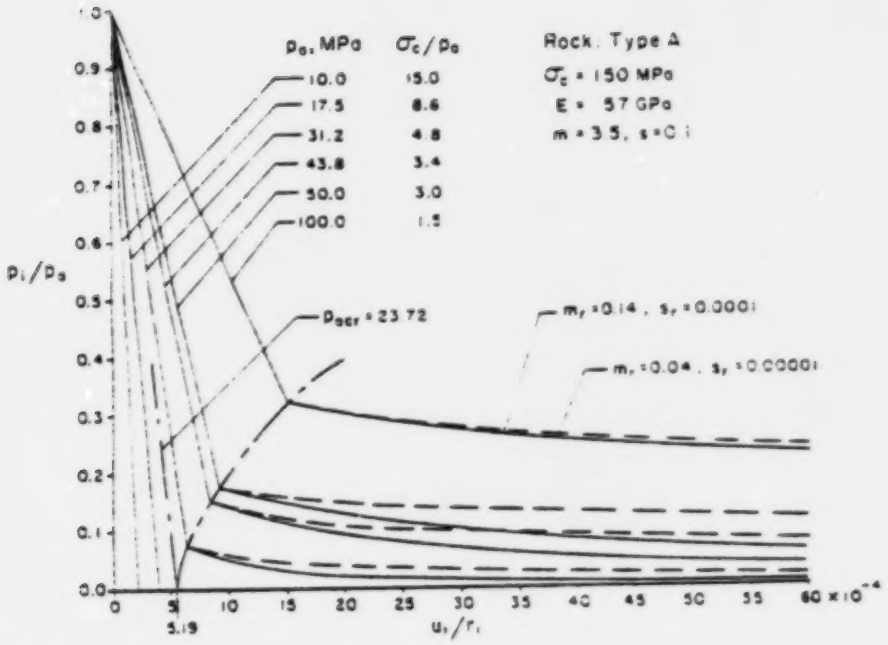


Fig. 16 - Load-deformation curves for rock Type A

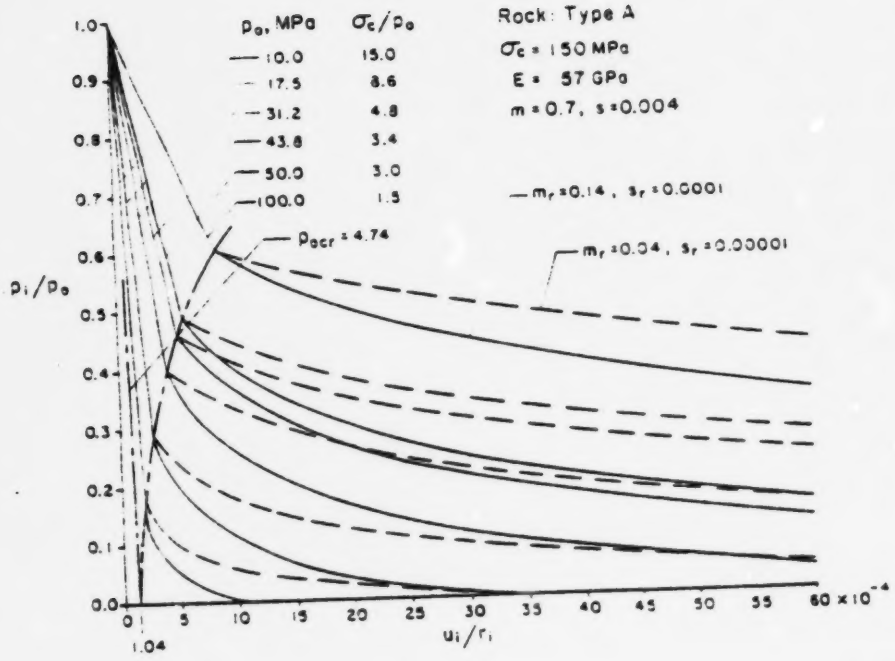


Fig. 17 - Load-deformation curves for rock Type A

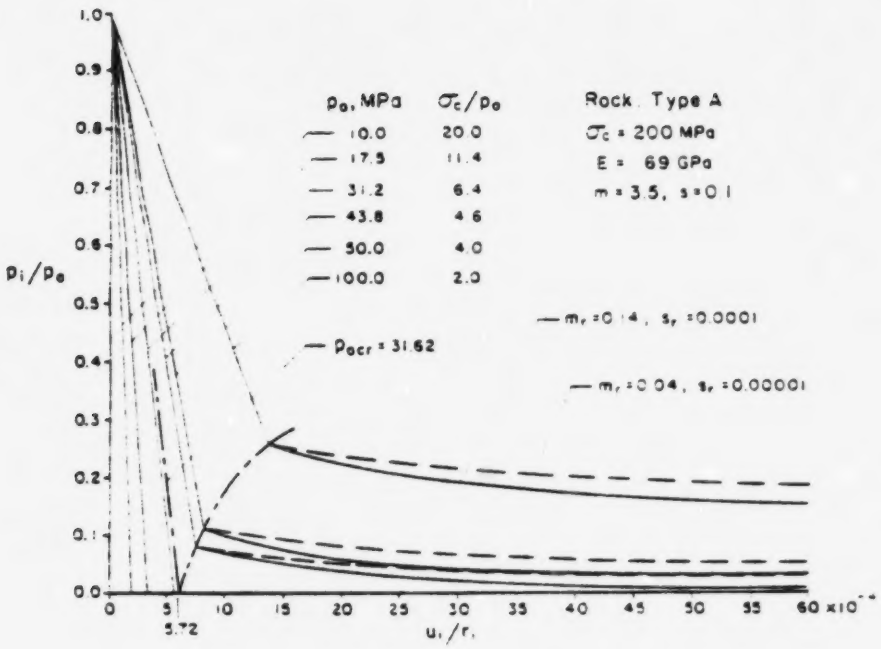


Fig. 18 - Load-deformation curves for rock Type A

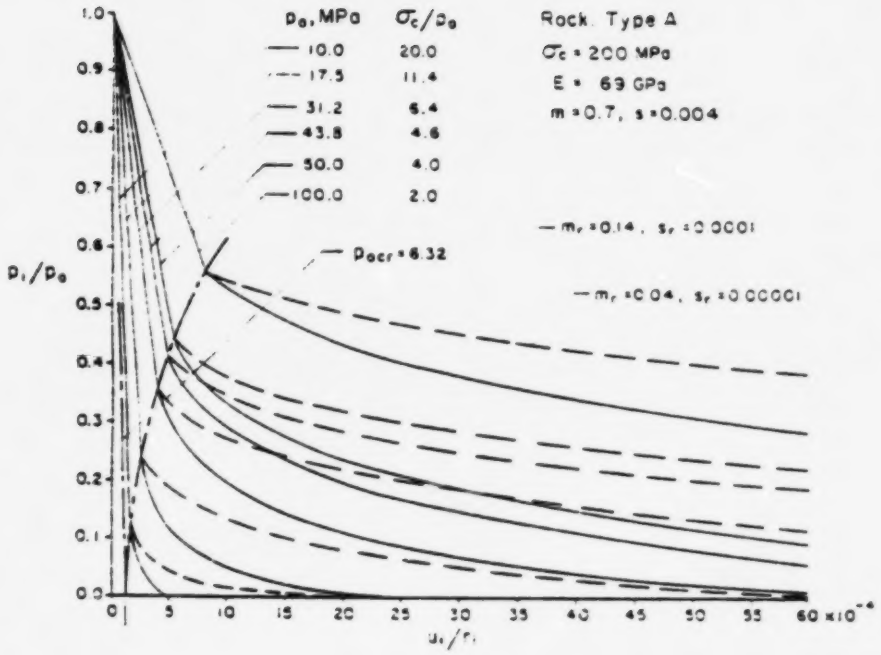


Fig. 19 - Load-deformation curves for rock Type A

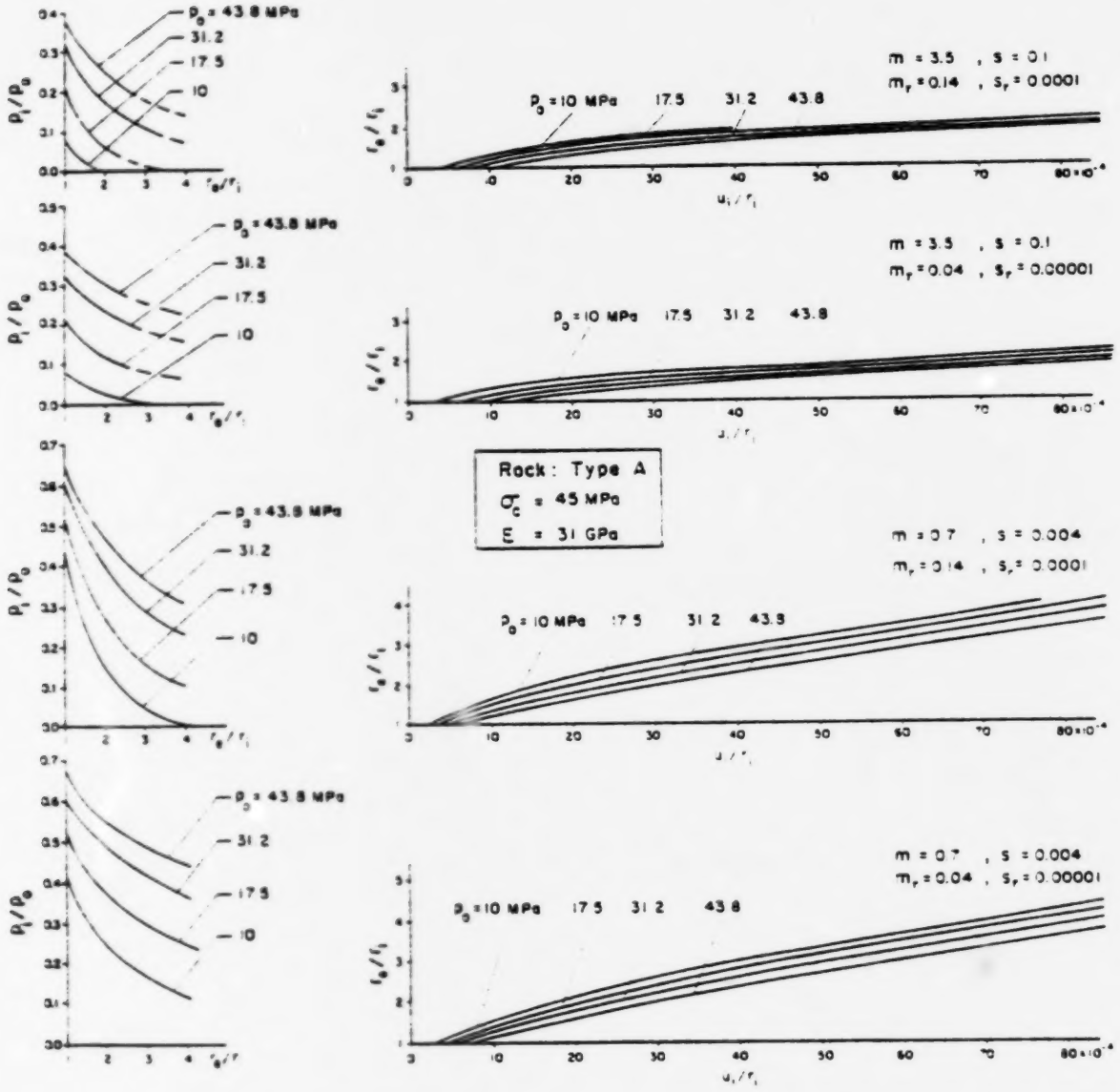


Fig. 20 - Extent of broken zones for rock Type A

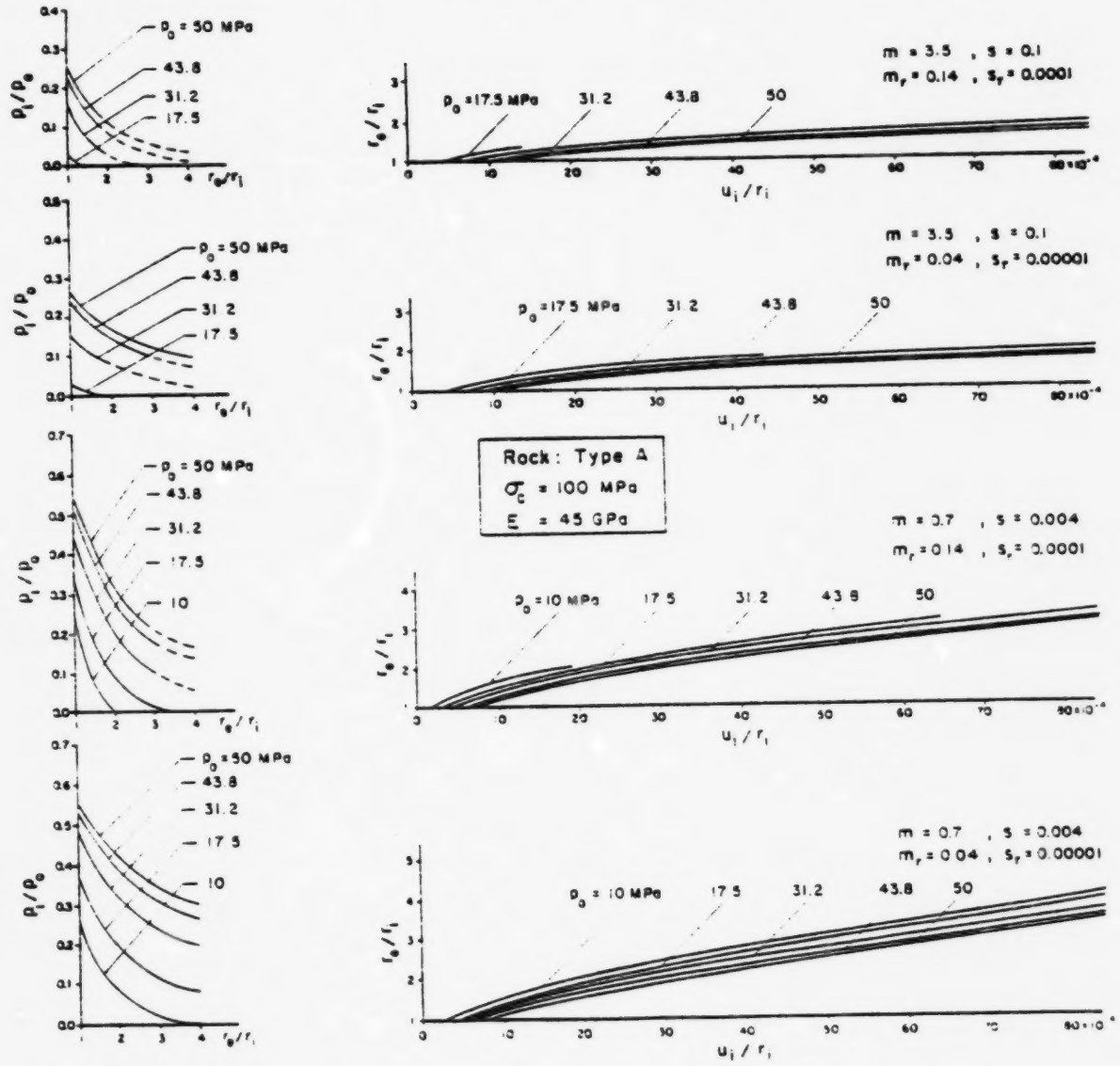


Fig. 21 - Extent of broken zones for rock Type A

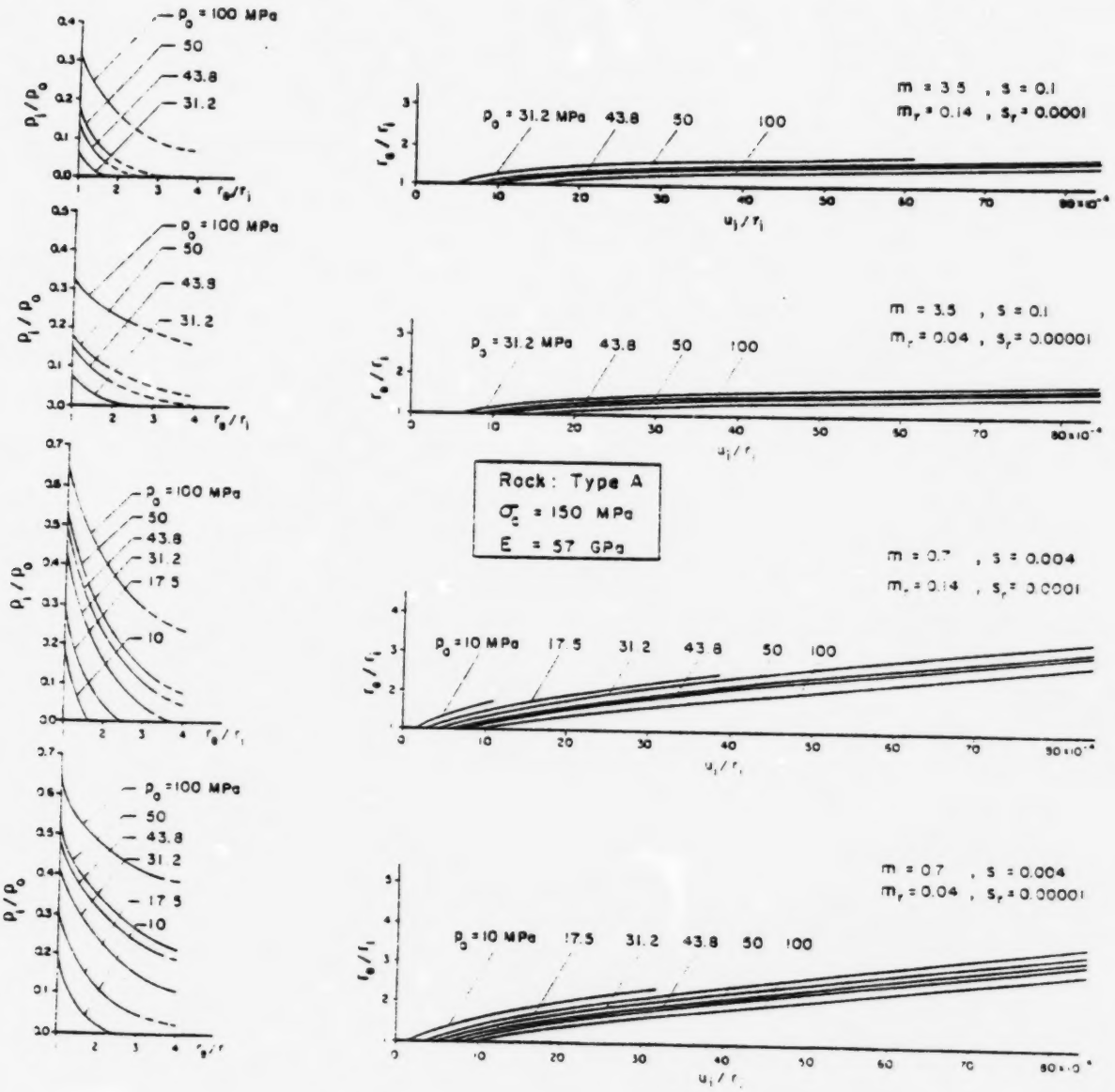


Fig. 22 - Extent of broken zones for rock Type A

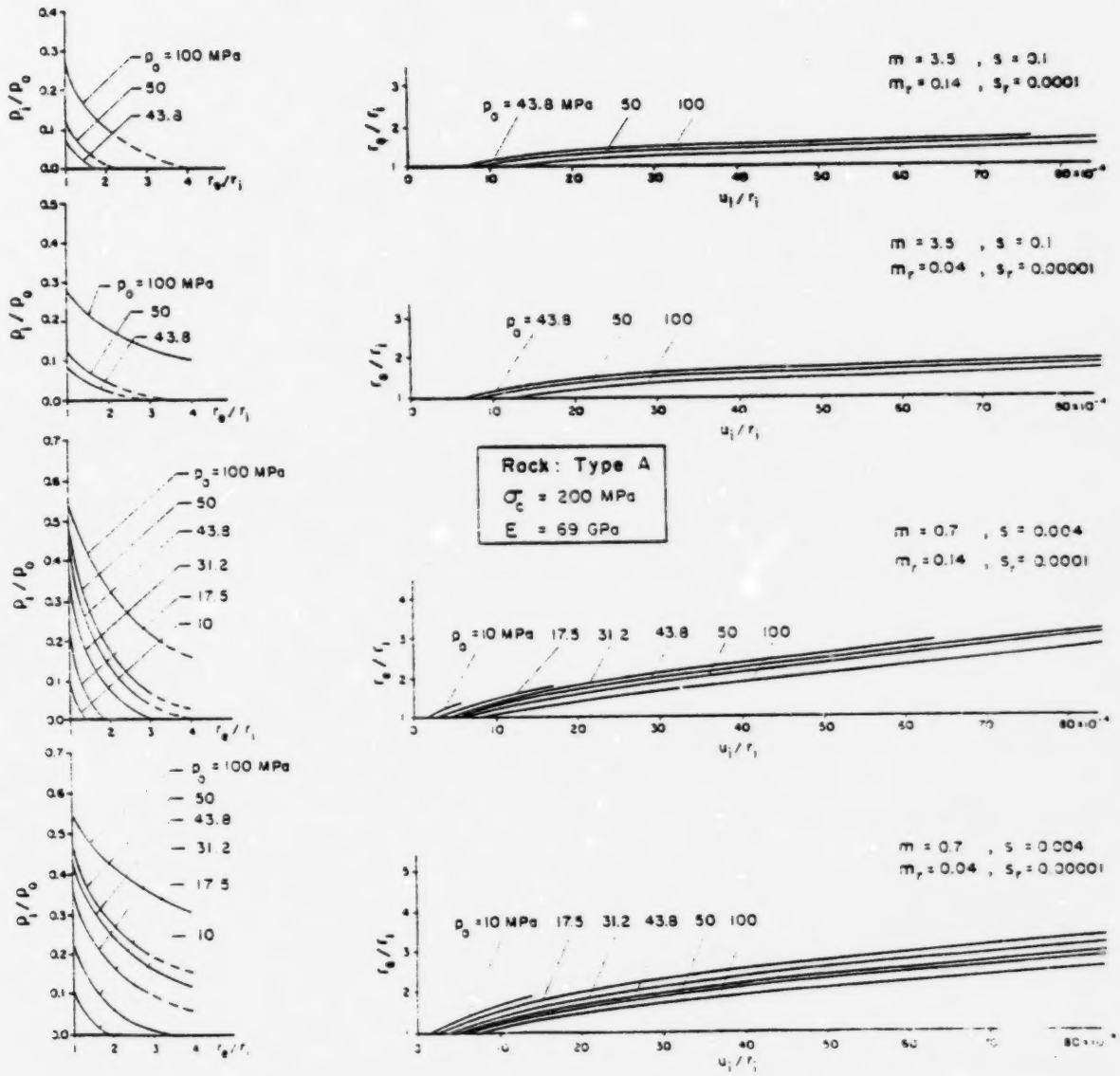


Fig. 23 - Extent of broken zones for rock Type A

ROCK: TYPE B

The computations were made for the systematic combinations of the selected values of variables listed in Table 16.

Table 16 - Listing of selected values of variables for rock Type B

| Variables | Selected values | |
|---|---|---|
| Material constants | Original rock mass quality | Very good $m = 5.0$, $s = 0.1$ |
| | | Good $m = 1.0$, $s = 0.004$ |
| | Broken rock mass quality | Fair $m_r = 0.2$, $s_r = 0.0001$ |
| | | Poor $m_r = 0.05$, $s_r = 0.00001$ |
| Paired uniaxial compressive strength and modulus of elasticity | $\sigma_c = 50$ MPa, $E = 22$ GPa<br>$\sigma_c = 130$ MPa, $E = 43$ GPa<br>$\sigma_c = 210$ MPa, $E = 65$ GPa<br>$\sigma_c = 300$ MPa, $E = 90$ GPa | |
| In situ stress, $p_o$ (MPa) | 10, 17.5, 31.2, 43.8, 50, 100 | |
| Poisson's ratio, $\nu$ | 0.25 | |
| Unit weight, $\gamma_r$, ($MN/m^3$) | 0.025 | |
| Radius of opening, $r_i$ (m) | 1.5, 3, 6, 9, 15 | |

The calculated values of $u_i/r_i$ are listed in Table 17. The elastic rays based on the results of Table 17 are shown in Fig. 24. The points of the transition curves, shown in Fig. 24, are calculated in Tables 18 and 19. The values of the calculated critical deformation ratios and critical in situ stresses are also given in Fig. 24.

The load-deformation curves for the lowest and highest values of the selected uniaxial compressive strength and elastic modulus pairs are plotted in Figs. 25 and 26 and Figs. 27 and 28, respectively.

Figures 29 and 30 illustrate the extent of broken zones corresponding to the lowest and highest values of selected $\sigma_c$ and E pairs, respectively.

Table 17 -Calculation and listing of $u_1/r_1$ values for rock Type B

| E | $\frac{1+\nu}{E}$ | $u_1/r_1$ for $p_3$ of | | | | | |
|---|---|---|---|---|---|---|---|
| | | 10 | 17.5 | 31.2 | 43.8 | 50 | 100 |
| 22,000 | $5.68\times10^{-5}$ | $5.68\times10^{-4}$ | $9.94\times10^{-4}$ | $1.77\times10^{-3}$ | $2.49\times10^{-3}$ | $2.84\times10^{-3}$ | $5.68\times10^{-3}$ |
| 43,000 | $2.91\times10^{-5}$ | $2.91\times10^{-4}$ | $5.09\times10^{-4}$ | $9.08\times10^{-4}$ | $1.27\times10^{-3}$ | $1.46\times10^{-3}$ | $2.91\times10^{-3}$ |
| 65,000 | $1.92\times10^{-5}$ | $1.92\times10^{-4}$ | $3.36\times10^{-4}$ | $5.99\times10^{-4}$ | $8.41\times10^{-4}$ | $9.60\times10^{-4}$ | $1.92\times10^{-3}$ |
| 90,000 | $1.39\times10^{-5}$ | $1.39\times10^{-4}$ | $2.43\times10^{-4}$ | $4.34\times10^{-4}$ | $6.09\times10^{-4}$ | $6.95\times10^{-4}$ | $1.39\times10^{-3}$ |

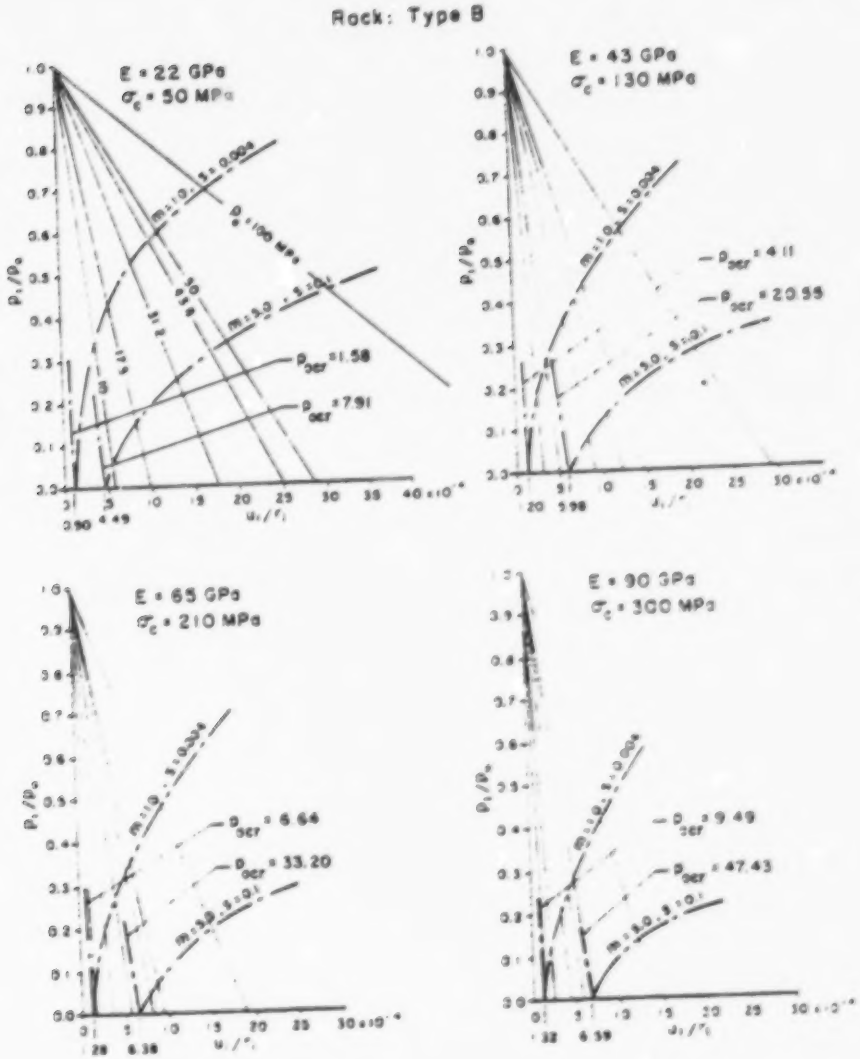


Fig. 24 - Elastic rays of rock Type B

Table 18 - Calculation and listing of $p_{1cr}/p_2$ values for case Type 4

| $p_2$ | | $\sigma_1$ | | | |
|---|---|---|---|---|---|
| | | 90 | 130 | 210 | 330 |
| 18 | $p_3/\sigma_2$ | 0.200 | 0.377 | 0.348 | 0.233 |
| | $5.0\ p_3/\sigma_2$ | 1.000 | 0.185 | 0.240 | 0.168 |
| | $\eta$ | 0.191 | 0.291 | 0.365 | 0.351 |
| | $\eta\ \sigma_2/p_2$ | 0.955 | 1.18₄ | 1.354 | 1.5₄₃ |
| | $p_{1cr}/p_2$ | 0.345 | -0.181 | -0.354 | -0.5₄₃ |
| 27.5 | $p_3/\sigma_2$ | 0.350 | 0.435 | 0.381 | 0.259 |
| | $5.0\ p_3/\sigma_2$ | 1.750 | 0.875 | 0.415 | 0.290 |
| | $\eta$ | 0.299 | 0.140 | 0.396 | 0.374 |
| | $\eta\ \sigma_2/p_2$ | 0.854 | 1.237 | 1.457 | 1.479 |
| | $p_{1cr}/p_2$ | 0.146 | -0.37⁷ | -0.157 | -0.379 |
| 41.2 | $p_3/\sigma_2$ | 0.624 | 0.540 | 0.1₄₃ | 0.0₄ |
| | $5.0\ p_3/\sigma_2$ | 3.120 | 1.400 | 0.7₄₃ | 0.1₄₄ |
| | $\eta$ | 0.469 | 0.821 | 0.6₄₄ | 0.4₄₄ |
| | $\eta\ \sigma_2/p_2$ | 2.752 | 2.921 | 1.013 | 1.0₄₃ |
| | $p_{1cr}/p_2$ | 2.248 | 2.079 | -0.013 | -0.1₄₃ |
| 61.8 | $p_3/\sigma_2$ | 0.979 | 0.137 | 0.209 | 0.1₄₃ |
| | $5.0\ p_3/\sigma_2$ | 4.180 | 1.685 | 1.045 | 0.7₄₃ |
| | $\eta$ | 0.604 | 0.290 | 0.1₄₃ | 0.1₄₃ |
| | $\eta\ \sigma_2/p_2$ | 3.649 | 3.991 | 1.447 | 1.0₄₃ |
| | $p_{1cr}/p_2$ | 3.351 | 2.139 | 0.553 | -0.0₄₃ |
| 93 | $p_3/\sigma_2$ | 1.300 | 0.385 | 0.024 | 0.1₄₃ |
| | $5.0\ p_3/\sigma_2$ | 5.300 | 1.925 | 1.1₄₃ | 0.8₄₃ |
| | $\eta$ | 0.998 | 0.320 | 0.2₄₃ | 0.1₄₃ |
| | $\eta\ \sigma_2/p_2$ | 3.999 | 3.939 | 0.924 | 1.0₄₃ |
| | $p_{1cr}/p_2$ | 3.334 | 2.0₄₃ | 0.3₄₃ | 0.0₄₃ |
| 130 | $p_3/\sigma_2$ | 2.300 | 0.799 | 0.1₄₃ | 0.1₄₃ |
| | $5.0\ p_3/\sigma_2$ | 10.000 | 3.995 | 2.1₄₃ | 0.5₄₃ |
| | $\eta$ | 1.281 | 0.466 | 0.2₄₃ | 0.1₄₃ |
| | $\eta\ \sigma_2/p_2$ | 3.542 | 3.713 | 0.7₄₃ | 0.8₄₃ |
| | $p_{1cr}/p_2$ | 2.458 | 2.287 | 0.2₄₃ | 0.1₄₃ |

$n = 5.0,\quad p = 2.2$

$$\eta = \frac{1}{2}\sqrt{\left(\frac{5+2}{6}\right)^2 - 5.0\ p_3/\sigma_2} - \left(\frac{5+2}{6}\right)^{1/2} = 5.2/6$$

$$\eta = \frac{1}{2}\left(1.663 - 5.0\ p_3/\sigma_2\right)^{1/2} - 0.629$$

Table 19- Calculation and listing of $p_{ter}/p_o$ values for rock Type 3

| $p_o$ | | $\sigma_c$ | | | |
|---|---|---|---|---|---|
| | | 50 | 130 | 2.2 | 300 |
| 10 | $p_o/\sigma_c$ | 0.200 | 0.077 | 0.048 | 0.033 |
| | 1.0 $p_o/\sigma_c$ | 0.200 | 0.077 | 0.048 | 0.033 |
| | M | 0.133 | 0.065 | 0.044 | 0.031 |
| | M $\sigma_c/p_o$ | 0.665 | 0.388 | 0.937 | 1.000 |
| | $p_{ter}/p_o$ | 0.335 | 0.156 | 0.063 | |
| 17.5 | $p_o/\sigma_c$ | 0.350 | 0.135 | 0.083 | 0.058 |
| | 1.0 $p_o/\sigma_c$ | 0.350 | 0.135 | 0.083 | 0.058 |
| | M | 0.198 | 0.100 | 0.069 | 0.052 |
| | M $\sigma_c/p_o$ | 0.566 | 0.741 | 0.831 | 0.897 |
| | $p_{ter}/p_o$ | 0.434 | 0.259 | 0.169 | 0.103 |
| 31.2 | $p_o/\sigma_c$ | 0.624 | 0.240 | 0.148 | 0.104 |
| | 1.0 $p_o/\sigma_c$ | 0.624 | 0.240 | 0.148 | 0.104 |
| | M | 0.291 | 0.152 | 0.107 | 0.080 |
| | M $\sigma_c/p_o$ | 0.466 | 0.633 | 0.718 | 0.769 |
| | $p_{ter}/p_o$ | 0.534 | 0.367 | 0.282 | 0.231 |
| 43.8 | $p_o/\sigma_c$ | 0.876 | 0.337 | 0.209 | 0.146 |
| | 1.0 $p_o/\sigma_c$ | 0.876 | 0.337 | 0.209 | 0.146 |
| | M | 0.364 | 0.193 | 0.136 | 0.102 |
| | M $\sigma_c/p_o$ | 0.412 | 0.573 | 0.650 | 0.698 |
| | $p_{ter}/p_o$ | 0.588 | 0.427 | 0.340 | 0.302 |
| 50 | $p_o/\sigma_c$ | 1.000 | 0.385 | 0.238 | 0.167 |
| | 1.0 $p_o/\sigma_c$ | 1.000 | 0.385 | 0.238 | 0.167 |
| | M | 0.391 | 0.211 | 0.151 | 0.114 |
| | M $\sigma_c/p_o$ | 0.391 | 0.548 | 0.634 | 0.684 |
| | $p_{ter}/p_o$ | 0.609 | 0.452 | 0.366 | 0.316 |
| 100 | $p_o/\sigma_c$ | 2.000 | 0.769 | 0.476 | 0.333 |
| | 1.0 $p_o/\sigma_c$ | 2.000 | 0.769 | 0.476 | 0.333 |
| | M | 0.594 | 0.332 | 0.243 | 0.181 |
| | M $\sigma_c/p_o$ | 0.297 | 0.432 | 0.511 | 0.457 |
| | $p_{ter}/p_o$ | 0.703 | 0.568 | 0.489 | 0.429 |

$a = 1.0$, $s = 0.004$

$$M = \frac{1}{2}\left(\left(\frac{1.0}{4}\right)^2 + 1.0\ p_o/\sigma_c + 0.004\right)^{1/2} - 1.0/8$$

$$M = \frac{1}{2}\left(0.067 + 1.0\ p_o/\sigma_c\right)^{1/2} - 0.125$$

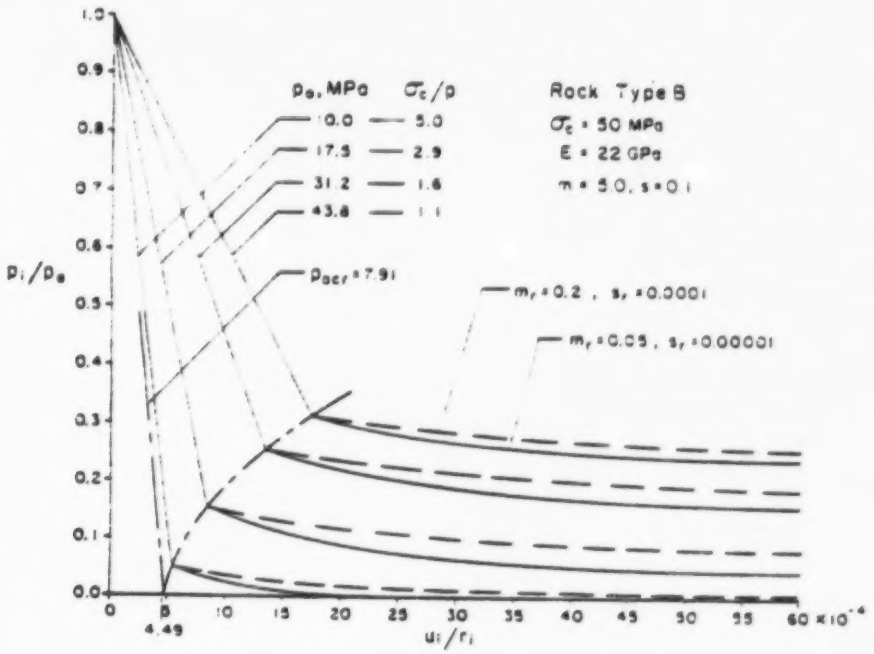


Fig. 25 - Load-deformation curves for rock Type B

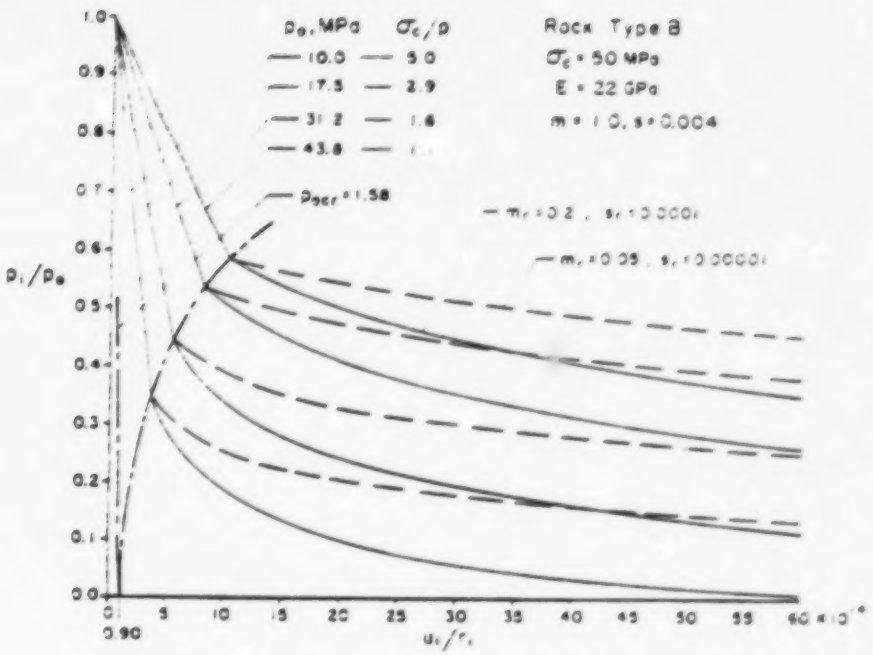


Fig. 26 - Load-deformation curves for rock Type B

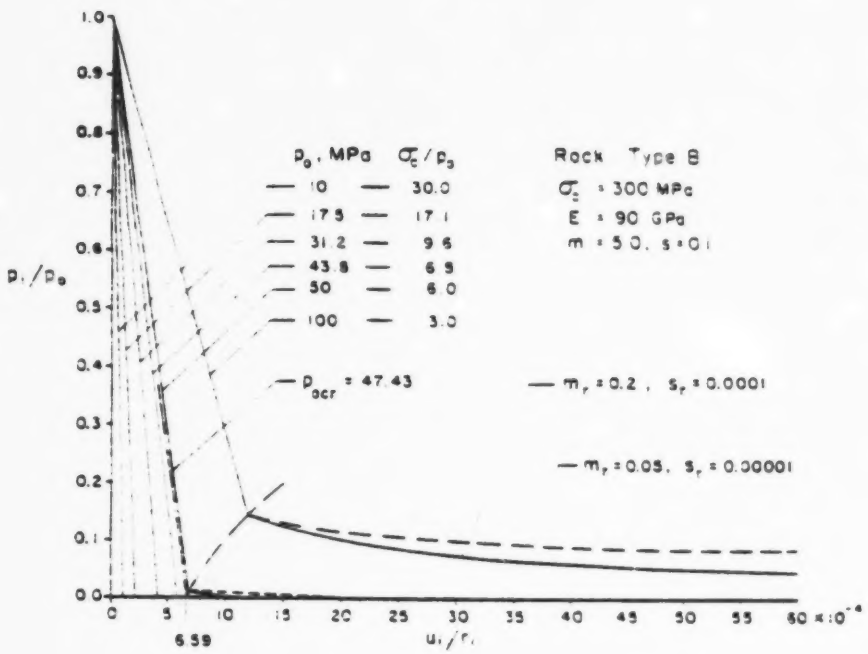


Fig. 27 - Load-deformation curves for rock Type B

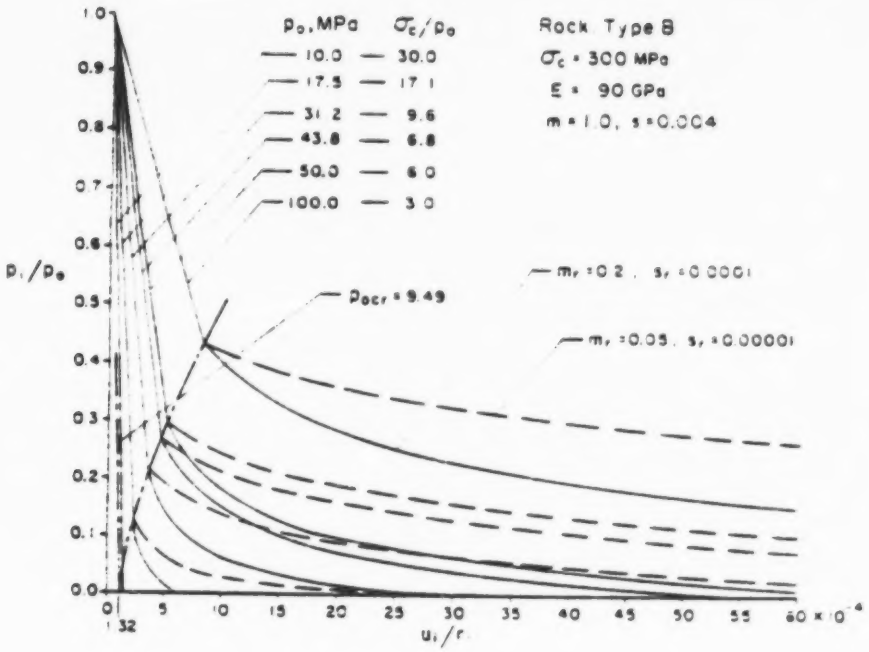


Fig. 28 - Load-deformation curves for rock Type B

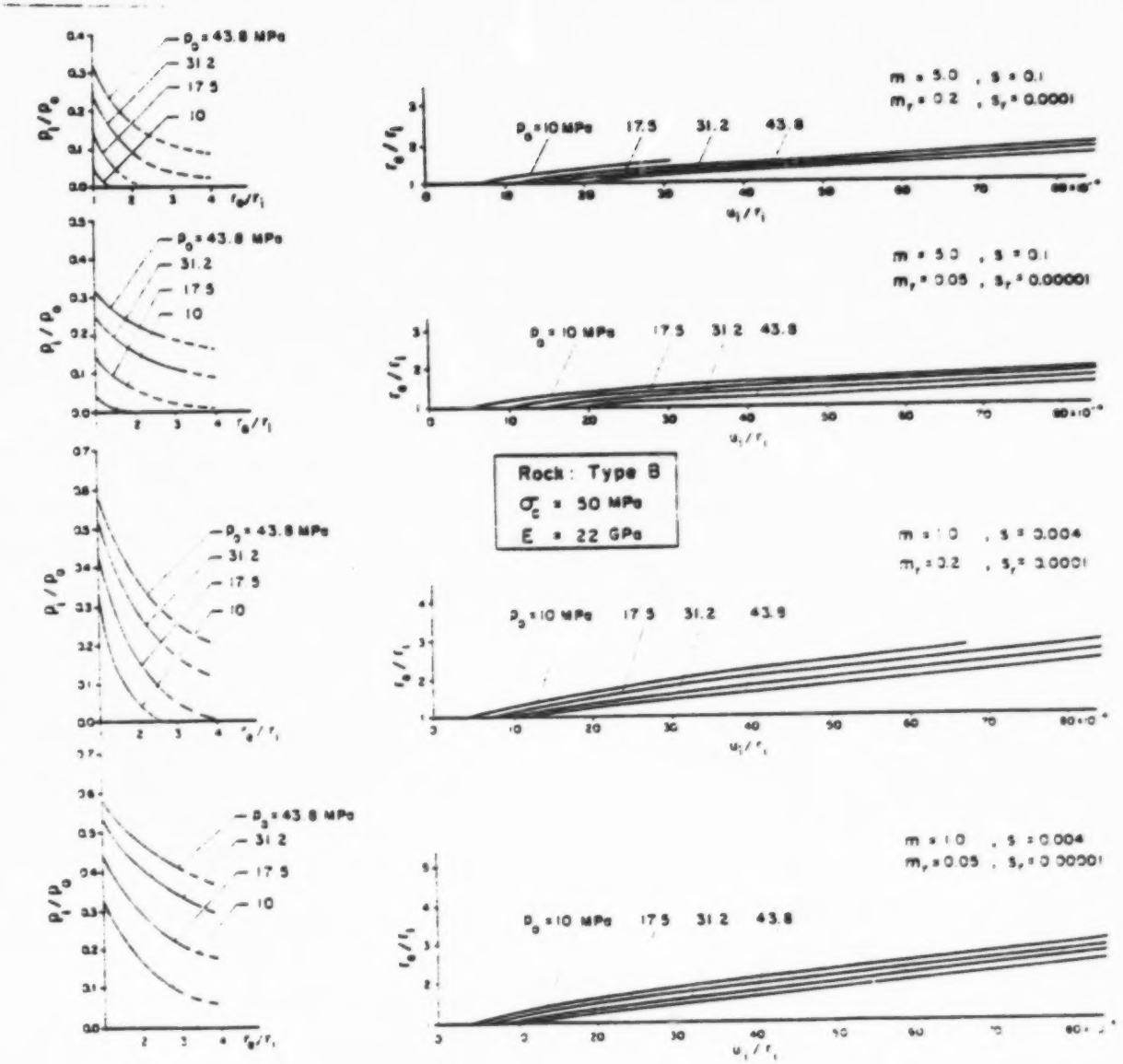


Fig. 29 - Extent of broken zones for rock Type B

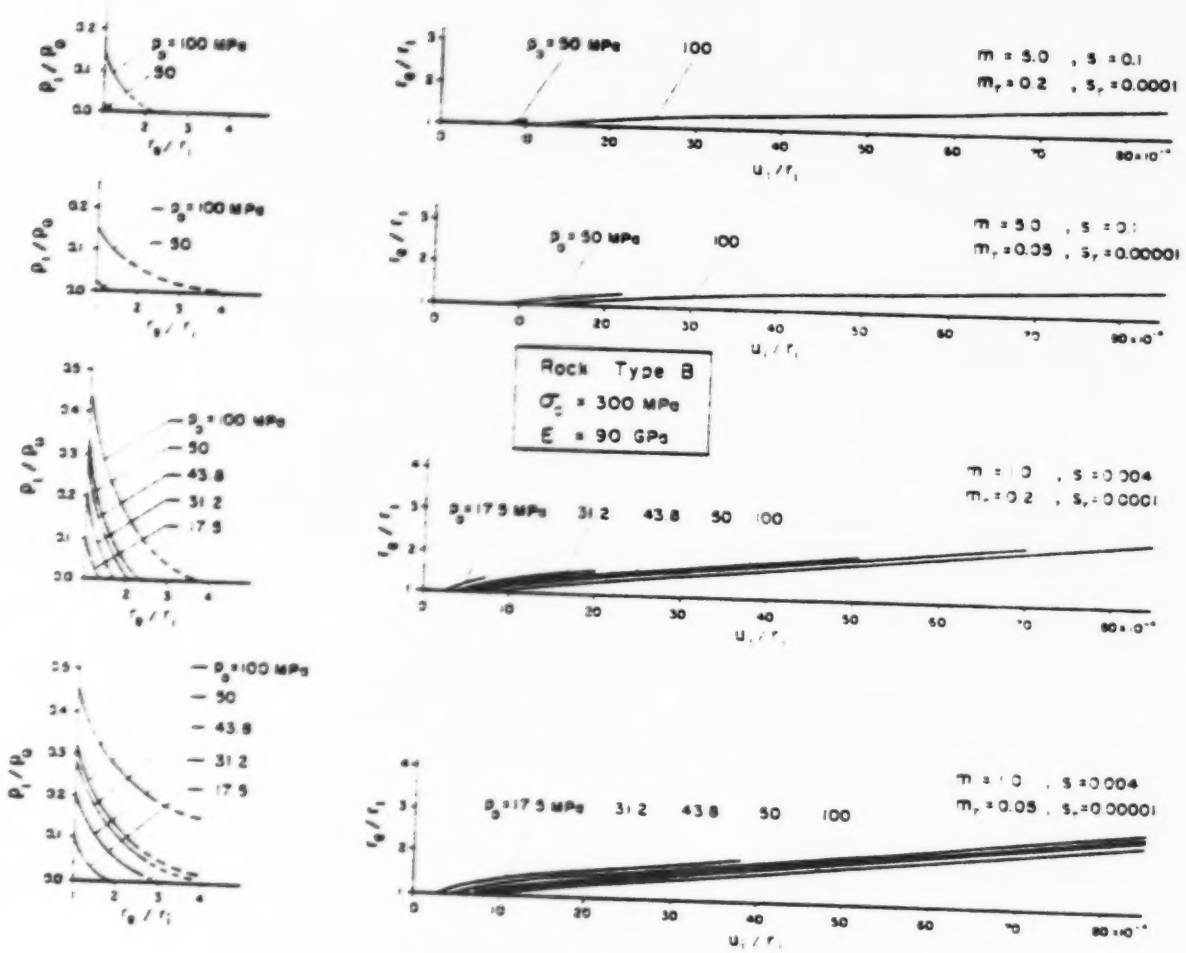


Fig. 30 - Extent of broken zones for rock Type B

ROCK: TYPE C

The computations were made for the systematic combinations of the selected values of variables listed in Table 20.

Table 20 - Listing of selected values of variables for rock Type C

| Variables | Selected values | |
|---|---|---|
| Material constants | Original rock mass quality | Very good $m = 7.5$, $s = 0.1$ |
| | | Good $m = 1.5$, $s = 0.004$ |
| | Broken rock mass quality | Fair $m_r = 0.3$, $s_r = 0.0001$ |
| | | Poor $m_r = 0.08$, $s_r = 0.00001$ |
| Paired uniaxial compressive strength and modulus of elasticity | $\sigma_c$ = 60 MPa, E = 18 GPa<br>$\sigma_c$ = 165 MPa, E = 40 GPa<br>$\sigma_c$ = 270 MPa, E = 63 GPa<br>$\sigma_c$ = 375 MPa, E = 86 GPa | |
| In situ stress, $p_o$ (MPa) | 11, 19.2, 34.4, 48.1, 55, 110 | |
| Poisson's ratio, $\nu$ | 0.25 | |
| Unit weight, $\gamma_r$, ($MN/m^3$) | 0.0275 | |
| Radius of opening, $r_i$ (m) | 1.5, 3, 6, 9, 15 | |

The calculated values of $u_i/r_i$ are listed in Table 21. The elastic rays based on the results of Table 21 are shown in Fig. 31. The points of the transition curves, shown in Fig. 31, are calculated in Tables 22 and 23. The values of the calculated critical deformation ratios and critical in situ stresses are also given in Fig. 31.

The load-deformation curves for the lowest and highest values of the selected uniaxial compressive strength and elastic modulus pairs are plotted in Figs. 32 and 33 and Figs. 34 and 35, respectively.

Figures 36 and 37 illustrate the extent of broken zones corresponding to the lowest and highest values of selected $\sigma_c$ and E pairs, respectively.

Table 21 - Calculation and listing of $u_i/r_i$ values for rock Type C

| E | $\frac{1+\nu}{E}$ | $u_i/r_i$ for $p_o$ of | | | | | |
|---|---|---|---|---|---|---|---|
| | | 11 | 19.2 | 34.4 | 48.1 | 55 | 110 |
| 18,000 | $6.94\times10^{-5}$ | $7.64\times10^{-4}$ | $1.33\times10^{-3}$ | $2.39\times10^{-3}$ | $3.34\times10^{-3}$ | $3.82\times10^{-3}$ | $7.64\times10^{-3}$ |
| 40,000 | $3.13\times10^{-5}$ | $3.44\times10^{-4}$ | $6.00\times10^{-4}$ | $1.08\times10^{-3}$ | $1.50\times10^{-3}$ | $1.72\times10^{-3}$ | $3.44\times10^{-3}$ |
| 63,000 | $1.98\times10^{-5}$ | $2.18\times10^{-4}$ | $3.81\times10^{-4}$ | $6.83\times10^{-4}$ | $9.54\times10^{-4}$ | $1.09\times10^{-3}$ | $2.18\times10^{-3}$ |
| 86,000 | $1.45\times10^{-5}$ | $1.60\times10^{-4}$ | $2.79\times10^{-4}$ | $5.00\times10^{-4}$ | $6.99\times10^{-4}$ | $7.99\times10^{-4}$ | $1.60\times10^{-3}$ |

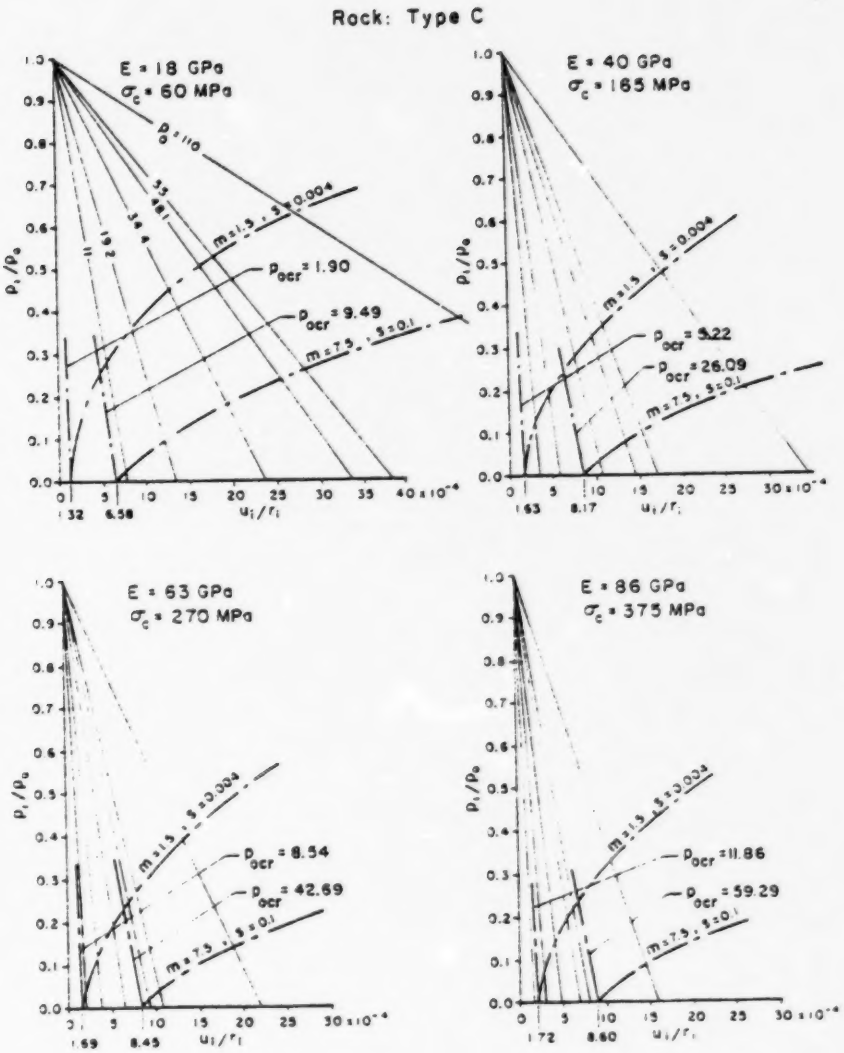


Fig. 31 - Elastic rays of rock Type C

Table 22- Calculation and listing of $P_{ter}/P_o$ values for rock Type 2

| $P_o$ | | $\sigma_c$ | | | |
|---|---|---|---|---|---|
| | | 60 | 165 | 270 | 375 |
| 11 | $P_o/\sigma_c$ | 0.183 | 0.067 | 0.041 | 0.029 |
| | $7.5\ P_o/\sigma_c$ | 1.373 | 0.503 | 0.308 | 0.218 |
| | M | 0.179 | 0.077 | 0.052 | 0.041 |
| | $M\ \sigma_c/P_o$ | 0.978 | 1.149 | 1.268 | 1.414 |
| | $P_{ter}/P_o$ | 0.022 | -0.149 | -0.268 | -0.414 |
| 19.2 | $P_o/\sigma_c$ | 0.320 | 0.116 | 0.071 | 0.051 |
| | $7.5\ P_o/\sigma_c$ | 2.400 | 0.870 | 0.533 | 0.383 |
| | M | 0.288 | 0.121 | 0.080 | 0.062 |
| | $M\ \sigma_c/P_o$ | 0.900 | 1.043 | 1.127 | 1.213 |
| | $P_{ter}/P_o$ | 0.100 | -0.043 | -0.127 | -0.213 |
| 34.4 | $P_o/\sigma_c$ | 0.573 | 0.208 | 0.127 | 0.092 |
| | $7.5\ P_o/\sigma_c$ | 4.298 | 1.560 | 0.953 | 0.690 |
| | M | 0.469 | 0.200 | 0.131 | 0.100 |
| | $M\ \sigma_c/P_o$ | 0.818 | 0.962 | 1.031 | 1.087 |
| | $P_{ter}/P_o$ | 0.182 | 0.038 | -0.031 | -0.087 |
| 48.1 | $P_o/\sigma_c$ | 0.802 | 0.292 | 0.179 | 0.129 |
| | $7.5\ P_o/\sigma_c$ | 6.015 | 2.190 | 1.335 | 0.960 |
| | M | 0.614 | 0.267 | 0.175 | 0.132 |
| | $M\ \sigma_c/P_o$ | 0.766 | 0.914 | 0.983 | 1.031 |
| | $P_{ter}/P_o$ | 0.234 | 0.086 | 0.017 | -0.031 |
| 55 | $P_o/\sigma_c$ | 0.917 | 0.333 | 0.204 | 0.147 |
| | $7.5\ P_o/\sigma_c$ | 6.878 | 2.498 | 1.530 | 1.103 |
| | M | 0.682 | 0.298 | 0.196 | 0.148 |
| | $M\ \sigma_c/P_o$ | 0.744 | 0.895 | 0.961 | 1.007 |
| | $P_{ter}/P_o$ | 0.256 | 0.105 | 0.039 | -0.007 |
| 110 | $P_o/\sigma_c$ | 1.833 | 0.667 | 0.407 | 0.293 |
| | $7.5\ P_o/\sigma_c$ | 13.748 | 5.003 | 3.053 | 2.198 |
| | M | 1.146 | 0.530 | 0.353 | 0.268 |
| | $M\ \sigma_c/P_o$ | 0.625 | 0.795 | 0.867 | 0.913 |
| | $P_{ter}/P_o$ | 0.375 | 0.205 | 0.133 | 0.086 |

$a = 7.5, \quad s = 0.1$

$$M = \frac{1}{2}\left(\left(\frac{7.5}{4}\right)^2 + 7.5\ P_o/\sigma_c + 0.1\right)^{1/2} - 7.5/8$$

$$M = \frac{1}{2}\left(3.616 + 7.5\ P_o/\sigma_c\right)^{1/2} - 0.938$$

22

Table 23 - Calculation and listing of $p_{ler}/p_o$ values for rock Type I

| $p_o$ | | $\theta_c$ | | | |
|---|---|---|---|---|---|
| | | 60 | 165 | 270 | 275 |
| 11 | $p_o/\theta_c$ | 0.183 | 0.067 | 0.041 | 0.039 |
| | 1.5 $p_o/\theta_c$ | 0.275 | 0.101 | 0.062 | 0.059 |
| | M | 0.136 | 0.060 | 0.039 | 0.039 |
| | M $\theta_c/p_o$ | 0.743 | 0.896 | 0.951 | 1.000 |
| | $p_{ler}/p_o$ | 0.257 | 0.104 | 0.049 | 0 |
| 14.2 | $p_o/\theta_c$ | 0.320 | 0.116 | 0.071 | 0.068 |
| | 1.5 $p_o/\theta_c$ | 0.480 | 0.174 | 0.107 | 0.102 |
| | M | 0.207 | 0.094 | 0.063 | 0.060 |
| | M $\theta_c/p_o$ | 0.647 | 0.810 | 0.887 | 0.941 |
| | $p_{ler}/p_o$ | 0.353 | 0.190 | 0.113 | 0.059 |
| 34.4 | $p_o/\theta_c$ | 0.573 | 0.208 | 0.127 | 0.123 |
| | 1.5 $p_o/\theta_c$ | 0.860 | 0.312 | 0.191 | 0.185 |
| | M | 0.312 | 0.150 | 0.102 | 0.099 |
| | M $\theta_c/p_o$ | 0.546 | 0.721 | 0.803 | 0.846 |
| | $p_{ler}/p_o$ | 0.454 | 0.279 | 0.197 | 0.154 |
| 48.1 | $p_o/\theta_c$ | 0.802 | 0.292 | 0.178 | 0.173 |
| | 1.5 $p_o/\theta_c$ | 1.203 | 0.438 | 0.267 | 0.260 |
| | M | 0.393 | 0.194 | 0.133 | 0.130 |
| | M $\theta_c/p_o$ | 0.490 | 0.664 | 0.747 | 0.751 |
| | $p_{ler}/p_o$ | 0.510 | 0.336 | 0.253 | 0.249 |
| 55 | $p_o/\theta_c$ | 0.917 | 0.333 | 0.204 | 0.197 |
| | 1.5 $p_o/\theta_c$ | 1.376 | 0.500 | 0.306 | 0.296 |
| | M | 0.429 | 0.214 | 0.148 | 0.144 |
| | M $\theta_c/p_o$ | 0.468 | 0.643 | 0.726 | 0.729 |
| | $p_{ler}/p_o$ | 0.532 | 0.357 | 0.274 | 0.271 |
| 110 | $p_o/\theta_c$ | 1.833 | 0.667 | 0.407 | 0.393 |
| | 1.5 $p_o/\theta_c$ | 2.750 | 1.001 | 0.611 | 0.590 |
| | M | 0.563 | 0.347 | 0.247 | 0.234 |
| | M $\theta_c/p_o$ | 0.362 | 0.520 | 0.607 | 0.662 |
| | $p_{ler}/p_o$ | 0.638 | 0.480 | 0.393 | 0.338 |

$\eta = 1.5, \quad s = 0.004$

$$M = \frac{1}{2}\left(\left(\frac{1.5}{4}\right)^2 + 1.5\ p_o/\theta_c + 0.004\right)^{1/2} - 1.5/8$$

$$M = \frac{1}{2}\left(0.145 + 1.5\ p_o/\theta_c\right)^{1/2} - 0.188$$

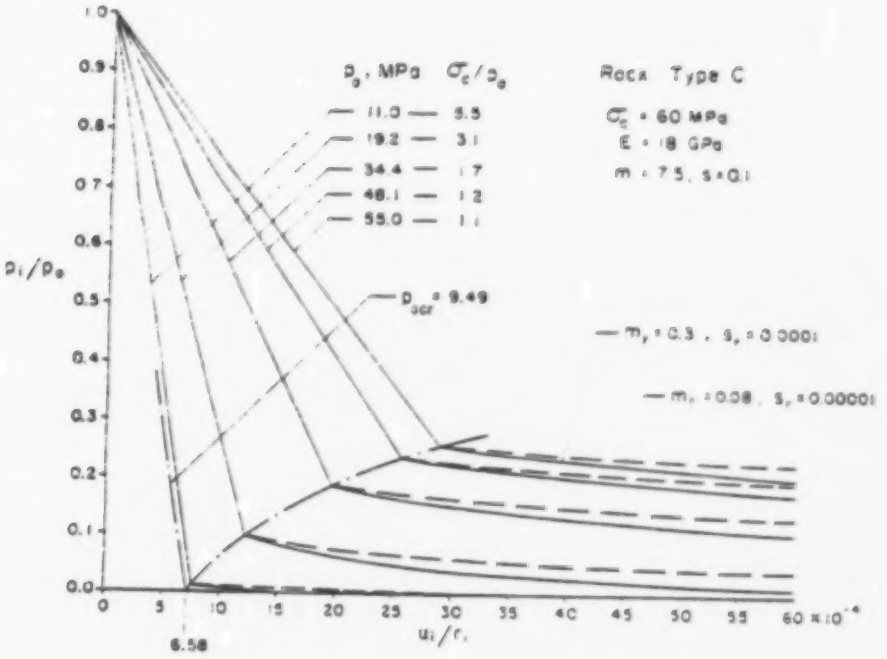


Fig. 32 - Load-deformation curves for rock Type C

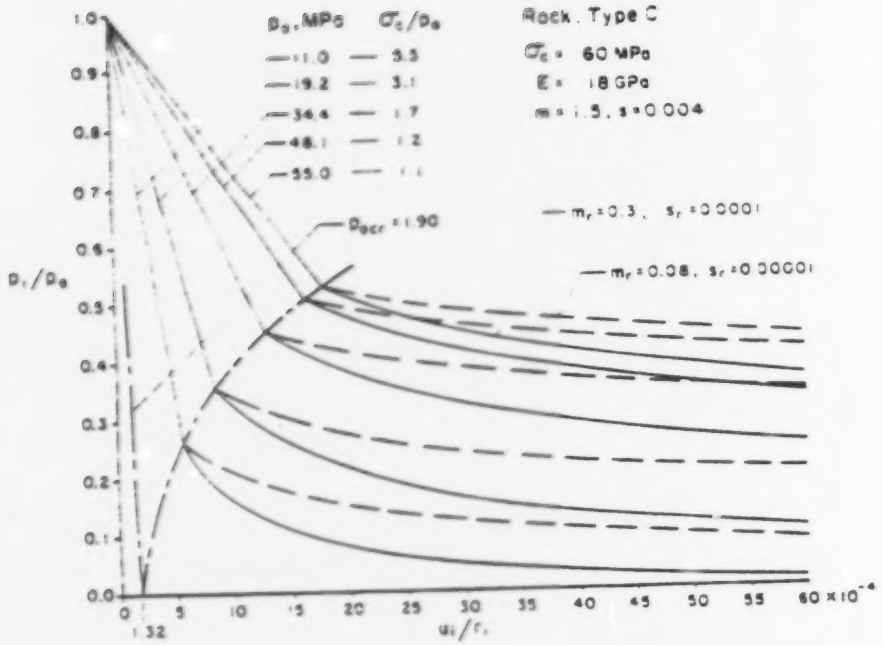


Fig. 33 - Load-deformation curves for rock Type C

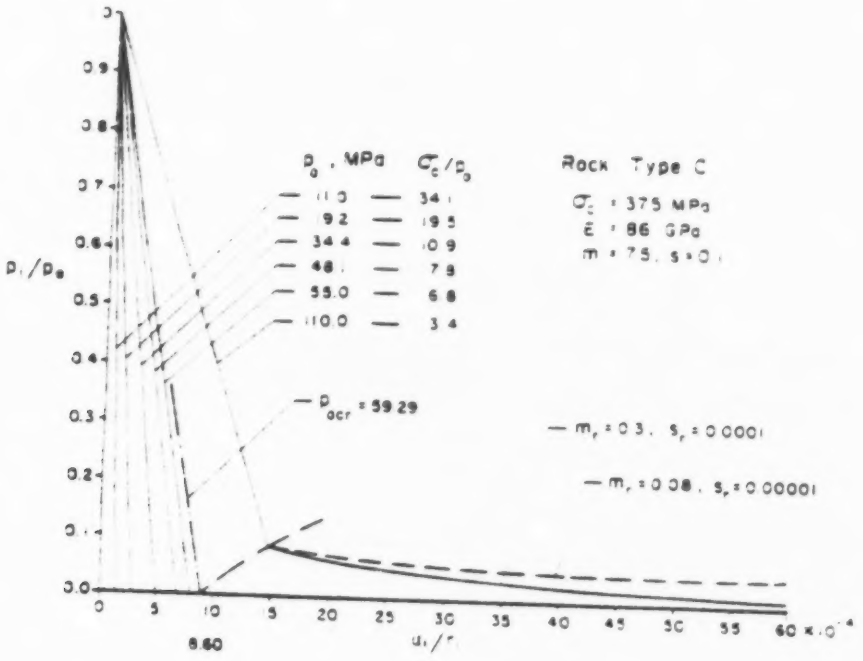


Fig. 34 - Load-deformation curves for rock Type C

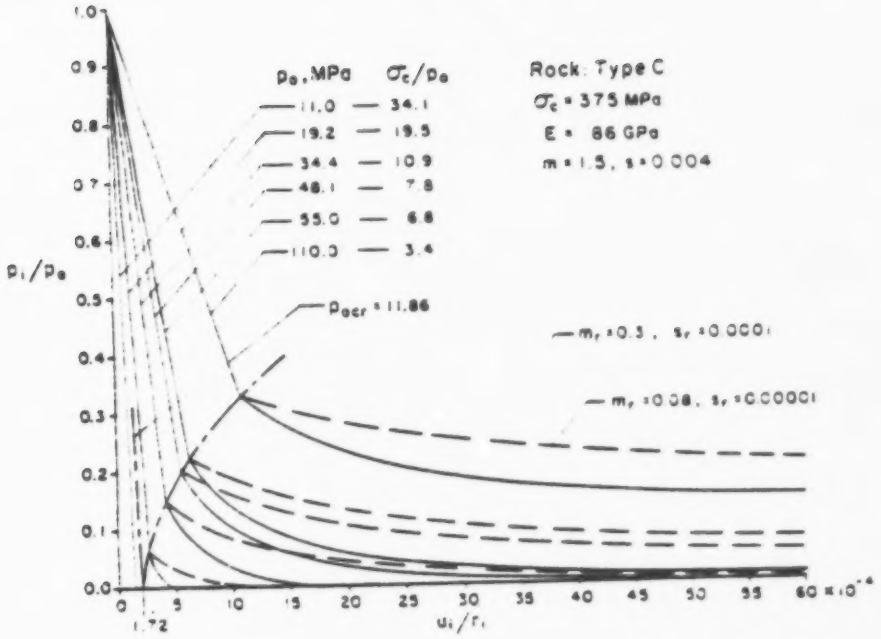


Fig. 35 - Load-deformation curves for rock Type C

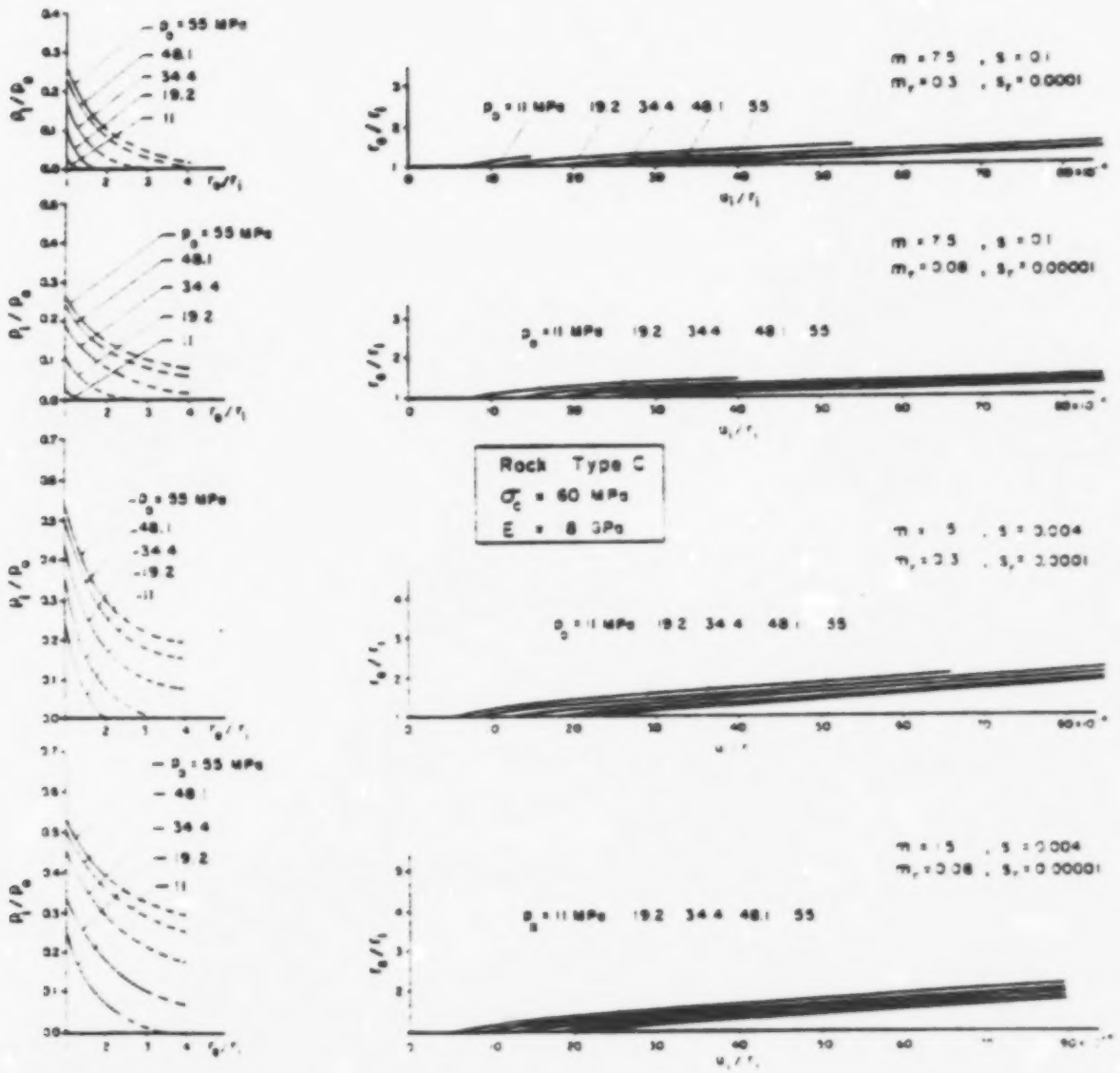


Fig. 36 - Extent of broken zones for rock Type C

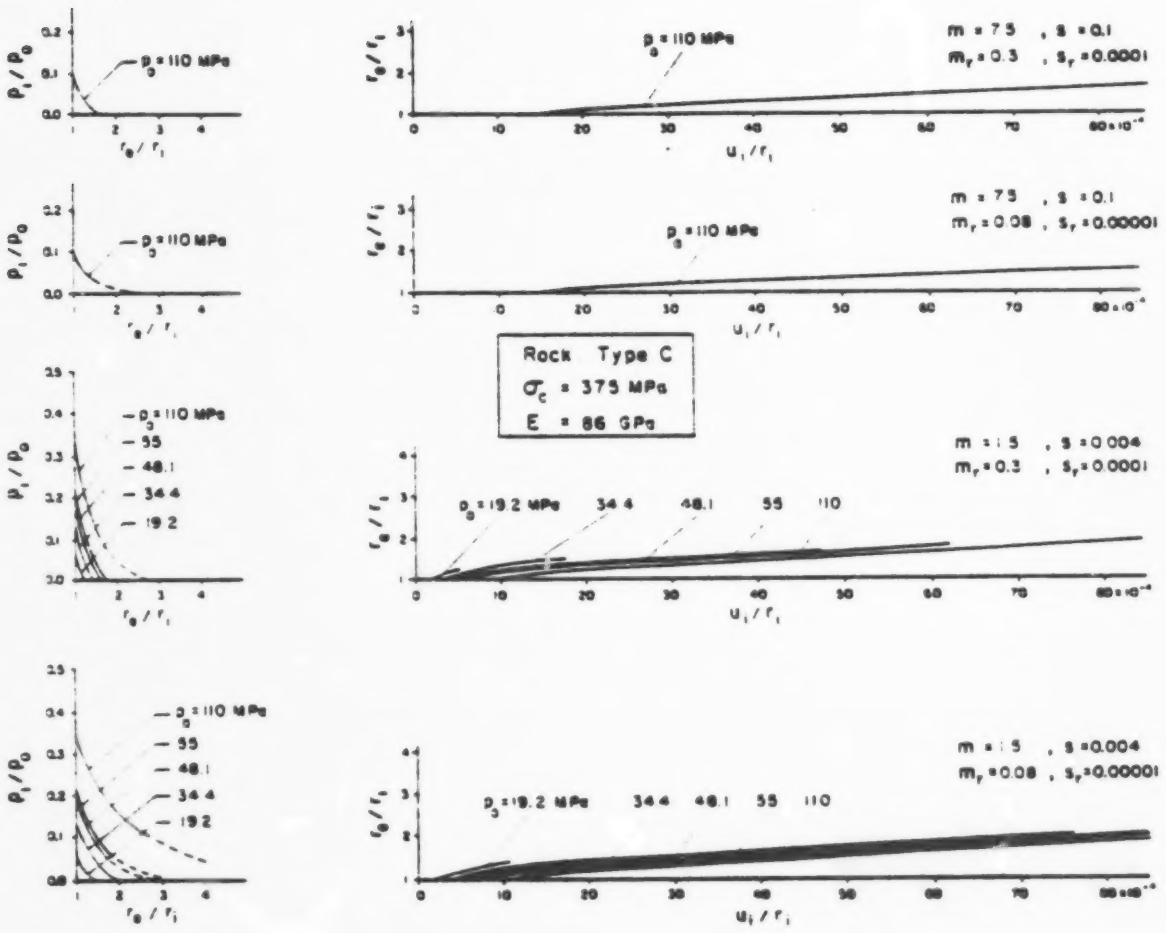


Fig. 37 - Extent of broken zones for rock Type C

ROCK: TYPE D

The computations were made for the systematic combinations of the selected values of variables listed in Table 24.

Table 24 - Listing of selected values of variables for rock Type D

| Variables | Selected values | |
|---|---|---|
| Material constants | Original rock mass quality | Very good $m = 8.5$, $s = 0.1$ |
| | | Good $m = 1.7$, $s = 0.004$ |
| | Broken rock mass quality | Fair $m_r = 0.34$, $s_r = 0.0001$ |
| | | Poor $m_r = 0.09$, $s_r = 0.00001$ |
| Paired uniaxial compressive strength and modulus of elasticity | $\sigma_c$ = 90 MPa, E = 41 GPa<br>$\sigma_c$ = 195 MPa, E = 62 GPa<br>$\sigma_c$ = 300 MPa, E = 84 GPa<br>$\sigma_c$ = 400 MPa, E = 104 GPa | |
| In situ stress, $p_o$ (MPa) | 12, 21, 37.5, 52.5, 60, 120 | |
| Poisson's ratio, $\nu$ | 0.25 | |
| Unit weight, $\gamma_r$, ($MN/m^3$) | 0.03 | |
| Radius of opening, $r_i$ (m) | 1.5, 3, 6, 9, 15 | |

The calculated values of $u_i/r_i$ are listed in Table 25. The elastic rays based on the results of Table 25 are shown in Fig. 38. The points of the transition curves, shown in Fig. 38, are calculated in Tables 26 and 27. The values of the calculated critical deformation ratios and critical in situ stresses are also given in Fig. 38.

The load-deformation curves for the lowest and highest values of the selected uniaxial compressive strength and elastic modulus pairs are plotted in Figs. 39 and 40 and Figs. 41 and 42, respectively.

Figures 43 and 44 illustrate the extent of broken zones corresponding to the lowest and highest values of selected $\sigma_c$ and E pairs, respectively.

Table 23.-Calculation and listing of $u_1/r_1$ values for rock Type 3

| E | $\frac{1 - \nu}{E}$ | $u_1/r_1$ for $p_2$ of | | | | | |
|---|---|---|---|---|---|---|---|
| | | 12 | 21 | 37.4 | 62.5 | 90 | 120 |
| 41,300 | $1.95 \times 10^{-5}$ | $3.66 \times 10^{-4}$ | $6.41 \times 10^{-4}$ | $1.16 \times 10^{-3}$ | $1.90 \times 10^{-3}$ | $1.93 \times 10^{-3}$ | $3.90 \times 10^{-3}$ |
| 92,300 | $2.32 \times 10^{-5}$ | $2.42 \times 10^{-4}$ | $4.24 \times 10^{-4}$ | $7.17 \times 10^{-4}$ | $1.06 \times 10^{-3}$ | $1.21 \times 10^{-3}$ | $2.42 \times 10^{-3}$ |
| 84,000 | $1.49 \times 10^{-5}$ | $1.79 \times 10^{-4}$ | $3.13 \times 10^{-4}$ | $5.59 \times 10^{-4}$ | $7.82 \times 10^{-4}$ | $9.04 \times 10^{-4}$ | $1.79 \times 10^{-3}$ |
| 104,300 | $1.20 \times 10^{-5}$ | $1.44 \times 10^{-4}$ | $2.52 \times 10^{-4}$ | $4.50 \times 10^{-4}$ | $6.30 \times 10^{-4}$ | $7.20 \times 10^{-4}$ | $1.44 \times 10^{-3}$ |

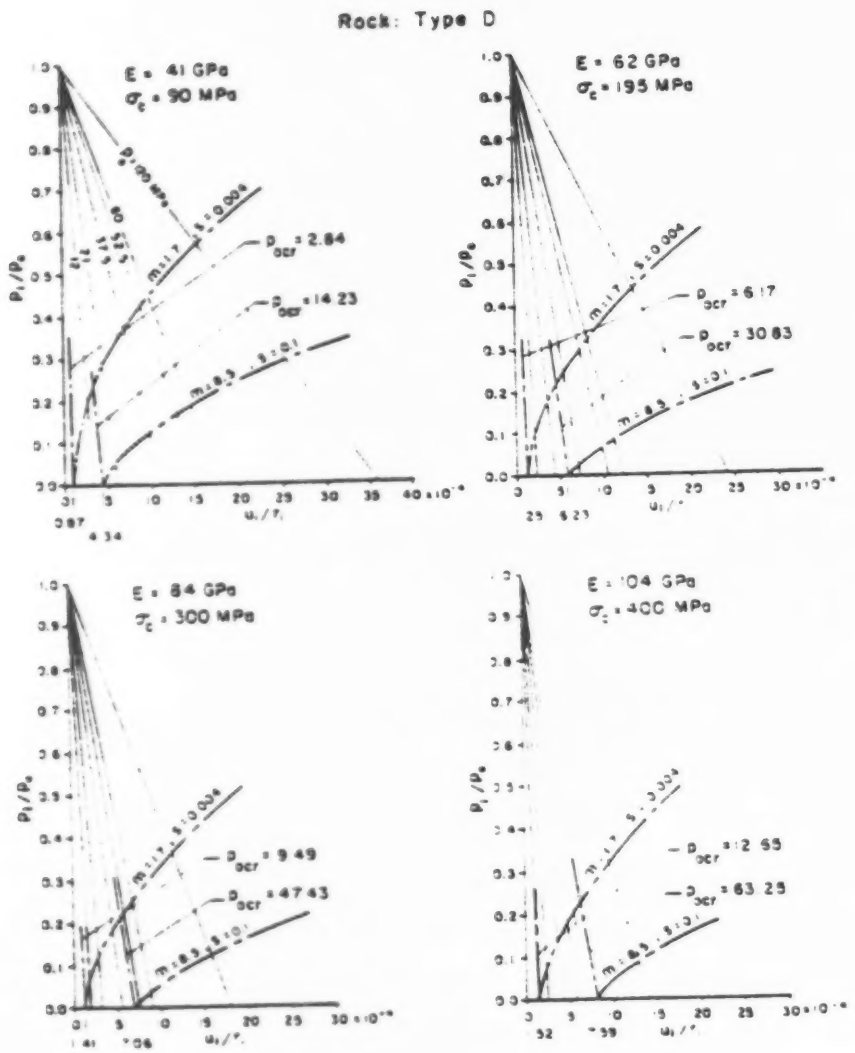


Fig. 38 - Elastic rays of rock Type D

Table 26- Calculation and listing of $P_{ter}/P_o$ values for rock type 3

| $P_o$ | | $\sigma_c$ | | | |
|---|---|---|---|---|---|
| | | 90 | 195 | 300 | 400 |
| 12 | $P_o/\sigma_c$ | 0.133 | 0.062 | 0.040 | 0.030 |
| | $8.5\ P_o/\sigma_c$ | 1.131 | 0.527 | 0.340 | 0.255 |
| | M | 0.136 | 0.071 | 0.050 | 0.04. |
| | $M\ \sigma_c/P_o$ | 1.023 | 1.145 | 1.250 | 1.36? |
| | $P_{ter}/P_o$ | -0.023 | -0.145 | -0.250 | -0.36? |
| 21 | $P_o/\sigma_c$ | 0.233 | 0.108 | 0.070 | 0.053 |
| | $8.5\ P_o/\sigma_c$ | 1.981 | 0.918 | 0.595 | 0.45. |
| | M | 0.221 | 0.113 | 0.079 | 0.062 |
| | $M\ \sigma_c/P_o$ | 0.948 | 1.046 | 1.114 | ..70 |
| | $P_{ter}/P_o$ | 0.052 | -0.046 | -0.114 | -0.17? |
| 37.5 | $P_o/\sigma_c$ | 0.417 | 0.192 | 0.125 | 0.. 94 |
| | $8.5\ P_o/\sigma_c$ | 3.545 | 1.632 | 1.063 | 0.794 |
| | M | 0.365 | 0.187 | 0.123 | 0.0.. |
| | $M\ \sigma_c/P_o$ | 0.875 | 0.978 | 1.032 | 1.074 |
| | $P_{ter}/P_o$ | 0.125 | 0.026 | -0.032 | -0.074 |
| 52.5 | $P_o/\sigma_c$ | 0.583 | 0.269 | 0.175 | 0.131 |
| | $8.5\ P_o/\sigma_c$ | 4.956 | 2.287 | 1.488 | ..14 |
| | M | 0.484 | 0.251 | 0.172 | 0.134 |
| | $M\ \sigma_c/P_o$ | 0.830 | 0.933 | 0.983 | 1.023 |
| | $P_{ter}/P_o$ | 0.170 | 0.067 | 0.017 | -0.023 |
| 90 | $P_o/\sigma_c$ | 0.987 | 0.308 | 0.300 | 0.150 |
| | $8.5\ P_o/\sigma_c$ | 5.870 | 2.618 | ..700 | 1.275 |
| | M | 0.541 | 0.282 | 0.194 | 0.15. |
| | $M\ \sigma_c\ P_o$ | 0.811 | 0.916 | 0.970 | ..07 |
| | $P_{ter}/P_o$ | 0.189 | 0.084 | 0.0.. | -0.0. |
| 120 | $P_o/\sigma_c$ | 1.333 | 0.615 | 0.400 | 0.300 |
| | $8.5\ P_o/\sigma_c$ | 11.331 | 5.229 | 3.400 | 2.550 |
| | M | 0.334 | 0.606 | 0.253 | 0.1.5 |
| | $M\ \sigma_c/P_o$ | 0.701 | 0.823 | 0.883 | 0.917 |
| | $P_{ter}/P_o$ | 0.299 | 0.177 | 0.117 | 0.083 |

$\sigma = 0.5$, $\sigma = 0.1$

$$M = \frac{1}{2}\left(\left(\frac{0.5}{4}\right)^2 + 8.5\ P_o/\sigma_c + 0.1\right)^{1/2} - 0.5/8$$

$$M = \frac{1}{2}\left(0.016 + 8.5\ P_o/\sigma_c\right)^{1/2} - 1.063$$

26

Table 27- Calculation and listing of $p_{ter}/p_o$ values for rock Type 3

| $p_o$ | | $\sigma_c$ | | | |
|---|---|---|---|---|---|
| | | 90 | 195 | 300 | 400 |
| 12 | $p_o/\sigma_c$ | 0.133 | 0.062 | 0.040 | 0.030 |
| | 1.7 $p_o/\sigma_c$ | 0.226 | 0.105 | 0.068 | 0.051 |
| | M | 0.107 | 0.056 | 0.038 | 0.030 |
| | M $\sigma_c/p_o$ | 0.805 | 0.903 | 0.950 | 1.000 |
| | $p_{ter}/p_o$ | 0.195 | 0.097 | 0.050 | 0 |
| 21 | $p_o/\sigma_c$ | 0.233 | 0.108 | 0.070 | 0.053 |
| | 1.7 $p_o/\sigma_c$ | 0.396 | 0.184 | 0.119 | 0.090 |
| | M | 0.168 | 0.091 | 0.063 | 0.049 |
| | M $\sigma_c/p_o$ | 0.721 | 0.843 | 0.900 | 0.934 |
| | $p_{ter}/p_o$ | 0.279 | 0.157 | 0.100 | 0.076 |
| 37.5 | $p_o/\sigma_c$ | 0.417 | 0.192 | 0.125 | 0.094 |
| | 1.7 $p_o/\sigma_c$ | 0.709 | 0.325 | 0.213 | 0.160 |
| | M | 0.250 | 0.144 | 0.102 | 0.081 |
| | M $\sigma_c/p_o$ | 0.624 | 0.750 | 0.816 | 0.862 |
| | $p_{ter}/p_o$ | 0.376 | 0.250 | 0.184 | 0.138 |
| 52.5 | $p_o/\sigma_c$ | 0.583 | 0.269 | 0.175 | 0.131 |
| | 1.7 $p_o/\sigma_c$ | 0.991 | 0.457 | 0.298 | 0.223 |
| | M | 0.329 | 0.188 | 0.134 | 0.106 |
| | M $\sigma_c/p_o$ | 0.564 | 0.699 | 0.766 | 0.803 |
| | $p_{ter}/p_o$ | 0.436 | 0.301 | [illegible] | [illegible] |
| 60 | $p_o/\sigma_c$ | 0.667 | [illegible] | [illegible] | [illegible] |
| | 1.7 $p_o/\sigma_c$ | 1.134 | 0.524 | [illegible] | [illegible] |
| | M | 0.361 | 0.208 | 0.149 | [illegible] |
| | M $\sigma_c/p_o$ | 0.541 | 0.675 | 0.745 | 0.793 |
| | $p_{ter}/p_o$ | 0.459 | 0.325 | 0.255 | 0.207 |
| 120 | $p_o/\sigma_c$ | 1.333 | 0.615 | 0.400 | 0.300 |
| | 1.7 $p_o/\sigma_c$ | 2.266 | 1.046 | 0.680 | 0.510 |
| | M | 0.570 | 0.342 | 0.242 | 0.204 |
| | M $\sigma_c/p_o$ | 0.428 | 0.556 | 0.630 | 0.680 |
| | $p_{ter}/p_o$ | 0.572 | 0.444 | 0.370 | 0.320 |

$a = 1.7$, $s = 0.004$

$$M = \frac{1}{2}\left(\left(\frac{1.7}{4}\right)^2 + 1.7\ p_o/\sigma_c + 0.004\right)^{1/2} - 1.7/8$$

$$M = \frac{1}{2}\left(0.185 + 1.7\ p_o/\sigma_c\right)^{1/2} - 0.213$$

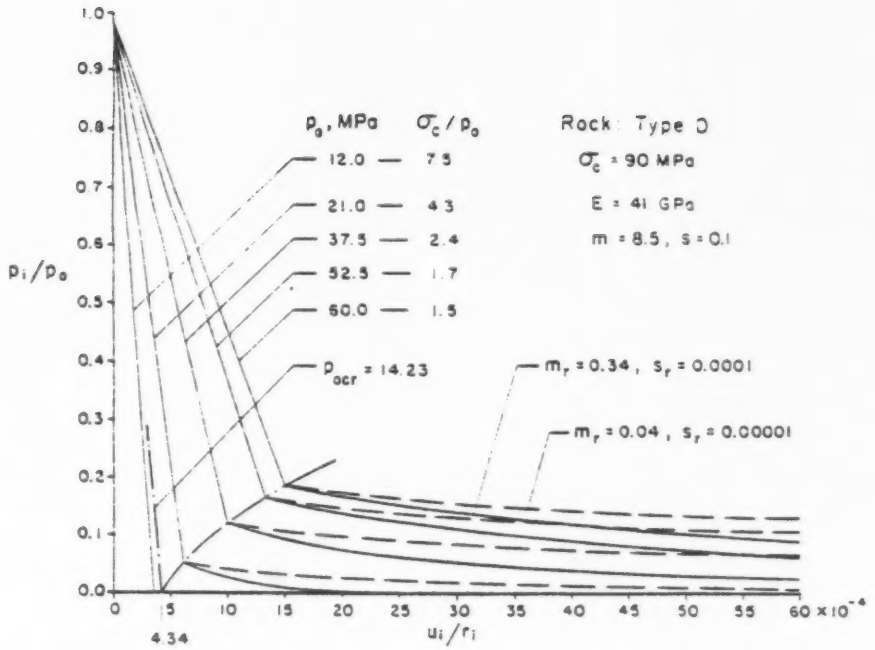


Fig. 39 - Load-deformation curves for rock Type D

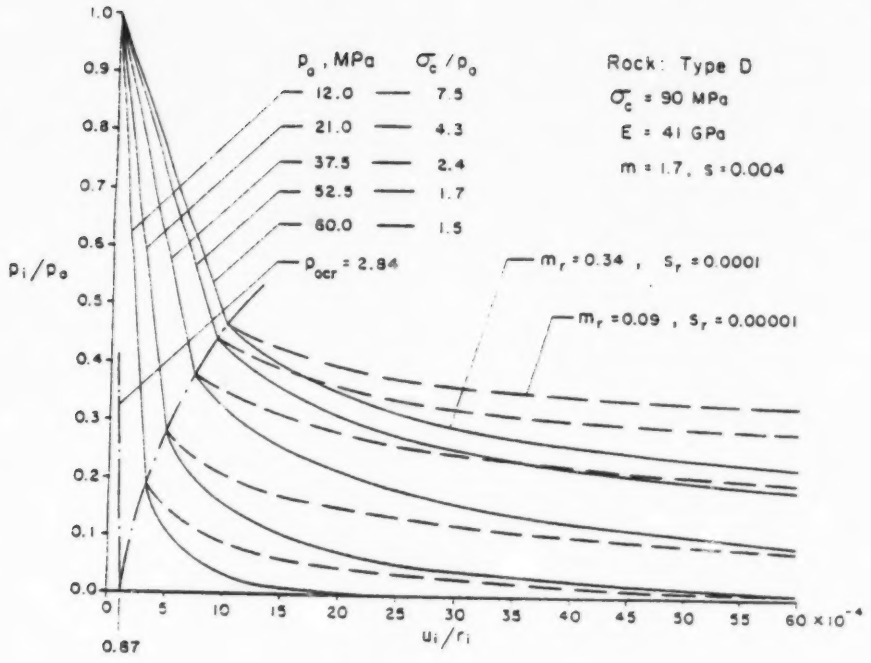


Fig. 40 - Load-deformation curves for rock Type D

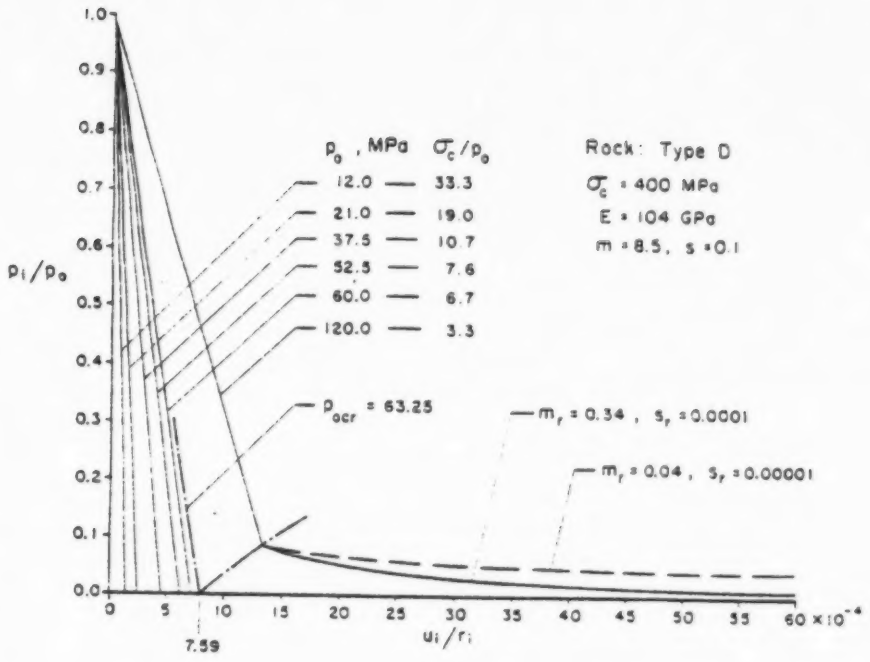


Fig. 41 - Load-deformation curves for rock Type D

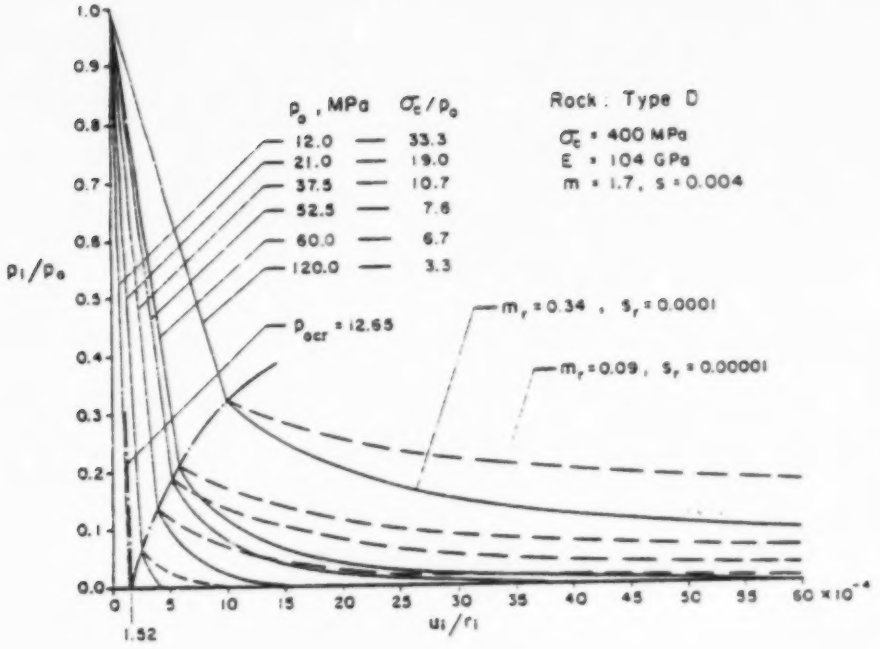


Fig. 42 - Load-deformation curves for rock Type D

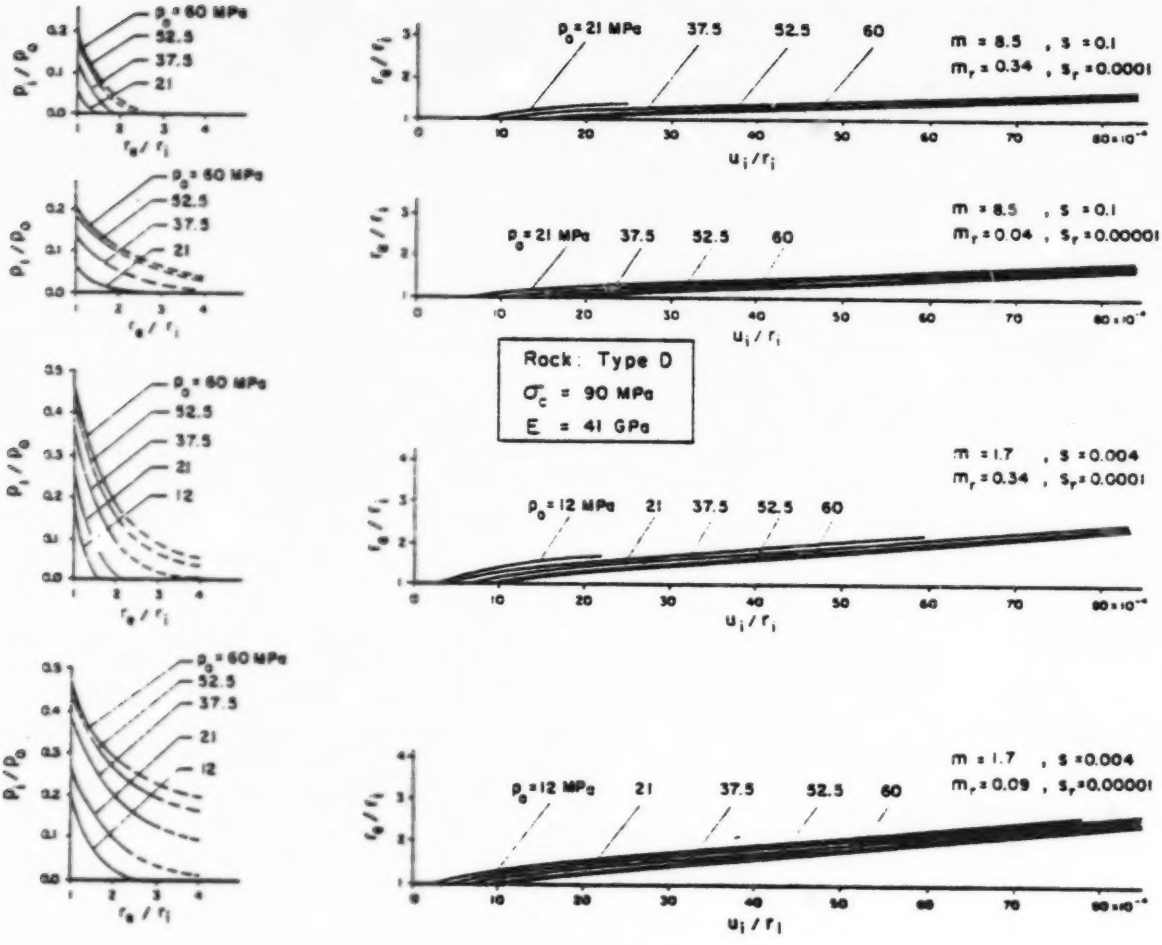


Fig. 43 - Extent of broken zones for rock Type D

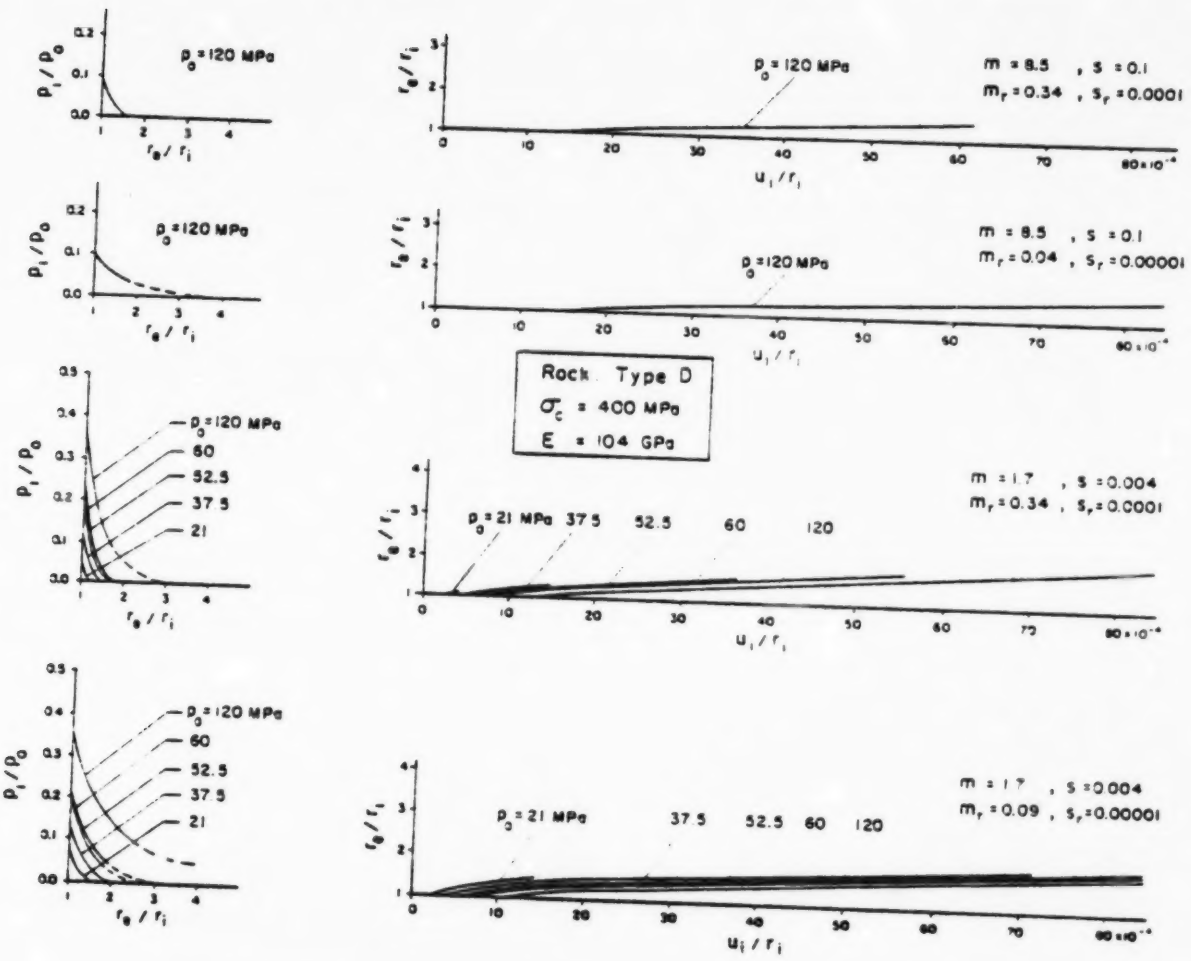


Fig. 44 - Extent of broken zones for rock Type D

ROCK: TYPE E

The computations were made for the systematic combinations of the selected values of variables listed in Table 28.

Table 28 - Listing of selected values of variables for rock Type E

| Variables | Selected values | |
|---|---|---|
| Material constants | Original rock mass quality | Very good m = 12.5, s = 0.1 |
| | | Good m = 2.5, s = 0.004 |
| | Broken rock mass quality | Fair $m_r$ = 0.5, $s_r$ = 0.0001 |
| | | Poor $m_r$ = 0.13, $s_r$ = 0.00001 |
| Paired uniaxial compressive strength and modulus of elasticity | $\sigma_c$ = 100 MPa, E = 41 GPa<br>$\sigma_c$ = 200 MPa, E = 58 GPa<br>$\sigma_c$ = 300 MPa, E = 76 GPa<br>$\sigma_c$ = 375 MPa, E = 88 GPa<br>$\sigma_c$ = 450 MPa, E = 101 GPa | |
| In situ stress, $p_o$ (MPa) | 12, 21, 37.5, 52.5, 60, 120 | |
| Poisson's ratio, $\nu$ | 0.25 | |
| Unit weight, $\gamma_r$, ($MN/m^3$) | 0.03 | |
| Radius of opening, $r_i$ (m) | 1.5, 3, 6, 9, 15 | |

The calculated values of $u_i/r_i$ are listed in Table 29. The elastic rays based on the results of Table 29 are shown in Fig. 45. The points of the transition curves, shown in Fig. 45, are calculated in Tables 30 and 31. The values of the calculated critical deformation ratios and critical in situ stresses are also given in Fig. 45.

The load-deformation curves for the lowest and highest values of the selected uniaxial compressive strength and elastic modulus pairs are plotted in Figs. 46 and 47 and Figs. 48 and 49, respectively.

Figures 50 and 51 illustrate the extent of broken zones corresponding to the lowest and highest values of selected $\sigma_c$ and E pairs, respectively.

Table 29 - Calculation and listing of $r_i/r_1$ values for rock type E

| E | $\frac{\sigma_c}{E}$ | $r_i/r_1$ for $\theta_0$ of | | | | | |
|---|---|---|---|---|---|---|---|
| | | 12 | 24 | 37.5 | 49.5 | 62 | 74 |
| 41.000 | $3.05\times10^{-5}$ | $3.38\times10^{-4}$ | $5.41\times10^{-4}$ | $1.14\times10^{-3}$ | $1.90\times10^{-3}$ | $3.83\times10^{-3}$ | $5.20\times10^{-3}$ |
| 58.000 | $2.15\times10^{-5}$ | $2.49\times10^{-4}$ | $4.54\times10^{-4}$ | $9.10\times10^{-4}$ | $1.63\times10^{-3}$ | $3.00\times10^{-3}$ | $4.33\times10^{-3}$ |
| 79.000 | $1.58\times10^{-5}$ | $1.97\times10^{-4}$ | $3.48\times10^{-4}$ | $6.89\times10^{-4}$ | $1.21\times10^{-3}$ | $2.44\times10^{-3}$ | $3.47\times10^{-3}$ |
| 98.000 | $1.27\times10^{-5}$ | $1.70\times10^{-4}$ | $2.98\times10^{-4}$ | $5.33\times10^{-4}$ | $1.06\times10^{-3}$ | $2.02\times10^{-3}$ | $2.93\times10^{-3}$ |
| 101.000 | $1.24\times10^{-5}$ | $1.49\times10^{-4}$ | $2.60\times10^{-4}$ | $4.59\times10^{-4}$ | $9.41\times10^{-4}$ | $1.84\times10^{-3}$ | $2.66\times10^{-3}$ |

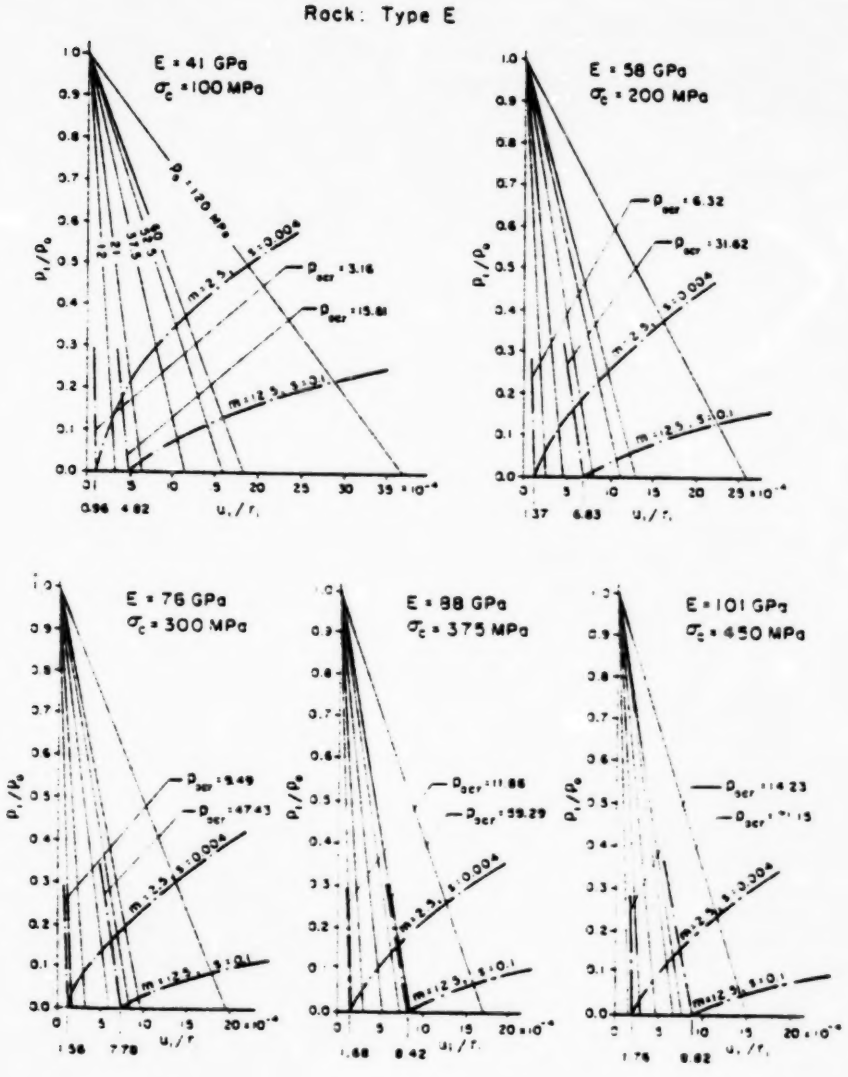


Fig. 45 - Elastic rays of rock Type E

Table 30-Calculation and listing of $p_{icr}/p_o$ values for rock type E

| $p_o$ | | $\sigma_c$ | | | | |
|---|---|---|---|---|---|---|
| | | 90 | 135 | 300 | 400 | 450 |
| 12 | $p_o/\sigma_c$ | 0.120 | 0.080 | 0.040 | 0.032 | 0.027 |
| | 12.5 $p_o/\sigma_c$ | 1.500 | 0.750 | 0.500 | 0.400 | 0.338 |
| | M | 0.123 | 0.066 | 0.047 | 0.039 | 0.034 |
| | M $\sigma_c/p_o$ | 1.025 | 1.100 | 1.175 | 1.219 | 1.259 |
| | $p_{icr}/p_o$ | -0.025 | -0.100 | -0.175 | -0.219 | -0.259 |
| 21 | $p_o/\sigma_c$ | 0.210 | 0.105 | 0.070 | 0.056 | 0.047 |
| | 12.5 $p_o/\sigma_c$ | 2.625 | 1.313 | 0.875 | 0.700 | 0.588 |
| | M | 0.204 | 0.109 | 0.076 | 0.062 | 0.054 |
| | M $\sigma_c/p_o$ | 0.971 | 1.038 | 1.086 | 1.107 | 1.143 |
| | $p_{icr}/p_o$ | 0.029 | -0.038 | -0.086 | -0.107 | -0.143 |
| 37.5 | $p_o/\sigma_c$ | 0.375 | 0.188 | 0.125 | 0.100 | 0.083 |
| | 12.5 $p_o/\sigma_c$ | 4.688 | 2.350 | 1.563 | 1.250 | 1.042 |
| | M | 0.344 | 0.185 | 0.127 | 0.104 | 0.088 |
| | M $\sigma_c/p_o$ | 0.917 | 0.948 | 1.016 | 1.040 | 1.057 |
| | $p_{icr}/p_o$ | 0.083 | 0.016 | -0.016 | -0.040 | -0.057 |
| 62.5 | $p_o/\sigma_c$ | 0.625 | 0.263 | 0.175 | 0.140 | 0.117 |
| | 12.5 $p_o/\sigma_c$ | 6.563 | 3.288 | 2.188 | 1.750 | 1.463 |
| | M | 0.484 | 0.250 | 0.171 | 0.141 | 0.119 |
| | M $\sigma_c/p_o$ | 0.884 | 0.951 | 0.989 | 1.007 | 1.020 |
| | $p_{icr}/p_o$ | 0.116 | 0.049 | 0.011 | -0.007 | -0.020 |
| 90 | $p_o/\sigma_c$ | 0.600 | 0.300 | 0.200 | 0.150 | 0.120 |
| | 12.5 $p_o/\sigma_c$ | 7.500 | 3.750 | 2.500 | 2.000 | 1.667 |
| | M | 0.521 | 0.282 | 0.195 | 0.150 | 0.122 |
| | M $\sigma_c/p_o$ | 0.868 | 0.940 | 0.975 | 0.994 | 1.014 |
| | $p_{icr}/p_o$ | 0.132 | 0.060 | 0.025 | 0.006 | -0.014 |
| 120 | $p_o/\sigma_c$ | 1.200 | 0.600 | 0.400 | 0.300 | 0.240 |
| | 12.5 $p_o/\sigma_c$ | 15.000 | 7.500 | 5.000 | 4.000 | 3.333 |
| | M | 0.930 | 0.521 | 0.365 | 0.299 | 0.254 |
| | M $\sigma_c/p_o$ | 0.775 | 0.868 | 0.913 | 0.934 | 0.951 |
| | $p_{icr}/p_o$ | 0.225 | 0.132 | 0.087 | 0.066 | 0.049 |

$m = 12.5$, $s = 0.1$

$$M = \frac{1}{2}\left(\left(\frac{12.5}{4}\right)^2 + 12.5\ p_o/\sigma_c - 0.1\right)^{1/2} - 12.5/8$$

$$M = \frac{1}{2}\left(9.866 + 12.5\ p_o/\sigma_c\right)^{1/2} - 1.563$$

Table 31 - Calculation and listing of $p_{ier}/p_o$ values for rock Type E

| $p_o$ | | $\sigma_c$ | | | | |
|---|---|---|---|---|---|---|
| | | 100 | 200 | 300 | 375 | 450 |
| 12 | $p_o/\sigma_c$ | 0.120 | 0.060 | 0.040 | 0.032 | 0.027 |
| | 2.5 $p_o/\sigma_c$ | 0.300 | 0.150 | 0.100 | 0.080 | 0.067 |
| | M | 0.104 | 0.056 | 0.039 | 0.032 | 0.027 |
| | M $\sigma_c/p_o$ | 0.867 | 0.933 | 0.975 | 1.000 | 1.000 |
| | $p_{ier}/p_o$ | 0.133 | 0.067 | 0.025 | 0 | 0 |
| 21 | $p_o/\sigma_c$ | 0.210 | 0.105 | 0.070 | 0.056 | [illegible] |
| | 2.5 $p_o/\sigma_c$ | 0.525 | 0.263 | 0.175 | 0.140 | [illegible] |
| | M | 0.167 | 0.093 | 0.064 | 0.051 | [illegible] |
| | M $\sigma_c/p_o$ | 0.795 | 0.886 | 0.914 | [illegible] | [illegible] |
| | $p_{ier}/p_o$ | 0.205 | 0.114 | 0.086 | 0.054 | [illegible] |
| 37.5 | $p_o/\sigma_c$ | 0.375 | 0.188 | 0.125 | [illegible] | [illegible] |
| | 2.5 $p_o/\sigma_c$ | 0.938 | 0.470 | 0.313 | [illegible] | [illegible] |
| | M | 0.264 | 0.152 | 0.108 | [illegible] | [illegible] |
| | M $\sigma_c/p_o$ | 0.704 | 0.809 | 0.864 | [illegible] | [illegible] |
| | $p_{ier}/p_o$ | 0.296 | 0.191 | 0.136 | [illegible] | [illegible] |
| 52.5 | $p_o/\sigma_c$ | 0.525 | 0.263 | 0.175 | [illegible] | [illegible] |
| | 2.5 $p_o/\sigma_c$ | 1.313 | 0.658 | 0.438 | [illegible] | [illegible] |
| | M | 0.340 | 0.200 | 0.143 | [illegible] | [illegible] |
| | M $\sigma_c/p_o$ | 0.648 | 0.760 | 0.817 | [illegible] | [illegible] |
| | $p_{ier}/p_o$ | 0.352 | 0.240 | 0.183 | [illegible] | [illegible] |
| 60 | $p_o/\sigma_c$ | 0.600 | 0.300 | 0.200 | [illegible] | [illegible] |
| | 2.5 $p_o/\sigma_c$ | 1.500 | 0.750 | 0.500 | [illegible] | [illegible] |
| | M | 0.375 | 0.222 | 0.160 | [illegible] | [illegible] |
| | M $\sigma_c/p_o$ | 0.625 | 0.740 | 0.800 | [illegible] | [illegible] |
| | $p_{ier}/p_o$ | 0.375 | 0.260 | 0.200 | [illegible] | [illegible] |
| 120 | $p_o/\sigma_c$ | 1.200 | 0.600 | 0.400 | 0.320 | [illegible] |
| | 2.5 $p_o/\sigma_c$ | 3.000 | 1.500 | 1.000 | 0.800 | [illegible] |
| | M | 0.608 | 0.375 | 0.278 | 0.234 | [illegible] |
| | M $\sigma_c/p_o$ | 0.507 | 0.625 | 0.695 | [illegible] | [illegible] |
| | $p_{ier}/p_o$ | 0.493 | 0.375 | 0.305 | 0.269 | 0.243 |

$m = 2.5, \quad s = 0.004$

$$M = \frac{1}{2}\left(\left(\frac{2.5}{4}\right)^2 + 2.5\ p_o/\sigma_c + 0.004\right)^{1/2} - 2.5/8$$

$$M = \frac{1}{2}\left(0.395 + 2.5\ p_o/\sigma_c\right)^{1/2} - 0.313$$

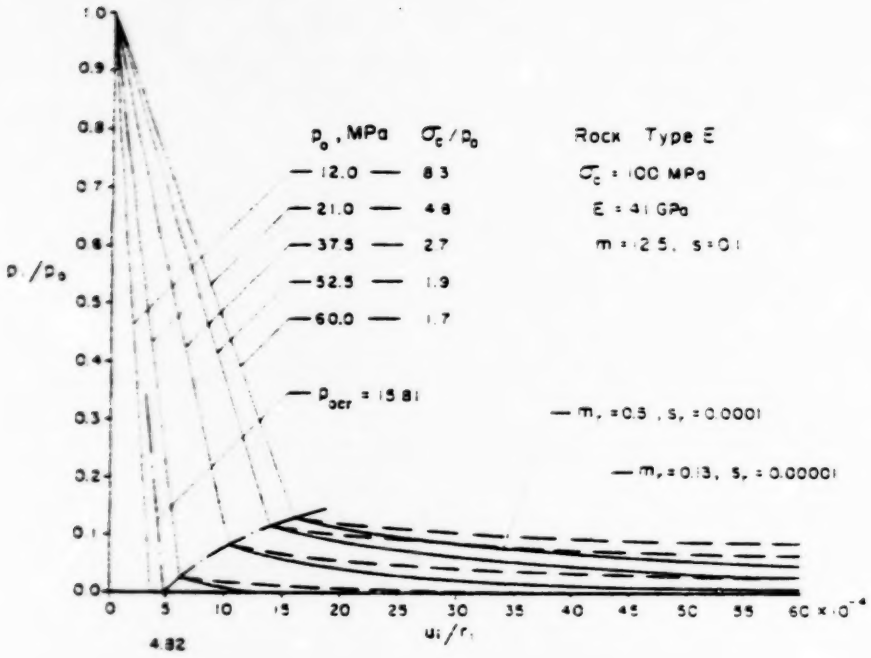


Fig. 46 - Load-deformation curves for rock Type E

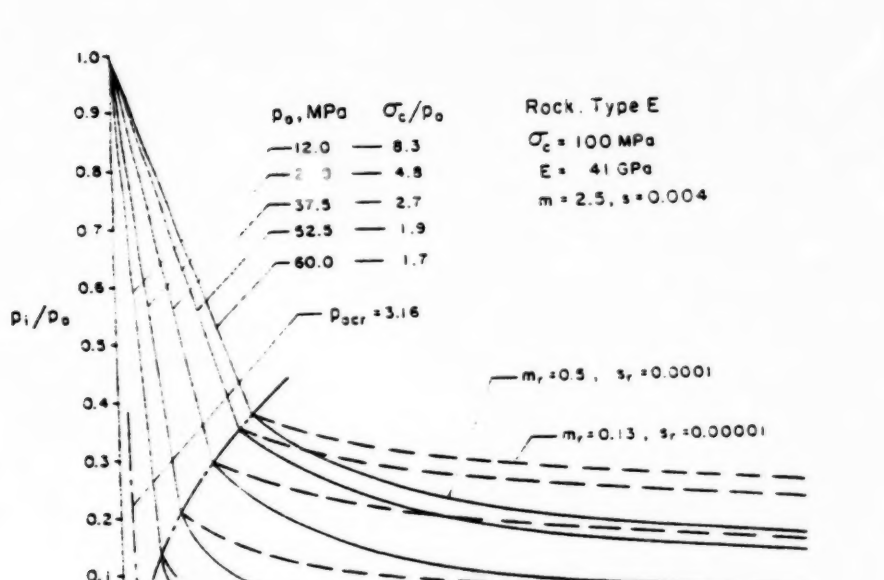


Fig. 47 - Load-deformation curves for rock Type E

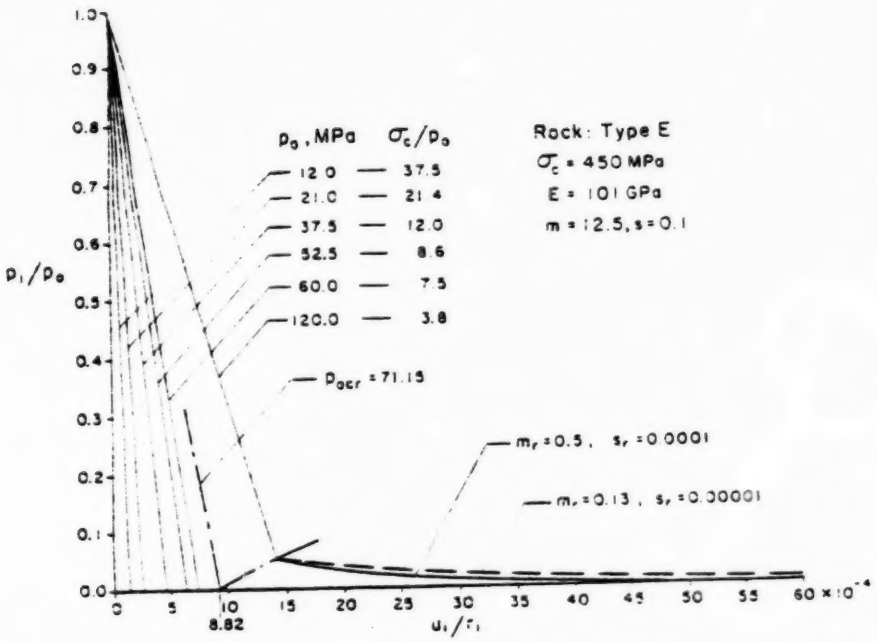


Fig. 48 - Load-deformation curves for rock Type E

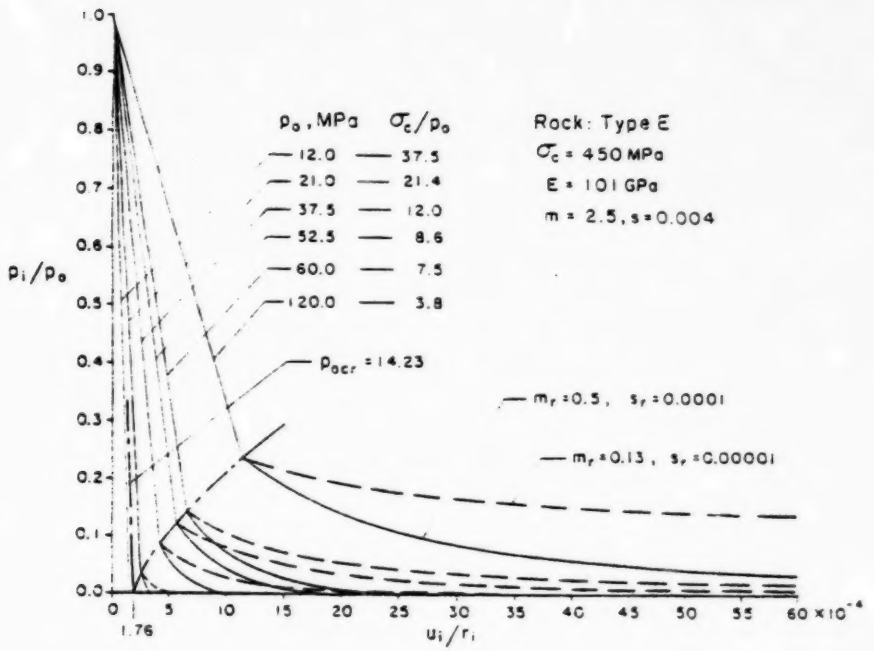


Fig. 49 - Load-deformation curves for rock Type E

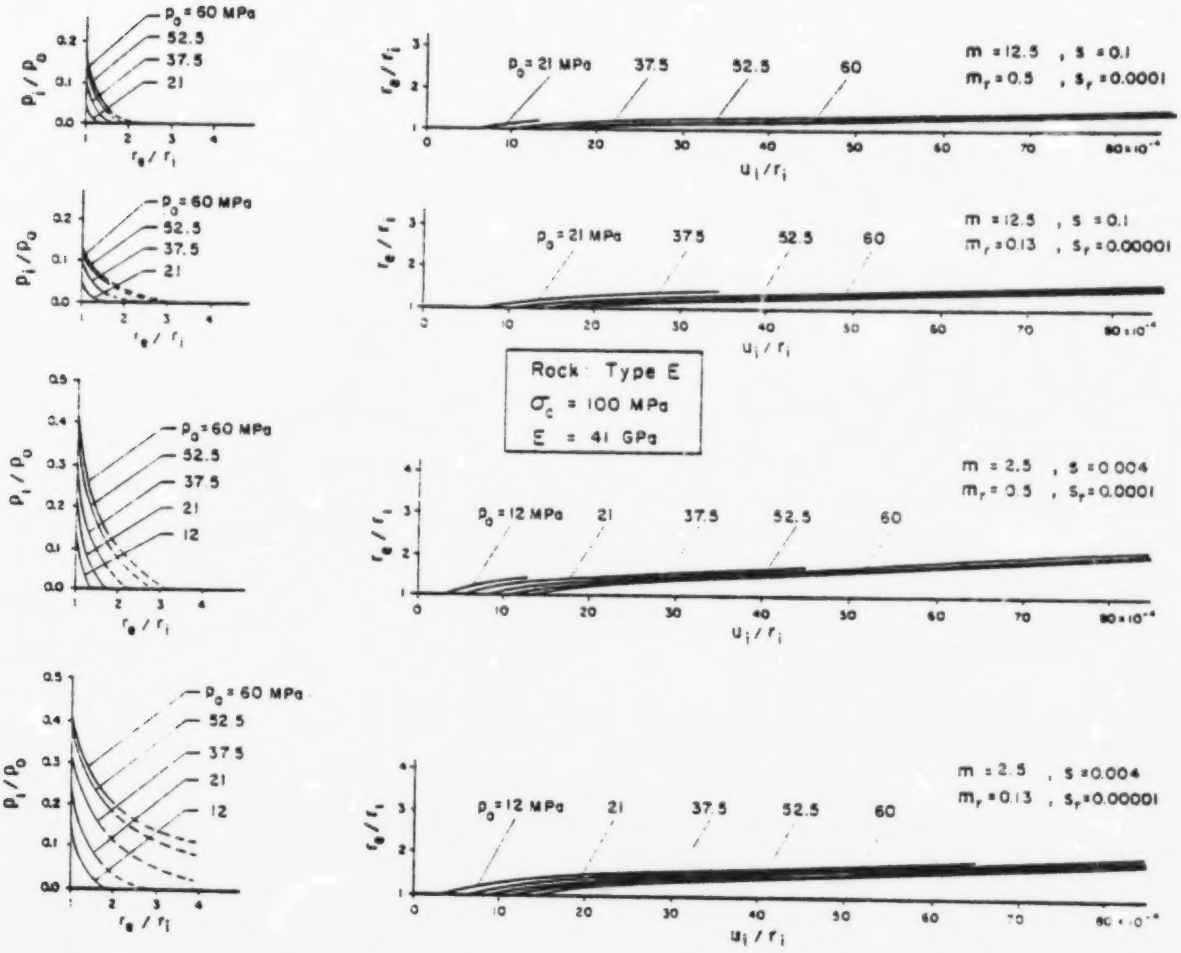


Fig. 50 - Extent of broken zones for rock Type E

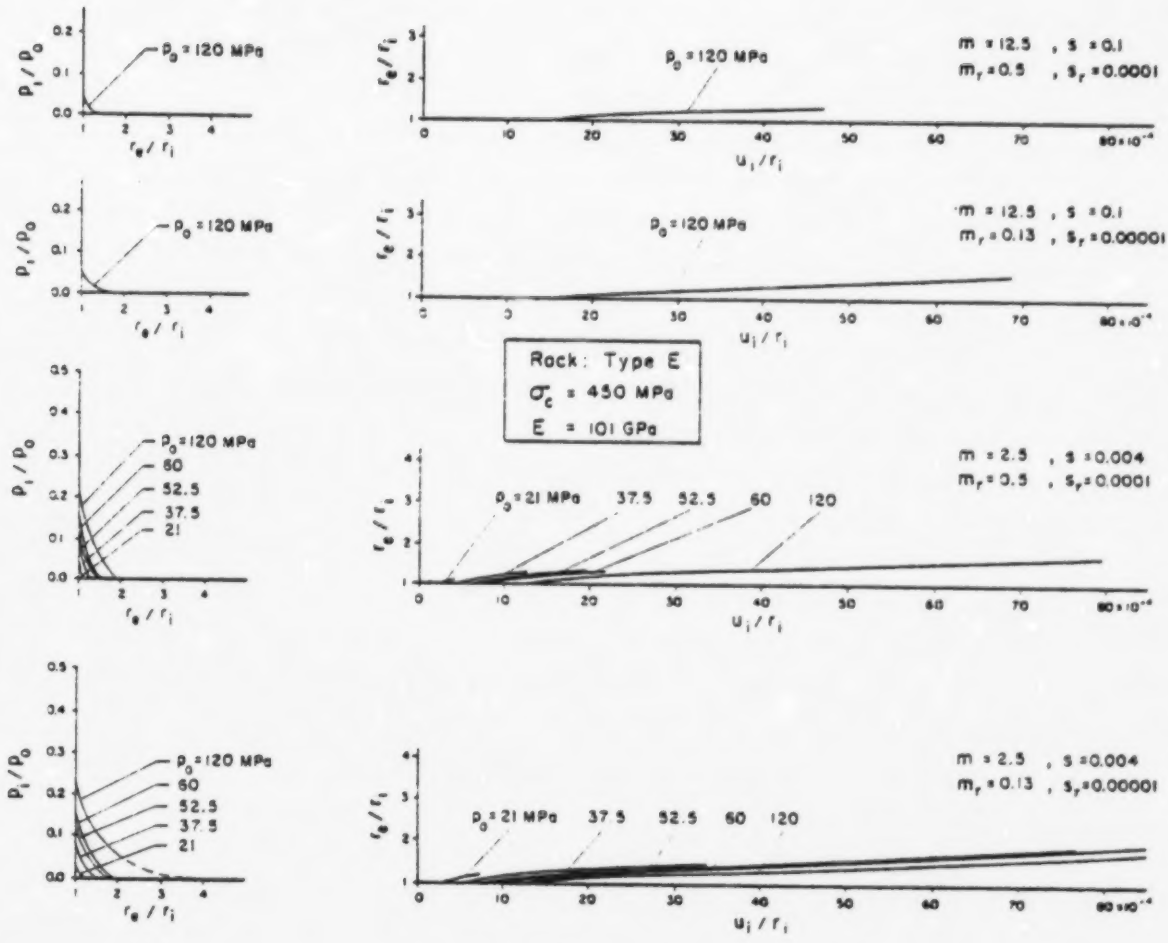


Fig. 51 - Extent of broken zones for rock Type E

## DISCUSSION OF RESULTS

The completed parametric analyses resulted two sets of curves which are given in the previous section.

The set of load-deformation curves may be used to design the required support system if the rock mass properties and stress conditions of the given case coincide with the selected values of any particular analysed case. The complete rock-support interaction design procedure has been explained previously by a detailed example. The set of broken zone curves may be used to estimate the dead-weight of loose rocks and the required length of rock bolts.

The actual support design, however, is outside of the scope of the present study. The purpose of the study was to correlate and sythesize all major factors involved in support design in order to establish a systemized data base required for the development of bolting guidelines for hard rocks.

In connection with the detailed example it had already been demonstrated that for a given rock mass (original), characterized by its strength and deformation properties ($\sigma_c$, m, s, E, $\nu$), the expected stability behaviour, for the given in situ stress conditions, can be defined in terms of critical stress and deformation values.

These important results of the study are summarised in Fig. 52. Accordingly, if the acting in situ stress is smaller than the critical in situ stress (i.e., $p_o < p_{ocr}$), the entire rock mass around a circular opening behave elastically. Because no broken zone develops, the opening is stable without support.

The limit of completely elastic radial deformation is determined by the critical radial deformation, $u_{icr}$.

Broken rock zone will develop if the acting in situ stress exceeds the magnitude of the critical in situ stress, i.e., $p_o > p_{ocr}$. The development of broken zone sets out at the periphery of the opening where the concentration of stresses takes effect. The extent of the broken zone is governed by the stress ratio of $p_i/p_o$.

The relationship between the critical stress ratio and the properties of the original rock mass is expressed by the equation of $p_{icr}/p_o = 1 - M\sigma_c/p_o$. The original rock mass, where $p_i/p_o > p_{icr}/p_o$ is in elastic condition; while, the broken rock mass, where $p_i/p_o < p_{icr}/p_o$ is in plastic condition.

The plastic deformation of the broken zone is governed by the properties of the broken rock mass which are manifested by the material constants of $m_r$ and $s_r$.

The significance of the obtained results, in analysing the stability condition of an opening situated in a rock mass of defined strength and deformation properties, can be underscored through the discussion of the underlying mathematical relationships.

The transition curve is defined by the equation:

$$p_{icr}/p_o = 1 - M\,\sigma_c/p_o \tag{3a}$$

where

$$M = \frac{1}{2}\left[\left(\frac{m}{4}\right)^2 + m\,p_o/\sigma_c + s\right]^{1/2} - \frac{m}{8} \tag{4}$$

The transition curve originates at the point of $p_{icr}/p_o = 0$, that is, where $p_i = p_{icr} = 0$.

Therefore,

$$0 = 1 - M\,\sigma_c/p_o \tag{3b}$$

and

$$p_o = M\,\sigma_c \tag{3c}$$

Because equation (3c) represents a special case, i.e., $p_i = p_{icr} = 0$, the in situ stress magnitude, $p_o$, is being designated as critical in situ stress, $p_{ocr}$, therefore,

$$p_{ocr} = M\,\sigma_c \tag{3d}$$

From equation (3d)

$$M = p_{ocr}/\sigma_c \tag{3e}$$

however, by equation (4)

$$M = \frac{1}{2}\left[\left(\frac{m}{4}\right)^2 + m\, p_o/\sigma_c + s\right]^{1/2} - \frac{m}{8}$$

therefore,

$$\frac{p_{ocr}}{\sigma_c} = \frac{1}{2}\left[\left(\frac{m}{4}\right)^2 + \frac{m\, p_{ocr}}{\sigma_c} + s\right]^{1/2} - \frac{m}{8}$$

The simplification of this expression yields the following equation:

$$p_{ocr} = \left(\frac{s\, \sigma_c^{\,2}}{4}\right)^{1/2} \tag{14}$$

Then, the end point of the elastic ray representing the critical in situ stress, $p_{ocr}$, can be calculated by the following equation:

$$\frac{u_{icr}}{r_i} = \frac{1 + \nu}{E}\, p_{ocr} \tag{15}$$

where, the designation of critical radial deformation, $u_{icr}$, emphasises the fact that it is a common point for the end of the elastic ray of $p_{ocr}$ and the origin of the transition curve.

The rearrangment of equation (14) yields the following forms:

$$p_{ocr}^{\,2} = \frac{s\, \sigma_c^{\,2}}{4} \tag{14a}$$

then,

$$\frac{p_{ocr}^{\,2}}{\sigma_c^{\,2}} = \frac{s}{4} \tag{14b}$$

and finally,

$$\frac{p_{ocr}}{\sigma_c} = (s)^{1/2}/_2 \tag{14c}$$

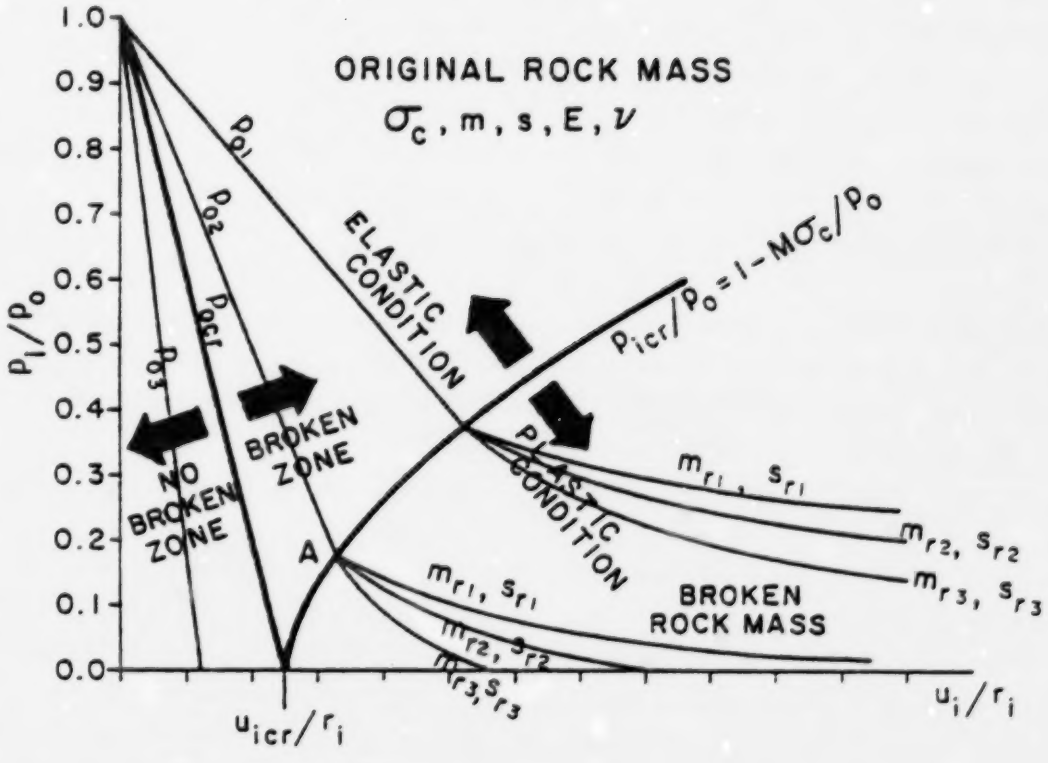


Fig. 52 - Critical stress and deformation of a rock mass and the expected stability behaviour

Note that the right side of equation (3e) is the same as the left side of equation (14c), therefore, it follows that $M = (s)^{1/2}/2$. Since this relationship is applicable only for the specifc case of $p_i = p_{icr} = 0$, the value of M for this case is to be designated as $M_{cr}$, then

$$M_{cr} = (s^{1/2})/2 \tag{16}$$

The derived relationship expressed by equations (14c) and (16) deserves some further deliberations.

The original rock mass is assumed to be linear-elastic and to be characterized by $\sigma_c$, m, s, E and $\nu$. The failure characteristics of this material are defined, after Hoek and Brown, by the equation

$$\sigma_1 = \sigma_3 + (m\ \sigma_c \sigma_3 + s\ \sigma_c^2)^{1/2} \tag{1}$$

From the differential equation of

$$\frac{d\ \sigma_r}{d_r} + \frac{(\sigma_r - \sigma_\theta)}{r} = 0 \tag{94}$$

the following equations can be obtained for the stresses in the elastic region:

$$\sigma_r = p_o - (p_o - \sigma_{re})\ (r_e/r)^2 \tag{95}$$

$$\sigma_\theta = p_o + (p_o - \sigma_{re})\ (r_e/r)^2 \tag{96}$$

Let us consider the specific case when $p_i = p_{icr} = 0$ and when $r = r_e$. Since in this case $\sigma_{re} = 0$, the stresses, expressed by equation (95) and (96), are:

$$\sigma_r = 0$$
$$\sigma_\theta = 2\ p_o$$

Then, by substituting $\sigma_1 = \sigma_\theta = 2p_o$ and $\sigma_3 = \sigma_r = 0$ into equation (1), we obtain:

$$2p_o = \left( s\, \sigma_c^{\,2} \right)^{1/2}$$

and then

$$\frac{p_o}{\sigma_c} = (s)^{1/2}/2$$

which is the same result as obtained by either equation (14c) or equation (16).

It can, therefore, be stated that the failure and consequently the stability of the rock mass at the immediate periphery of the opening is governed by a single parameter, namely by the material constant s.

The application of the critical stress and deformation concept is shown in Figs. 53 and 54.

The data presented in Fig. 53 correspond to rock Type A. In Fig. 53(a) the assumed quality of the original rock mass is very good. The data points of the graphs were calculated by the equations discussed above. As can be seen, the values of $p_{ocr}$ and $u_{icr}/r_i$ change with the input data pair of $\sigma_c$ and E. The ratio of $p_{ocr}/\sigma_c$, however, ramains constant, because it is governed only by the constant value of s = 0.1. Some authors prefer to use the reciprocate value, i.e. $\sigma_c/p_{ocr}$, and refer to it as the competence factor (e.g., [8]).

Similar data are presented in Fig. 53(b) which corresponds to a good quality Type A rock mass. Note the decreased stability, as indicated by the decreased values of $p_{ocr}$ and $u_{icr}/r_i$ and also by the much steeper transition curves.

The reduced stability is caused by the lower values of material constants. The decrease in $p_{ocr}$ and $u_{icr}/r_i$ values is due entirely to the change in the value of s, i.e. from s = 0.1 (very good quality rock mass) to s = 0.004 (good quality rock mass). The reduction in the value of m, i.e., fro 3.5 to 0.7, causes the steepening of the transition curves. The constant ratio of $p_{ocr}/\sigma_c$ = 0.032 corresponds to the s = 0.004 value, as defined by equation (14c).

The effects of the material constants on the stability of the rock mass around the opening are even more pronounced in Fig. 54, because of the significantly different values of $\sigma_c$, E and m of the presented graphs.

Figure 54(a) compares the stability of Type A and Type E very good quality rock masses. The similar comperative data are presented in Fig. 54(b) for good quality rock masses. Note again the constant values of $p_{ocr}/\sigma_c$ = 0.158 and $p_{ocr}/\sigma_c$ = 0.032, related to s = 0.1 and s = 0.004 values, respectively.

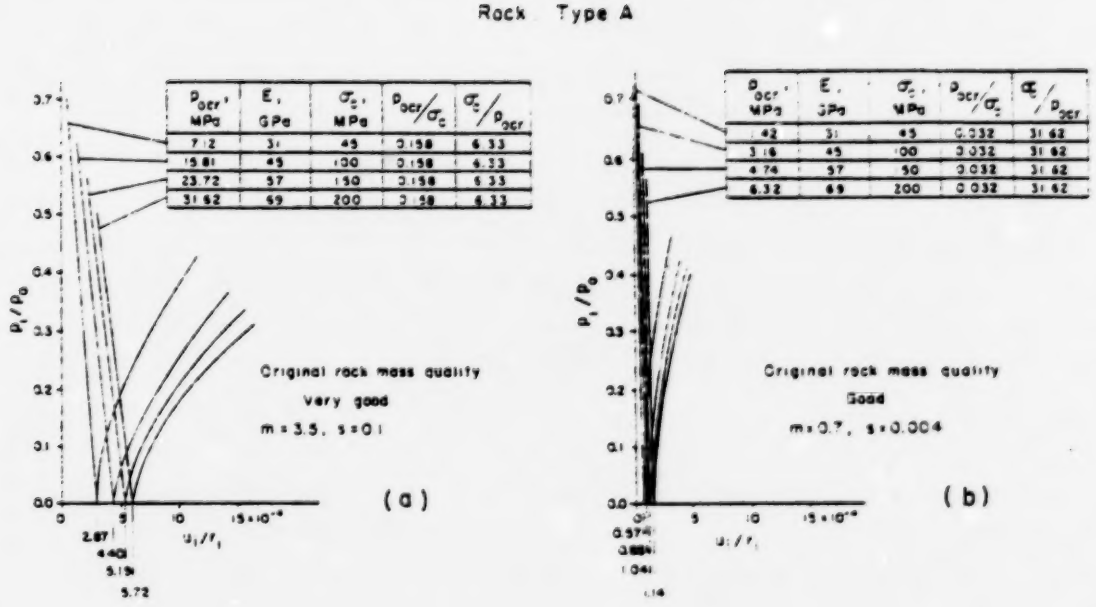
Rock Type A
$p_{ocr}$, MPa | E, GPa | $\sigma_c$, MPa | $p_{ocr}/\sigma_c$ | $\sigma_c/p_{ocr}$
7.12 | 31 | 45 | 0.158 | 6.33
15.81 | 45 | 100 | 0.158 | 6.33
23.72 | 57 | 150 | 0.158 | 6.33
31.62 | 69 | 200 | 0.158 | 6.33
$p_i/p_o$
Original rock mass quality
Very good
m = 3.5, s = 0.1
(a)
$u_i/r_i$
2.87
4.40
5.19
5.72
$p_{ocr}$, MPa | E, GPa | $\sigma_c$, MPa | $p_{ocr}/\sigma_c$ | $\sigma_c/p_{ocr}$
.42 | 31 | 45 | 0.032 | 31.62
3.16 | 45 | 100 | 0.032 | 31.62
4.74 | 57 | 50 | 0.032 | 31.62
6.32 | 69 | 200 | 0.032 | 31.62
$p_i/p_o$
Original rock mass quality
Good
m = 0.7, s = 0.004
(b)
$u_i/r_i$
0.574
0.884
1.041
1.16

Fig. 53 - Variation of critical stresses and deformations for rock Type A

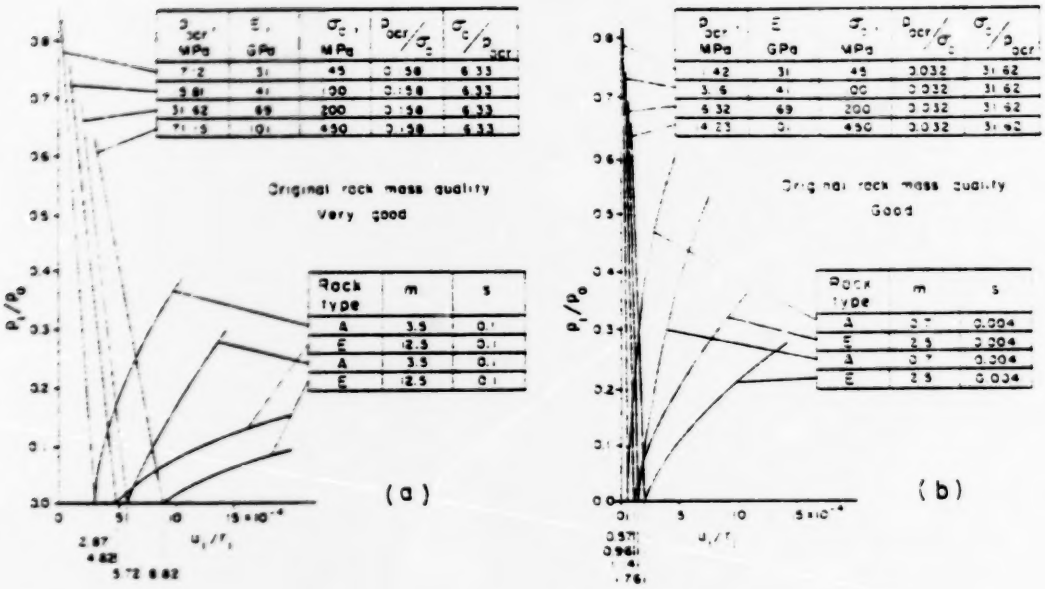


Fig. 54 - Variation of critical stresses and deformation for rock Types A and E

## CONCLUSIONS AND RECOMMENDATIONS

1. The significance of each involved variable with respect to the stability of underground openings had been determined.
2. One of the important results of the study is the formulation of the concept of critical stress and deformation analysis.
3. The critical stress and deformation analysis provides an effective and simple method in analysing the expected stability behaviour of an underground opening.
4. The critical stress and deformation analysis can be used to estimate the support requirements and to make an initial selection of support types.
5. The conditions, in the terms of rock mass properties and in situ stresses, of effective rock bolting support, can be defined on the basis of critical stress and deformation analysis and of the correlated data of this completed study.
6. The ultimate objective of the Material Properties and Support Project is to provide guidelines on support design, installation, testing and monitoring. The guidelines on rock bolting requires field measurement data on the supporting capacity of rock bolt types and systems, correlated with the essential strength and deformation properties of rock mass. This type of data are presently not available.
7. It is possible, however, to proceed with a draft version of the proposed bolting guidelines, based on the results obtained by this study as well as other available information.
8. The method of stability analysis used in this study is based on the empirical equation of $\sigma_1 = \sigma_3 + (m\ \sigma_3\ \sigma_c + s\ \sigma_c^2)^{1/2}$, developed by Hoek and Brown. The recommended material constant values of m and s are adequately accurate to perform preliminary analyses or to establish the sensitivity of the design to changes in rock mass properties, like in the case of this study. There is no doubt, this empirical equation will be widely used in the future for rock mechanics analysis and design. It is desirable, therefore, that the rock mechanics field and laboratory investigations to be directed towards of establishing the rock mass strength and deformation properties data in the terms required by this method of analysis.
9. Two areas of further investigations are identified. Investigations should be conducted to establish the relationship between the supporting capacity of the various bolt types, bolting systems and the quality and properties

of various rock masses. The second objective of this investigation is to verify or, if required, to modify the specifications of the draft bolting guidelines. The other area of investigations is related to the development of a much needed data bank on the pre- and post-failure strength and deformation properties of various major rock types of the Canadian mines.

## REFERENCES


1. Gyenge, M. "Evaluation of support system: rock bolting - first interim report"; CANMET, Energy, Mines and Resources Canada; Division Report MRP/MRL 82-1(TR), 41 p; January 1982.

2. Hoek, E. and Brown E.T. "Underground excavations in rock"; Institute of Mining and Metallurgy, London; 527 p; 1981.

3. Coates, D.F. and Cochrane, T.S. "Development of design specifications for rock bolting from research in Canadian mines"; CANMET, Energy, Mines and Resources Canada; Research Report R224, 29 p; 1970.

4. Lama, R.D. and Vutukuri, V.S. "Handbook on mechanical properties of rocks - Testing techniques and results - Volume II"; Trans Tech Publications, Germany; 481 p; 1978.

5. Touloukian, Y.S. and Ho, C.Y. "Physical properties of rocks and minerals"; McGraw-Hill/CINDAS Data Services on Material Properties Volume II-2, McGraw-Hill; 548 p; 1981.

6. Unpublished internal reports on test results; Mining Research Laboratories, CANMET, Energy, Mines and Resources Canada.

7. Ladanyi, B. "Use of the long-term strength concept in the determination of ground pressure on tunnel linings"; 3rd Congr., Intnl. Soc. Rock Mech., Denver; 1974, Vol. 2B, pp. 1150-1146.

8. Tanimoto, C. "Tunnelling in rock with rockbolts and shotcrete"; Kyoto Univ., Japan, Lecture note; 1980.

POOR

QUALITY

ORIGINAL